69-8604

JOHNSON, Albert Wayne, 1938-

MEASURED LIFETIMES OF ELECTRONIC, VIBRATIONAL AND ROTATIONAL LEVELS OF THE NITROGEN MOLECULE.

The University of Oklahoma, Ph.D., 1968
Physics, molecular

University Microfilms, Inc., Ann Arbor, Michigan

THE UNIVERSITY OF OKLAHOMA

GRADUATE COLLEGE

MEASURED LIFETIMES OF ELECTRONIC, VIBRATIONAL AND ROTATIONAL LEVELS OF THE NITROGEN MOLECULE

A DISSERTATION

SUBMITTED TO THE GRADUATE FACULTY

in partial fulfillment of the requirements for the

degree of

DOCTOR OF PHILOSOPHY

by

ALBERT WAYNE JOHNSON

NORMAN, OKLAHOMA

1968

MEASURED LIFETIMES OF ELECTRONIC, VIBRATIONAL AND

ROTATIONAL LEVELS OF THE NITROGEN MOLECULE

APPROVED BY

Richard B Fowler

J M Canfield

Lyle Lewis

Robert M. St John

R. A. Day

ACKNOWLEDGEMENT

I am indebted to many for the completion of the project which this dissertation describes. Dr. T. M. Holzberlein designed and developed the invertron, which was the basic tool of this experiment. In addition, Dr. Holzberlein assisted, encouraged and advised me in many aspects of the experiment.

Drs. S.J.B. Corrigan, Stanley Babb and C.C. Lin contributed their time to discuss some of the experimental or theoretical aspects of this research. Invaluable assistance and advice was obtained from Jim Hood and Gene Scott in the manufacture of various components and from Norman Alexandre and Ron Stermer in the design and construction of the vacuum systems. Gary Copeland, Manny Polizzi and Dick Thompson almost daily worked with me to build and design the equipment or to take data. Stanley Robertron gave to me invaluable information in the operation of the vacuum ultraviolet spectrograph. Indeed, the information and assistance obtained from the faculty, staff and students of the Physics Department at the University of Oklahoma is of manifold extent.

The advice, assistance and personal encouragement which Dr. R. G. Fowler gave to me largely accounts for any of the successful accomplishments of this research.

My wife, Gail, did many of tne numerical calculations and most of the typing and preparation of this dissertation. But the faith and under-

standing of my wife is that which has been the determining factor for all of my achievements in graduate school.

Appreciation is extended to Kirtland Air Force Base for the financial funding of this project.

TABLE OF CONTENTS

TABLE OF CONTENTS (CONT'D.)

LIST OF TABLES

LIST OF TABLES (CONT'D.)

LIST OF FIGURES

LIST OF FIGURES (CONT'D.)

LIST OF FIGURES (CONT'D.)

GLOSSARY OF ACRONYMS

1. CRT -- Cathode Ray Tube
2. DTG -- Delayed Trigger Generator
3. EFS -- Exponential Function Synthesizer
4. GPG -- Gate Pulse Generator
5. LPG -- Logic Pulse Generator
6. PHA -- Pulse Height Analyzer
7. RM -- Rate Meter
8. RMA -- Rate Meter Amplifier
9. SWG -- Square Wave Generator
10. TPC -- Time Pickoff Control
11. TPAC - Time to Pulse Height Converter

MEASURED LIFETIMES OF ELECTRONIC, VIBRATIONAL AND ROTATIONAL LEVELS OF THE NITROGEN MOLECULE

CHAPTER I

INTRODUCTION

Due to the atmospheric content of the earth, the nitrogen molecule plays an important role in electron and photon energy transport in our environment. To describe the mechanism of photon energy transport, the oscillator strengths and transition probabilities must be known. The oscillator strengths and transition probabilities are determinable from the lifetimes of the corresponding levels if the relative intensities of the emitted radiation are known also. Due to this importance and due to considerable confusion in previous measurements, the experimental investigation herein to be described of the lifetimes of the nitrogen molecule was undertaken.

Previous Work

The $B\,^3\Pi_g$ state of nitrogen decays by spontaneous emission to the $A\,^3\Sigma_u^+$ state. This produces the relatively strong, near infrared first positive band system. The spontaneous emission lifetime measurement of this state is difficult due to competing collisional depopulation because of the relatively long lifetime. Jeunehomme[1] measured the pressure dependent lifetimes of the vibrational levels v'=0 through v'=10 and obtained values which ranged from 8.0 to 4.4 microseconds, respectively,

after extrapolation to zero pressure. Brenner[2] examined the rotational equilibrium time in the nitrogen afterglow and claimed that the lifetime of the $B^3\Pi_g$ state is greater than 2.4 microseconds. Wuster[3] measured the absorption oscillator strength of the zero-zero vibrational transition in a shock heated nitrogen gas. The value he obtained for the oscillator strength was 0.0028.

The electronic state of the molecular ion (N_2^+), which has received the most attention in direct lifetime measurements, is the $B^2\Sigma_u^+$. This level decays by spontaneous emission to the $A^2\Sigma_g^+$ level. The resulting spectral bands are referred to as the first negative systems. Bennett and Dalby[4] were the first to measure directly the lifetime of the v'=0 vibrational level of the $B^2\Sigma_u^+$ state via the 3914 Å band to be 65.8 nanoseconds. Fink and Welge[5] used a phase shift technique and obtained a value of 45 nanoseconds for the v'=0 level. Sebacher[6] used a 10KeV pulsed electron gun and measured the lifetime of v'=0 to be 65 nanoseconds. Fowler and Holzberlein[7] viewed the radiation decay directly and obtained a value of about 70 nanoseconds for the $B^2\Sigma_u^+$ state. Jeunehomme[8] observed the radiation decay following a terminated, radio frequency discharge. By applying a gate to the photomultiplier, he was able to sample the radiation decay and accumulate a decay curve. The lifetime Jeunehomme reported for the state was 71.5 nanoseconds. Hesser and Dressler[9] obtained a value of 59 nanoseconds with a phase shift technique.

The $C^3\Pi_u$ state of nitrogen has been examined by a number of investigators. This state decays spontaneously to the $B^3\Pi_g$ state to produce the second positive band system. In all previous measurements, peculiar

and previously inexplicable pressure and electron energy dependences have been reported. Bennett and Dalby[4] did the original work on this state also. They found the lifetime to be electron energy dependent. Arbitrarily, they analyzed their data to yield a lifetime of 44.5 nanoseconds. Fink and Welge[5] extrapolated to the energy of excitation onset to obtain 27 microseconds as the lifetime of the v'=0 level. Jeunehomme[8] extrapolated his pressure dependent values to give 49 nanoseconds. He arbitrarily disregarded the low pressure measurements. Nichols and Wilson[10] measured the lifetime of the v'=0 and v'=1 levels of the $C^3\Pi_u$ state with a delayed coincidence photon counting technique. A pulsed proton beam was used as the excitation source. They extrapolated to zero pressure from a relatively high pressure region (50 - 400 Torr) to obtain lifetimes of 45.4 and 31.2 nanoseconds for the v'=0 and v'=1 levels, respectively.

A compilation and comparison of the above mentioned three states of nitrogen is presented in a tabular form in Chapter IV of this report.

This Work

The lifetimes of the $B^3\Pi_g$ and $C^3\Pi_u$ states of N_2 and of the $B^2\Sigma_u^+$ state of N_2^+ were investigated in an attempt to clarify the ambiguities and inaccuracies which previous measurements have demonstrated. The peculiar electron energy and pressure dependences of the $C^3\Pi_u$ and $B^2\Sigma_u^+$ states were also investigated and the results herein reported. A possible explanation for the previous ambiguities will be presented.

A band of a diatomic molecule produced by a vibrational transi-

tion is the result of many rotational transitions. The lifetimes of the individual rotational levels of the $B^2\Sigma_u^+$ (v'=0) were measured to test the common assumption that the lifetimes are all the same. The results of these measurements will be given.

The rotational temperature of the $B^2\Sigma_u^+(v'=0)$ of N_2^+ was also measured. The results of these measurements will be presented and a comparison will be made to the measured temperature of the containment vessel.

The Birge-Hopfield band system is produced by a transition from the $b^1\Pi_u$ to $X^1\Sigma_g^+$ states of the nitrogen molecule. An attempt was made to measure the lifetimes of the upper level. However, due to predissociation of this level, the radiation intensity was too weak and the resulting lifetimes probably too short to measure. An intensity comparison of the Lyman-α line of hydrogen was made to the Birge-Hopfield bands to obtain the ratio of the probability of predissociation to spontaneous emission of the $b^1\Pi_u(v'=1)$ level of nitrogen. This comparison will be described and the results presented in Chapter IV.

CHAPTER II

THEORY AND MATHEMATICAL ANALYSES

General Relations Between Transition Parameters

For electric dipole radiation, the line strength, S(M,N), of a transition connecting upper level M to lower level N may be expressed as follows.

$$S(M,N) = \Sigma_{m,n} \left| (m \left| \bar{P} \right| n) \right|^2 \tag{1}$$

$\left| (m|\bar{P}|n) \right|^2$ is the squared matrix component connecting a state m of the level M with a state n of the level N. $\bar{P}$ is the electric dipole moment for the system. Natural excitation and unpolarized radiation will be assumed in all that follows.

The transition probability, A(M,N), for the transition from level M to level N may be described in terms of the line strength.

$$A(M,N) = \frac{64\pi^4 \nu^3(M,N)\ S(M,N)}{3hc^3\ (2J_M + 1)} \tag{2}$$

h and c denote Planck's constant and the speed of light, respectively. $\nu(M,N)$ is the frequency of the emitted radiation for the M to N transition. The factor $(2J_M + 1)$ is the number of states in level M and is necessary simply because of the summation involved in the definition of the line strength. Treatment in this manner is justified since the total transi-

tion probability of every state in a given level is the same.[11] The lifetime, τ_M, of a given level may be expressed as:

$$\tau_M = [\Sigma_N A(M,N)]^{-1} = [\Sigma_N \frac{64\pi^4 \nu^3(M,N)\ S(M,N)}{3hc^3\ (2J_M + 1)}]^{-1} \tag{3}$$

The lifetime of every state in a given level is the same.

If the lifetime, τ_M, is known, the transition probabilities may be determined from a measurement of the relative intensities of the emitted radiation from the level M. The total intensity, I(M,N), of a particular transition M to N, in units of photons per second is:

$$I(M,N) = A(M,N)\ N_M \tag{4}$$

N_M is the number of atoms in level M. A summation of Eq. (4) over all lower levels N results in the following equation, with the use of Eq. (3).

$$A(M,N) = \frac{I(M,N)}{\Sigma_N I(M,N)} \quad \frac{1}{\tau_M} \tag{5}$$

The absorption oscillator strength, f(N,M), of a transition from N to M may be described in terms of either the transition probability or the line strength.

$$f(N,M) = \frac{2J_M + 1}{2J_N + 1} \quad \frac{mc^3}{8\pi^2 e^2\ \nu^2(M,N)}\ A(M,N) \tag{6}$$

or

$$f(N,M) = \frac{8\pi^2 m}{3he^2}\ \frac{\nu(M,N)}{(2J_N + 1)}\ S(M,N) \tag{7}$$

m and e denote the mass and charge of the electron, respectively. The relations embodied in the equations in this section may be used with no

difficulty for molecular electronic transitions if Λ (the projection of the total electron orbital angular momentum on the internuclear axis) and S (the total electron spin) does not change. If Λ is zero for one transition and not zero for another transition, all of the factors (2J + 1) relating to the Λ non-zero level must be multiplied by 2. This statement assumes that S(M,N) is summed over both possible orientations of Λ. The most important use of this factor of 2 is in Eq. (6) which relates the two measurable quantities f(N,M) and A(M,N).

Lifetimes of Rotational and Vibrational Levels of Diatomic Molecules

Molecular transition factors are usually described with different notation. To properly define the necessary notation, the quantum mechanical description of the diatomic molecule will be briefly considered. In the Born-Oppenheimer approximation to the diatomic molecule, the wave function, $\gamma_{evK\Lambda M}$, of a given state is separable into three functions.

$$\gamma_{evK\Lambda M} = \gamma_e(\bar{r}_e, R)\ \frac{1}{R}\gamma_v(R)\ \gamma_{K\Lambda M}(\theta,\phi) \tag{8}$$

γ_e is the electronic wave function which depends on the coordinates of the electrons, $\bar{r}_e$, with respect to the molecular fixed axis and on the distance, R, of separation of the two nuclei. The angle variables (θ,ϕ) reference the molecular fixed coordinates to space fixed coordinates. The quantum number Λ describes the projection of the electron angular momentum along the internuclear axis. $\frac{\gamma_v(R)}{R}$ is the vibrational wave function and $\gamma_{K\Lambda M}(\theta,\phi)$ is the rotational wave function. The Schroedinger wave equation is approx-

imately separable with the use of Eq. (8) for Hund's coupling cases a and b.[12]

The separated rotational wave equation may be further simplified with the following definition.

$$\gamma_{K\Lambda M} = F(\theta)\, e^{iM\phi}$$

The rotational wave equation as expressed by Kronig[13] will yield the following expression.

$$\left[\frac{1}{\sin\theta}\frac{d}{d\theta}\left\{\sin\theta\frac{d}{d\theta}\right\} + \frac{1}{\sin^2\theta}\{-M^2 + 2M\Lambda\cos\theta - \Lambda^2\cos^2\theta\} - K\right]F = 0 \tag{9}$$

Define a new variable, x.

$$x = 1/2(1 - \cos\theta)$$

The variable substitution reduces Eq. (9) to:

$$\frac{d(x(1-x))}{dx}\frac{dF}{dx} + \left[K - \frac{(M + \Lambda(2x - 1))}{4x(1 - x)}\right]F = 0 \tag{10}$$

Eq. (10) now has the same form as the separated equation describing the symmetrical top which has been examined by Rademacker and Reiche.[14]

Similar to Eq. (1) for an electric dipole transition, the line strength, $S^{e'v'K'\Lambda'}_{e''v''K''\Lambda''}$, connecting one level with another, may be described as follows, valid to within the previous approximations.

$$S^{e'v'K'\Lambda'}_{e''v''K''\Lambda''} = S^{K'\Lambda'}_{K''\Lambda''}\left|\int\gamma_{v'}(R)\left\{\int\gamma_{e'}(\bar{r}_e,R)\,\bar{P}_e(\bar{r}_e)\,\gamma_{e''}(\bar{r}_e,R)\,dV_e\right\}\gamma_{v''}(R)\,dR\right|^2 \tag{11}$$

A sum over the upper and lower states of M' and M'' has already been performed. $\bar{P}_e$ is the electric dipole moment. $S^{K'\Lambda'}_{K''\Lambda''}$ are the Honl-London factors which are well tabulated for most common cases by Herzberg.[15] These Honl-London factors are obtained from the early work done on the symmetrical top, since the form of the Schroedinger equation for the symmetrical top is identical to Eq. (10). The squared term in Eq. (11) is referred to as the band strength and designated by $p^{e'e''}_{v'v''}$. Henceforth, the electronic designation on $p^{e'e''}_{v'v''}$ will be dropped as all the following discussion is to be applied to electronic transitions which have unique e' and e''. The inside integral in the band strength is the electronic transition component. If it is a slowly varying function of R, it may be removed from the integral over R. The electronic transition component is usually designated as R_e.

$$S^{e'v'K'\Lambda'}_{e''v''K''\Lambda''} = S^{K'\ \Lambda'}_{K''\ \Lambda''} \quad (\bar{R}_{v'v''})\ q_{v'v''}$$

$q_{v'v''}$ is the square of the vibrational overlap integral and is called the Franck-Condon Factor. $\bar{R}_{v'v''}$ is the R-centroid and is dependent on the particular v' to v'' transition.

For a transition from a rotation-vibration level in a given electronic state to a rotation-vibration level in another given electronic state, the transition probability, $A^{e'v'K'\Lambda'}_{e''v''K''\Lambda''}$, may be described with Eq. (11), similar to Eq. (2).

$$A^{e'v'K'\Lambda'}_{e''v''K''\Lambda''} = \frac{64\pi^4\nu^3(v'K':v''K'')}{3hc^3} \frac{S^{K'\Lambda'}_{K''\Lambda''}}{(2K'+1)} p_{v'v''} \qquad (12)$$

$\nu(v'\ K':v''K'')$ is the frequency of the emitted radiation due to the transi-

tion which is being considered.

A simple expression results if the transition probability from a given rotational (K') and vibrational (v') level is summed over all lower rotational (K") levels in a given lower vibrational (v") level.

$$\sum_{K''} A^{v'K'}_{v''K''} = \sum_{K''} \frac{64\pi^4}{3hc^3} \nu^3(v'\ K':v''K'') \frac{S^{K'}_{K''} p_{v'v''}}{(2K' + 1)} \tag{13}$$

The e',e", Λ' and Λ" notation has been dropped in Eq. (13) since it is assumed to be completely specified and unique in all that follows. The frequency of the transitions in a given band are nearly equal. Thus, the frequency term may be removed from the sum in Eq. (13) and still give approximately the correct results. The only terms then left in the sum which depends on K" are the Honl-London factors. It is easy to verify that, for all the Honl-London factors tabulated by Herzberg,[15] the following is correct.

$$\Sigma_{K''} S^{K'}_{K''} = (2K' + 1) \tag{14}$$

Eq. (13) may be written as follows, with the use of Eq. (14).

$$\Sigma_{K''} A^{v'K'}_{v''K''} = \frac{64\pi^4}{3hc^3} \nu^3(v',v'')\ p_{v'v''} \tag{15}$$

ν(v',v") is the frequency between the zero rotational levels. Eq. (15) then states that, to the approximations employed, the transition probabilities from all rotational levels of a given vibrational level to a given lower vibrational level are the same. Hence, the sum of the transition probabilities in Eq. (15) may be designated by only the vibrational levels, A(v',v"). The lifetime of the vibrational level may now be written simi-

larly to Eq. (3).

$$\tau_{v'} = [\Sigma_{v''} A(v',v'')]^{-1} = [\frac{64\pi^4}{3hc^3} \Sigma_{v''} \nu^3(v',v'') p_{v'v''}]^{-1} \quad (16)$$

Thus the theory predicts that the lifetimes of all the rotational levels are the same to within the approximations made.

The variation of the lifetime (due only to the ν^3 factor in Eq. (13)) with rotational level will now be determined for a particular vibrational level of the nitrogen molecule. The first negative system of nitrogen results from a $^2\Sigma \rightarrow {}^2\Sigma$ transition. The Honl-London factors (S_J^X) for this type of transition have been tabulated by Mulliken.[16]

$$S_J^{P1} = S_J^{R1} = \frac{J^2 - 1/4}{J}$$

$$S_J^{P2} = S_J^{R2} = \frac{J^2 - 1/4}{J} \quad (17)$$

$$S_J^{RQ21} = S_J^{PQ12} = \frac{2J - 1}{4J(J - 1)}$$

J is to be taken as the largest of the two values J' or J''. The two factors for both the R and P branch are due to the splitting of each rotational level into two levels by the electron spin interaction. J is now the quantum number for the combination of electron spin and nuclear rotation in Hund's Coupling case b and takes on the values K ± 1/2. The extra branches $^RQ_{21}$ and $^PQ_{12}$ are due to a change in J equal to zero transition where the change in K is still plus or minus one. The frequencies of the R_1 and R_2 branches are approximately equal for a given value of K. The same holds for P_1 and P_2. The frequencies of the transitions corresponding to the Honl-London factors $^RQ_{21}$ and $^PQ_{12}$ are approximately equal to the

frequencies corresponding to R_1 or R_2 and P_1 or P_2, respectively. If the equations in (17) are substituted into Eq. (13), the following approximate equation results.

$$\sum_{K''} A^{v'J'}_{v''J''} = \tag{18}$$

$$\frac{64\,\pi^4\,p_{v'v''}}{3hc^3\,(2K'+1)} \left\{\nu_P^3(v'J':v''J'')\left(\frac{(J'+1)^2-1/4}{(J'+1)}\right) + \nu_R^3(v'J':v''J'')\left(\frac{J'^2-1/4}{J'}\right) + \nu_Q^3(v'J':v''J'')\left(\frac{2J'+1}{4J'(J'+1)}\right)\right\}$$

The sum in Eq. (18) is limited to three terms due to the selection rules for these transitions. The frequencies $\nu_P(v'J':v''J'')$ and $\nu_R(v'J':v''J'')$ are the frequencies of the P_1 or the P_2 and the R_1 or R_2 branches, respectively. The frenquency $\nu_Q(v'J':v''J'')$ is equal to $\nu_P(v'J':v''J'')$ or $\nu_R(v'J':v''J'')$ according to whether J' is K'+1/2 or K'-1/2, respectively. Notice that the coefficient on $\nu_Q(v'J':v''J'')$ approaches $(2J')^{-1}$ as J' becomes large while the coefficients of $\nu_P(v'J':v''J'')$ and $\nu_R(v'J':v''J'')$ approach J'. Thus for large J'levels, the Q terms become small.

For the J' levels which are equal to K'+1/2, the summed transition probability in Eq. (18) becomes:

$$\sum_{J''} A^{v'J'}_{v''J''} =$$

$$\frac{64\pi^4}{3hc^3}\,p_{v'v''}\left\{\nu_P^3(v'J':v''J'')\,\frac{K'+1}{2K'+1} + \nu_R^3(v'J':v''J'')\,\frac{K'}{2K'+1}\right\} \tag{19}$$

Eq. (19) is also correct for the J' levels which are equal to K'-1/2. The summed transition probability in Eq. (19) has a form identical to the summed transition probability of a $^1\Sigma \rightarrow {}^1\Sigma$ transition. This is

exactly as is to be expected since the interaction of the electron spin and nuclear rotation was not included in the approximation used to derive Eq. (19). Since both J' levels of a given K' level have the same transition probabilities, the J' notation of Eq. (19) will be changed to K'.

$$\sum_{J''} A^{v'J'}_{v''J''} \quad \rightarrow \quad \sum_{K''} A^{v'K'}_{v''K''}$$

Let R(v',v'',K') be the ratio of this summed transition probability of an arbitrary level to that of the K'=0 level.

$$R(v',v'',K') = \frac{\sum_{K''} A^{v'K'}_{v''K''}}{\sum_{K''} A^{v'0}_{v''K''}} = \frac{\nu_P^3(v'K':v''K'')\ (K'+1) + \nu_R^3(v'K':v''K'')\ K'}{\nu_P^3(v'0:v''1)\ (2K'+1)} \tag{20}$$

Table 1 gives this ratio, as calculated for the two bands, B $^2\Sigma_u^+(v'=0) \rightarrow X\ ^2\Sigma_g^+(v'=0)$ and B $^2\Sigma_u^+(v'=0) \rightarrow X\ ^2\Sigma_g^+(v'=1)$ of the nitrogen molecular ion. The frequencies used were taken from the measurements of Childs.[17] $\bar{R}(K')$ in Table 1 is the average of the other two R ratios listed.

The lifetimes of the v' and K' levels may now be expressed with the frequency corrected transition probabilities of Eq. (19).

$$\tau_{v',K'} = \{ \sum_{v''} \sum_{K''} A^{v'K'}_{v''K''} \}^{-1} \tag{21}$$

$$= \{\frac{64\pi^4}{3hc^3} \sum_{v''} P_{v'v''} \frac{\nu_P^3(v'K':v''K'')(K'+1) + \nu_R^3(v'K':v''K'')\ K'}{(2K'+1)} \}^{-1}$$

With the use of the ratios defined in Eq. (20), a lifetime ratio may be

Table 1. Theoretical Ratios of Transition Probabilities (R) and Theoretical Ratios of Lifetimes (Z) of the Rotational Levels of the $B^2\Sigma_u^+(v' = 0)$ Level Due Only to the Frequency Terms.

K'	R(0,0,K')	R(0,1,K')	$\bar{R}(K')$	Z
0	1	1	1	1
1	1.000	1.000	1.000	1.000
3	1.000	1.000	1.000	1.000
5	1.001	1.001	1.001	0.999
7	1.001	1.001	1.001	0.999
9	1.002	1.002	1.002	0.998
11	1.002	1.003	1.002	0.998
13	1.003	1.004	1.003	0.997
15	1.004	1.005	1.004	0.996
17	1.005	1.007	1.006	0.994
19	1.007	1.008	1.007	0.993
21	1.007	1.010	1.008	0.992
23	1.010	1.012	1.011	0.989
25	1.012	1.014	1.013	0.987
27	1.014	1.016	1.015	0.985
29	1.016	1.019	1.017	0.983
31	1.018	1.022	1.020	0.980
33	1.020	1.024	1.022	0.978
35	1.023	1.028	1.025	0.976

formed.

$$\frac{\tau_{v',K'}}{\tau_{v',0}} = \frac{\sum_{v''} p_{v'v''} \nu_P^3(v'0:v''1)}{\sum_{v''} p_{v'v''} \nu_P^3(v'0:v''1)\ R(v',v'',K')} \tag{22}$$

$R(v',v'',K'')$ is approximately independent of v''. This approximation is very good for the first negative system of N_2^+ as is demonstrated in Table 1, since the two tabulated transitions constitute over 90% of the total radiation emitted from the $B^2\Sigma_u^+(v'=0)$ level. If $\bar{R}(K')$ is now substituted into Eq. (22) for $R(v',v'',K')$ and then factored from the sum, the lifetimes of the rotational levels of the zero vibrational level of $B^2\Sigma_u^+$ of N_2^+ can be expressed in terms of the zero rotational level.

$$\tau_{0,K'} = \frac{\tau_{0,0}}{\bar{R}(K')} = Z\ \tau_{0,0}$$

Z is also given in Table 1.

Time Dependence of Excited Particle Concentration

The parameter referred to as the lifetime of a given electronic state may be utilized to describe mathematically the density of excited particles after the excitation mechanism has ceased. If spontaneous emission is the only population or depopulation mechanism, the differential equation describing the rate of change of the density of excited particles, N*, is:

$$\frac{dN^*}{dt} = -\sum_j A_j\ N^* \tag{24}$$

A_j is the transition probability of a transition from the state of the N* particles to a lower state, j. Solution of Eq. (24) and use of the definition in Eq. (3) gives:

$$N^* = N_o^* e^{-t/\tau} \tag{25}$$

N_o^* is the density of the excited particles at time zero. More general population mechanisms are discussed by Holzberlein.[18]

The mathematical description of a particular case of depopulation mechanisms will now be considered for later use. Assume that the important population and depopulation mechanisms are spontaneous emission, volume collisional depopulation, and wall collisional depopulation due to diffusion. The mathematical analogue for these conditions is:

$$\frac{dN^*}{dt} = -AN^* - N_o \sigma v N^* + DV^2 N^* \tag{26}$$

A stands for the sum of all the transition probabilities from the excited level which N* occupies, N_o is the density of particles in the ground state, σ is the cross section for the volume collisional depopulation of the excited level which N* occupies, v is the velocity of the collision, D is the diffusion coefficient for the nitrogen molecule and ∇^2 is the Laplacian operator. Inherent in Eq. (26) is the assumption that all excited particles, N*, which contact the wall of the invertron are depopulated without the emission of a photon which the excited particle characteristically emits in free space.

Since the results of this analysis will be applied to the invertron, the Laplacian operator of Eq. (26) is best expressed in cylindrical coordinates. The immediately simplifying assumption of no angular or axial dependence of the excited particle density will be made. The lack of

axial dependence is a reasonable assumption since the invertron excitation region has a ten to one length (ℓ) to radius (a) ratio. Eq. (26) is now separable by expressing N* as follows.

$$N^* = R(r)\ T(t) \tag{27}$$

R(r) is an assumed function of the radius, r, and T(t) is an assumed function of time, t, only. Substitution of Eq. (27) into Eq. (26) and utilization of $(-p^2)$ as the separation constant leads to the following equations.

$$\frac{dT}{dt} = -(p^2 + A + N_o\sigma v)T \tag{28}$$

$$r^2 \frac{d^2R}{dr^2} + r \frac{dR}{dr} + \frac{p^2r^2}{D} R = 0 \tag{29}$$

Solution of Eq. (28) and (29) yields the following result, after the requirement of finiteness is imposed on the solution.

$$N^* = C \exp(-p^2 - A - N_o\sigma v)t \quad J_o \left\{\frac{p\ r}{\sqrt{D}}\right\} \tag{30}$$

J_o is the zero order Bessel function. Let the boundary conditions be as follows.

$$t = 0 \qquad \begin{cases} N^* = N_o^* & r < a \\ N^* = 0 & r > a \end{cases} \tag{31}$$

This leads to the general solution:

$$N^* = N_o^* \sum_{n=1}^{\infty} \exp\left\{\left(\frac{-\alpha_n^2\ D}{a^2} - A - N_o\sigma v\right)t\right\} \frac{2J_o[\alpha_n \frac{r}{a}]}{\alpha_n\ J_1[\alpha_n]} \tag{32}$$

The α_n's are zero roots of J_o and a is the radius of the invertron. The time dependency of the total emitted light, I(t), for a given

transition may be expressed now by integrating N* from Eq. (32) over the volume of the invertron. The result of such an integration is:

$$I(t) = 4\pi a^2 N_o^* \ell A^* \sum_{n=1}^{\infty} \frac{e^{-\bar{A}_n t}}{\alpha_n^2} \tag{33}$$

A* is the transition probability for the particular transition under study and the effective transition probability, $\bar{A}$, is defined as follows.

$$\bar{A}_n = A + N_o \sigma v + \frac{\alpha_n^2 D}{a^2} \tag{34}$$

The third term on the right hand side of Eq. (34) can be evaluated with the use of the measured diffusion coefficients of Winter[19] and of Winn.[20] For the use of this analysis, D is expressed in terms of the concentration of the neutral particles at the temperature of the gas in the invertron.

$$D = \frac{9.2 \times 10^{18}}{N_o} \tag{35}$$

N_o has units of particles per cubic centimeter. The first (n = 1) exponential term in Eq. (33) can now be expressed with Eq. (34) and (35).

$$\bar{A} = A + N_o \sigma v + \frac{0.52}{N_o} \tag{36}$$

The subscript on $\bar{A}$ has been dropped. N_o is now expressed in units of 10^{15} particles per cubic centimeter and the values of the radius of the invertron (a) and the first zero root of J_o is used in Eq. (36). $N_o \sigma v$ is often referred to as the collision frequency.

An interesting and useful series can be obtained from Eq. (33). At zero time, the intensity is known independent of Eq. (33) and can be expressed as follows.

$$I(t = 0) = (\pi a^2)\ \ell\ A^* N^*_o \tag{37}$$

Eq. (33) also expresses the intensity of radiation at time zero.

$$I(t = 0) = (4)\ (\pi a^2)\ \ell\ A^*N^*_o \sum_{n=1}^{\infty} \left(\frac{1}{\alpha_n{}^2}\right) \tag{38}$$

Equating (37) and (38) then yields the following infinite series.

$$1/4 = \sum_{n=1}^{\infty} \left(\frac{1}{\alpha_n{}^2}\right) \tag{39}$$

The fraction (f) of the intensity due only to the first term in the series of Eq. (33) can now be determined for t equal zero.

$$f = \left(\frac{4}{\alpha_n{}^2}\right) = 0.7 \tag{40}$$

Thus the first term of the series (hereafter referred to as the first mode) contributes most of the total intensity.

Another factor contributes to the dominance of the first mode. The higher modes decay more rapidly than the first mode. For example, in Eq. (33), the first term of the exponential in the sum includes $\alpha_n{}^2$. The ratio of the equivalent lifetimes of this term for the second mode to the first mode is greater than five to one. The initial boundary conditions used in Eq. (32) assumed a constant concentration. Due to the faster decay of the higher modes, the correct boundary conditions would have a functional dependency of N^*_o on r which decreased with increasing r. This would have the effect of weighting the zero mode even more than Eq. (40) implies.

Time Dependency of Decay Curve for Multiple Photoelectron Distortion

The time dependency of the decay curve, when Timing and Detection

System III: Delayed Coincidence is used, is a function of the average number of photoelectrons per excitation pulse to the invertron. This time dependency can be derived in analytic form in the following way.

Assume that P_c is the probability that a photon emitted in the invertron will create a photoelectron in the photomultiplier after passage through the monochromator. Let A be the reciprocal of the lifetime of a certain state, and let A' be the transition probability for decay of that same state to produce a photon whose wavelength is under observation. Let N be the initial number of excited atoms of the same particular state. From time t to t + dt, the probability, dP, that an excited atom will produce a photoelectron and that this is the first photoelectron produced for a given pulse to the invertron may be described as:

$$dP = P_e P_c P_f dP_d \tag{41}$$

P_e is the probability that a particular atom exists at time t, dP_d is the probability that this atom decays into the observed mode during t to t + dt, P_f is the probability that all other atoms have failed by time t, and P_c is as previously defined. Each of the separate probabilities will be considered. First, P_f will be obtained.

Note that the probability that no other photoelectron has been created by time t is equal to the probability that all other particles in the particular excited level have failed to create a photoelectron by time t. To find this probability of failure of all other atoms, consider the probability of success, P_s, for a given excited atom by a time t.

$$P_s = [1 - \exp(-At)]P_c \tag{42}$$

Now the probability of failure of a given excited atom is:

$$(1 - P_s) = \{1 - P_c[1 - \exp(-At)]\}$$

The probability of failure of all atoms other than the one for which Eq. (41) was written is P_f and may be written as:

$$\begin{aligned} P_f &= \{1 - P_c[1 - \exp(-At)]\}^{N-1} \\ &= 1 - (N - 1)[1 - \exp(-At)]P_c - \frac{(N-1)(N-2)}{2!}P_c^2[1 - \exp(-At)]^2 \\ &\quad + \ldots . \\ &\approx \sum_{n=0}^{\infty} \frac{(NP_c)^n [1 - \exp(-At)]^n (-1)^n}{n!} \end{aligned} \tag{43}$$

The validity of the last approximation is based upon the fact that

$$\frac{(NP_c)^n}{n} \ll 1 \qquad n = \text{integer}$$

is correct for much smaller values of n than is the expression,

$$(N - n) \ll N$$

Now define:

$$NP_c = M \tag{44}$$

M is the average number of photoelectrons produced per excitation pulse.

The combination of Eq. (43) and (44) gives:

$$P_f = \sum_{n=0}^{\infty} \frac{(-1)^n M^n [1 - \exp(-At)]^n}{n} = \exp\{-M[1 - \exp(-At)]\} \tag{45}$$

The other terms in Eq. (41) are well known.

$$P_e = \exp(-At) \tag{46}$$

$$dP_d = A' \, dt \tag{47}$$

Insertion of the values from Eq. (45), (46) and (47) into Eq. (41) gives:

$$dP = A' \exp(-At) P_c \exp\{-M[1-\exp(-At)]\} \, dt$$

Now the intensity, I', of the observed radiation is:

$$I' = \frac{NdP}{dt} = NA'P_c \exp(-At) \exp\{-M[1 - \exp(-At)]\}$$

The time dependent part, I(t), is the part of interest.

$$I(t) = \exp(-At) \exp\{-M[1 - \exp(-At)]\} \tag{48}$$

An interesting demonstration, which lends credibility to the results of Eq. (48), is to show the relation of Eq. (48) to a Poisson distribution. The justification for applying a Poisson distribution is the same as the justification used to obtain the approximation in Eq. (43). To show the relation, consider the average number of photoelectrons not counted using a Poisson distribution. When zero or one photoelectrons occur for an invertron pulse, no photoelectrons are lost, *ie* all are counted. When x photoelectrons occur for an invertron pulse, x minus one photoelectrons are not counted. Poisson statistics then gives the average number of photoelectrons lost per pulse as:

$$\sum_{x=2}^{\infty} \frac{\exp(-M) \, M^x (x-1)}{x!} = M \sum_{x'=1}^{\infty} \frac{\exp(-M) M^{x'}}{x'!} - \sum_{x=2}^{\infty} \frac{\exp(-M) M^x}{x!} \tag{49}$$

Now the fraction of photoelectrons lost per pulse, F_L, is given by dividing

Eq. (49) by the average number of photoelectrons per pulse.

$$F_L = \sum_{x'=1}^{\infty} \frac{\exp(-M)M^{x'}}{x'!} - \frac{1}{M} \sum_{x=2}^{\infty} \frac{e^{-x}M^x}{x!} \tag{50}$$

The fraction of photoelectrons lost may also be calculated from the time dependent function, Eq. (48). The best way to do this is to calculate the fraction not lost, F_n.

$$F_n = \frac{\int_o^{\infty} I(t)dt}{\int_o^{\infty} e^{-At}dt} \tag{51}$$

The denominator in Eq. (51) expresses the total number of photoelectrons that occur. A constant multiplier has been omitted in both denominator and numerator. Eq. (51) may be easily integrated to give:

$$F_n = \frac{[1 - \exp(-M)]}{M}$$

The fraction lost then becomes:

$$F_L = 1 - F_n = 1 - \frac{[1 - \exp(-M)]}{M} \tag{52}$$

It can be shown that Eq. (50) and Eq. (52) are equivalent by multiplying Eq. (52) by exp(M).

$$\exp(M)F_L = \exp(M) - \frac{\exp(M)}{M} + \frac{1}{M} \tag{53}$$

Eq. (53) can be expanded using the normal infinite series expansion for exp(M). After the similar terms are cancelled, Eq. (53) becomes identical to Eq. (50) after multiplying, as correction, Eq. (53) by exp(-M) after the series expansion and cancellation.

To demonstrate the distortion of the true time dependency as compared

to the observed time dependency of the decay curve, for values of M not small, the distorted curve is plotted in Figure 1 for two values of M (1 and 0.3) along with the true curve, exp(-At), which is the same as M equal zero.

In practice, M cannot be measured directly since a measurement of the number of counts will miss the fraction lost. However, Eq. (52) can be manipulated to yield M from the ratio of the measured counts (CM) to the total number of possible counts (CP). From Eq. (52),

$$F_L = 1 - \frac{1}{M}[1 - \exp(-M)] = \frac{CT - CM}{CT} \tag{54}$$

CT is the true number of counts. In addition,

$$M = \frac{CT}{CP} \tag{55}$$

Eq. (54) and (55) contain two unknowns, M and CT, each of which are uniquely determinable. The determination of M from Eq. (54) and Eq. (55) follows.

$$M = -\ln[1 - (\frac{CM}{CP})] \tag{56}$$

For small values of $\frac{CM}{CP}$, M may be approximated as follows.

$$M = (\frac{CM}{CP}) + \frac{(\frac{CM}{CP})^2}{2} + \frac{(\frac{CM}{CP})^3}{3} \tag{57}$$

For $(\frac{CM}{CP})$ less than 0.1, M may be taken to be equal to $(\frac{CM}{CP})$ with less than 1% error in the results. For values of $(\frac{CM}{CP})$ larger than 0.1, Eq. (56) should be used to determine M. Failure to make this correction will result in underestimates of the decay time.

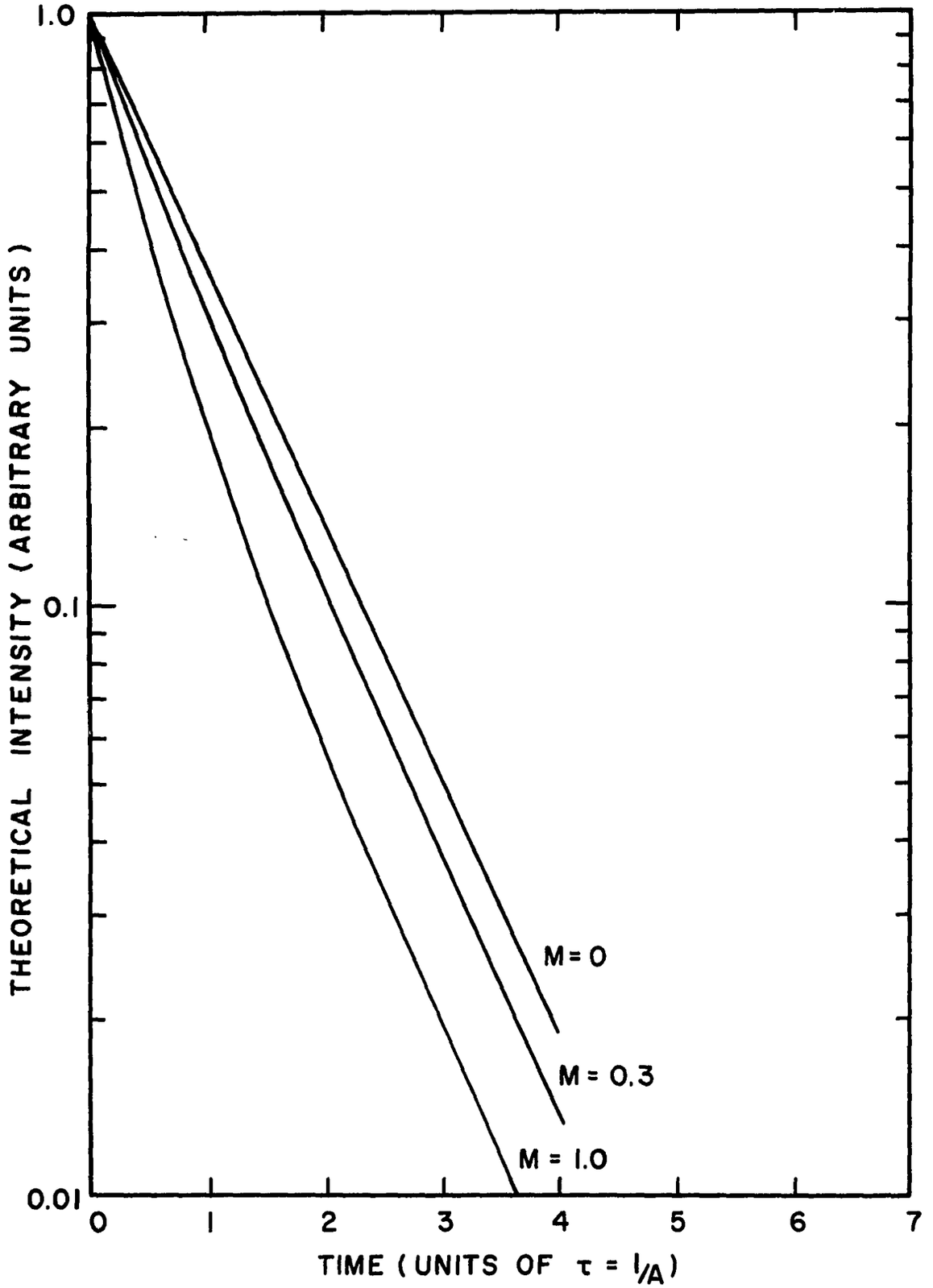

Figure 1. Theoretical Distortion of Decay Curve.

CHAPTER III

EXPERIMENTAL APPARATUS

Introduction

The equipment used in this experiment can be divided into three general categories:

1) Invertron and associated vacuum system

2) Monochromator and photomultiplier

3) Electronic equipment.

The invertron was an electron gun of a special design used to create atoms and molecules in excited states. The associated vacuum system was used to maximize purity of the gas and to produce sufficiently low pressure for the proper operation of the invertron. The monochromator was used to select the proper wavelength emitted by the excited atom or molecule which was characteristic of a desired excited state. The photomultiplier was used to detect the emitted radiation. The electronic equipment was used for two purposes. The first electronic equipment group was used to produce the excitation pulse which was applied to the invertron for electron acceleration. The second group of electronic equipment was used to detect the photomultiplier output and display it in some observable manner.

Figure 2 is a photograph of some of the experimental equipment.

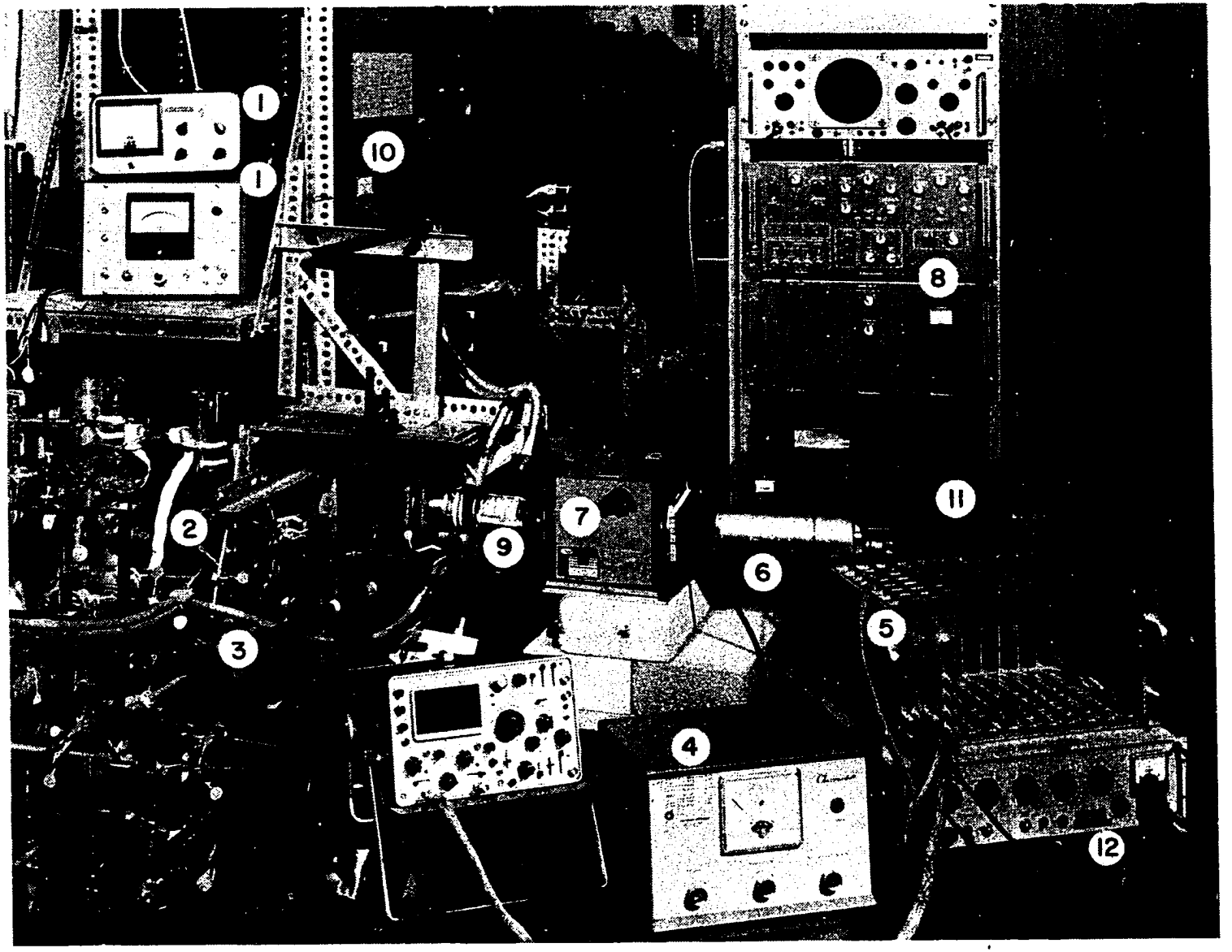

Figure 2. Experimental Apparatus.

NUMBER IDENTIFICATION OF EXPERIMENTAL APPARATUS

(Figure 2)

1. Vacuum Gauge
2. Vacuum System
3. Excitation Cable
4. Rate Meter
5. Time-to-Pulse Height Converter
6. Photomultiplier
7. Monochromator
8. Multichannel Analyzer
9. Invertron Surrounded by Heating Coils
10. Induction Heater
11. Printer
12. Photomultiplier Power Supply

Invertron and Associated Vacuum System

The invertron was originally developed by Holzberlein.[21] The invertron used in this experiment has been only slightly modified. Figure 3 is an illustration of the modified invertron. The cathode of the invertron was a nickel cylinder about 10 centimeter long and 1 centimeter radius. A barium oxide coating was used to increase the electron emission from the surface of the cathode which was heated with an induction heater. The grid structure was located inside the cathode. (Thus, the name, invertron, is due to the inverted nature of the electron gun from usual ones of cylindrical shape.) For the work reported in this paper, only one of the grids shown in Fig. 3 was used.

The grid structure was a tantalum mesh or tantalum rods supported by the cylindrical tantalum supports. The main body of the device was machined from stainless steel. The lucite or teflon spacers (both were used) insured electrical insulation of the grid bases and the cathode base. Viton A O-rings were used for vacuum sealing of the parts. The quartz window allowed optical viewing of the excitation zone. Not shown in the figure is a masonite support epoxied to the cathode base for the main support of the device. Also not shown is a doughnut shaped, aluminum disc used to hold in place the O-ring which sealed the quartz envelope to the cathode base.

The operation of the invertron when the excitation pulse is applied to the grid has been analyzed by Russell.[22] The application of the excitation voltage is not followed immediately by the complete, radial penetration of the electrons into the excitation zone. Only after a sufficient ion density has built up in the middle of the device to reduce the

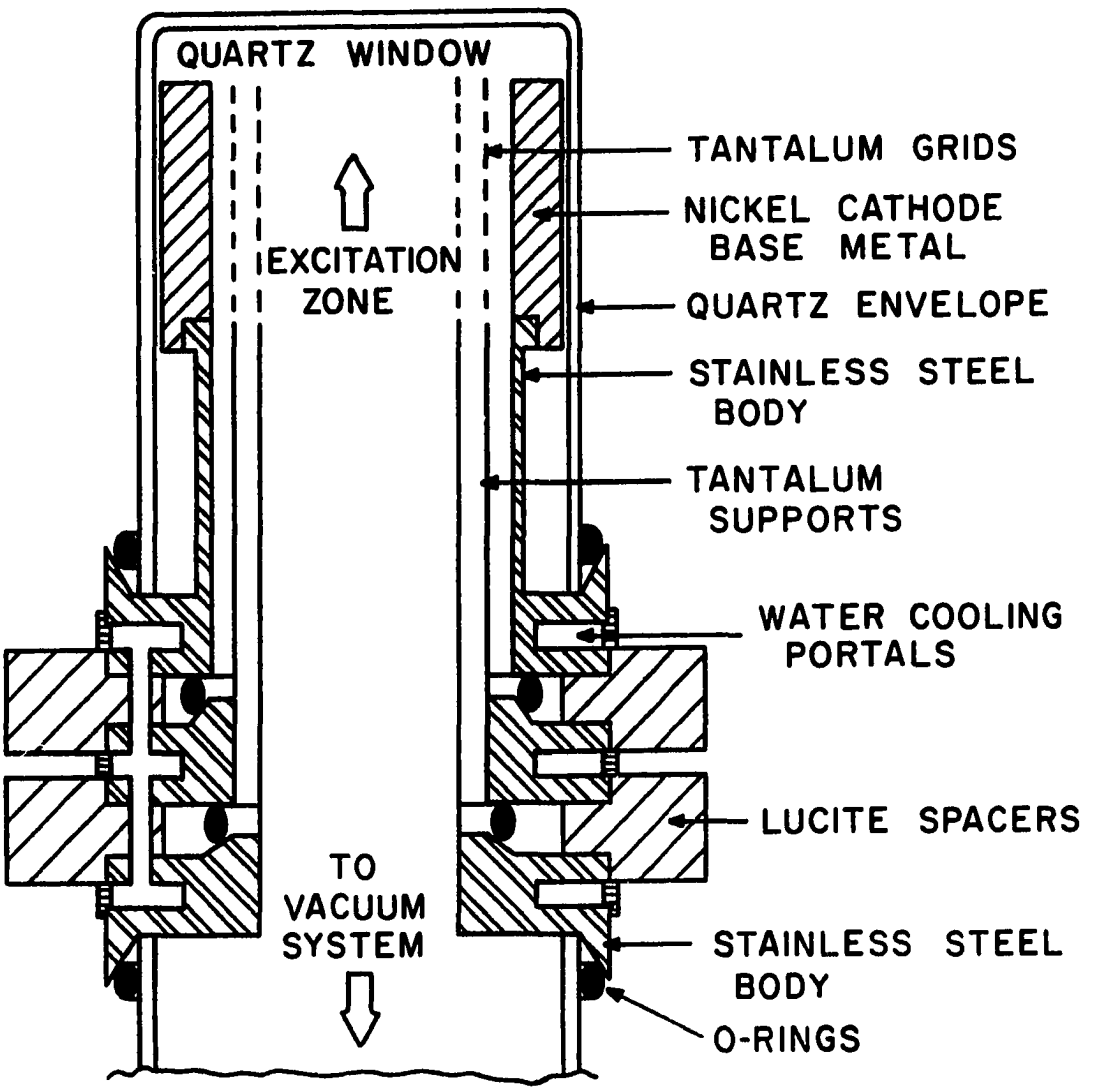

Figure 3. Cross Section of Invertron.

space charge does the electron current flow along a diameter into and out of the central region. However, with the use of a preionization pulse, immediate penetration of the electrons can be effected.

The vacuum system, which was used with the invertron for the measurements made in the quartz transparent wavelength region, was composed of a mercury diffusion pump, a mechanical backing pump, a mercury McLeod gauge, an ionization gauge, a thermocouple gauge, a dosing system for the gases, and assorted glass connections and glass valves. A base pressure of less than 10^{-6} Torr was attainable with the vacuum system. The leak rate of the system, when closed off from the pumps, was less than 10^{-3} Torr per seven days.

The invertron vacuum system used on the vacuum ultraviolet spectrograph differed from the previously described one as follows. An oil diffusion pump instead of a mercury diffusion pump was used. A palladium thimble for admitting hydrogen was connected to the vacuum system. Nitrogen was admitted into the vacuum system from a tank of research grade gas obtained from Matheson. The nitrogen continually flowed through the system and was admitted through coils cooled to liquid nitrogen temperatures. The base pressure attainable was less than 10^{-6} Torr. With the nitrogen tank closed off, the leak rate was less than 10^{-3} Torr per hour.

Monochromators and Photomultiplier Tube

A ¼-meter and a ½-meter Jarrell-Ash monochromators were used for the wavelength resolution of the visible and near visible radiation. The ½-meter Ebert mounting monochromator was used exclusively for the rotational studies. Drive mechanisms were already available or were built to allow

the scanning of a spectrum.

The vacuum ultraviolet monochromator was designed and built by the University of Oklahoma staff. Robertson[23] did the original focusing of the instrument. A 1200 lines per millimeter grating was inserted after the original focusing. The refocused instrument had a resolution of less than 5Å between 1100 to 1500Å. Although the instrument was capable of better focusing than was attained, the resolution was sufficient for this experiment. This vacuum monochromator was operated at a base pressure of 2×10^{-7} Torr.

Photomultipliers were used with all the monochromators to detect the radiation. An EMI 9558 tube was used for the red and infrared studies of the nitrogen molecule. This tube has a venetian blind dynode chain and consequently is a relatively slow tube ($\simeq$10 nanoseconds.) Since the lifetimes which were measured with the use of this photomultiplier tube were greater than 1 microsecond, there was negligible effect on the measured lifetimes due to the photomultiplier response time. An RCA 8575 photomultiplier tube was used for all the other measurements. The fall time of this tube is between 1 and 2 nanoseconds. The output signal is fed from the inside of the tube to the outside connections via a 50 ohms line. Since the photoelectron pulses were detected by zero-level crossing of the signal, the resolution time of the tube was much less than one nanosecond. Thus, the time of the device had negligible effect on the measured lifetimes of forty nanoseconds or greater.

A scintillator was used for conversion of the vacuum ultraviolet radiation into a wavelength which would pass through the face of the

photomultiplier tube. Both p-terphenyl and p-quaterphenyl were used successfully. Benzene solutions were sprayed onto the vacuum side of a quartz window. The p-terphenyl had the higher photon conversion ratio. A plastic scintillator was also used. The trade name was Pilot B, manufactured by Pilot Chemicals, Inc. Although the conversion ratio of the plastic scintillator was not as large as the p-terphenyl, the ease of use made this scintillator highly desirable. The plastic scintillator was machined to be the window in the vacuum system, thus eliminating the use of a quartz disc. The main advantage of the plastic scintillator was that it did not noticeably evaporate, while the other scintillators lasted only from one to two days.

Electronic Equipment

To produce the excited electronic levels of the molecules, a positive voltage was applied to the grid of the invertron. The resulting electron current then excited tha gas. To measure the lifetime of an excited level, the source of excitation must terminate, thus allowing the excited level to decay with its characteristic lifetime. The termination of excitation was effected with two devices. One device was a terminated coaxial cable which automatically turns off. The other device was a mercury switch used as a shunt across the invertron after a positive voltage had been applied. These pulse generating devices are described below.

The time dependency of the radiation emitted from the excited gas was monitored with three devices which are categorized by these titles: (1) Direct Observation; (2) Sampling Scope; and (3) Delayed Coincidence.

These devices are described below in the sections titled, Detection and Timing Device. Decay constants were then obtained from the time dependent intensity as measured with the detection and timing devices.

Some auxillary electronic equipment necessary for the lifetime measurements reported herein are also described below.

Pulse Generating Device I: Coaxial Cable

A charged coaxial cable was used to generate the voltage pulse to drive the invertron. When a coaxial cable is charged to a given voltage and then switched across its characteristic impedance, a square pulse is generated of amplitude one-half the original charged value, and of width twice the length of the cable where one foot length is taken equal to one nanosecond length, approximately. A gas thyratron (2D21) was used as the switch across the 50 ohm cable. Hereafter, this device will be referred to as the Square Wave Generator. (See Appendix) The center of the coaxial cable was connected to a power supply (0 to 4000 volts) via a resistor. This resistor must be connected directly to the center conductor with short leads so the reflected wave in the cable will see essentially an open circuit. To ensure this, the resistor must be much larger than the characteristic impedance of the cable.

The cable was usually charged to between 1500 and 2000 volts. When voltages of this magnitude were applied to a selected 2D21, the rise time of conduction of the 2D21 was less than one nanosecond; consequently, the rise time of the excitation voltage applied to the invertron was less than one nanosecond. The fall time of this square wave was determined by the length of the cable; that is, the width of the pulse. Since the

invertron required a time greater than 100 nanoseconds to start at pressures of less than 0.01 Torr, a basic limitation of cut-off times was encountered when the real coaxial cable was used, although even a one microsecond wide pulse generated by a real cable showed a cut-off time which was small compared to a 10 nanosecond lifetime. In order to measure lifetimes which are about one nanosecond, a second pulse generating device was developed.

Pulse Generating Device II: Mercury Switch and Pulse Forming Network

Mercury switches were observed to have a very fast turn on time (less than 0.3 nanoseconds) when applied as the switch across the real cable. Since the turn off time of the pulse is all important for lifetime measurements, little was to be gained by using the mercury switch as the start switch; however, a method was developed whereby the fast start of conduction of the relay was used to crowbar a pulse. In order to describe this method, a description of the Western Electric #218A switch will be given.

There are five external connections to the 218A mercury switch. The switching arm (pin 5) closes contacts 1 to 2 and 3 to 4, alternately, with a possible frequency range of 60 to 240 Hertz. The jitter time of the closing of pin 1 to 2 was about 100 microseconds at a frequency of 60 Hertz. It was accidentally noticed that the arm always touched pin 1 about 10 microseconds before pin 2, with a jitter time of about 0.5 microsecond in the 10 microseconds delay.

This observed operation of striking one pin before the other was

used in a system to take advantage of the fast switching capability of the mercury switch. The relay was driven from a Variac at 60 Hertz. When the switching arm touched pin 1, an adjustable delay circuit (Delayed Trigger Generator) was activated by the connection of pin 5 to ground via pin 1. The output from this delay circuit was used to trigger a 2D21 in a pulse forming network. The output of the pulse forming network was a pulse 8 microseconds wide and 500 to 1000 volts amplitude fed into about 50 ohms. (This circuit is described more in the Appendix.) A resistor divider chain determined the voltage which was then applied across the grid and cathode of the invertron. Pin 2 was connected to the grid of the invertron. Since the cathode was connected to ground, the switching arm, upon closing pin 1 to 2, acted as a shunt across the invertron. Thus, an excitation pulse of duration 1 to 8 microseconds could be applied to the invertron with a measured fall time of less than 0.3 nanosecond, the limit of the response time of available oscilloscopes.

Detection and Timing Device I: Direct Observation

When the excitation voltage to the invertron was turned off, the production of excited states by electron bombardment ceased. The excited states of the gas then began to decay. Those decaying by emission of a photon could be detected with a photomultiplier attached to the exit slit of a monochromator. The monochromator was, of course, used to separate the emitted radiation so that a particular excited level could be observed. All of the detection and timing systems utilized a photomultiplier and monochromator. They differed only in the

handling of the output from the photomultiplier.

With the Direct Observation, the output from the photomultiplier was fed directly into a Tektronix 555 oscilloscope with a real time sweep. An oscillogram of the resulting single trace on the CRT was made for later analysis.

Detection and Timing Device II: Sampling Scope

In this system the output of the photomultiplier was fed into a Tektronix 1S1 sampling unit and displayed on the CRT for photographing. The sampling unit had an internal gate which opened at prescribed intervals after a start signal was received. While the gate was open, the signal entering the unit was sampled. A dot was then displayed upon the CRT with the vertical displacement of the dot proportional to the sampled voltage and the horizontal displacement proportional to the time between the start signal and the opening of the gate. Another start signal began the operation over, with the gate opening at a prescribed later time. Thus, by repeating the process over and over, a facsimile of the entering signal was produced on the CRT, if the entering signal was repetitive. The resolution time of the sampling unit was 0.3 nanosecond as compared to about 4 nanoseconds maximum with the real time oscilloscopes.

In addition to the better resolution time, the sampling unit had the capability of improving the signal to noise ratio. The sampling unit stored a voltage which was proportional to the vertical displacement of the previously displaced dot. The next voltage sample was taken and compared to the stored voltage to obtain a difference voltage. A new voltage was obtained by dividing the difference voltage by z (the

smoothing factor) and adding to the sampled voltage. This new voltage then become the stored voltage and was displayed as a dot on the CRT.

Consideration must be given to the curve distortion when the smoothing control is used. To maintain the response time of the sampling unit, the dot density on the CRT must be increased when the smoothing factor is increased. A criteria for determination of dot density will now be developed.

Let β be the time between samples. This is a parameter related to the dot density, since the dot density (n) in units of dots per centimeter is equal to the sweep speed (S) in units of seconds per centimeters divided by β (in units of seconds).

$$n = \frac{S}{\beta} \tag{58}$$

Now assume that a negative step function is applied to the sampling unit when smoothing is being used. The effective decay time of the displayed signal will be longer than the zero decay time of the step function. Indeed, the first dot after the step will be intermediate between the peak before the step (A) and the bottom of the step (taken to be zero). By this first dot, a time β will have elapsed. At the second dot, a time 2β will have elapsed, and so forth. The amplitude (A_1) at the first dot position can be described as follows:

$$A_1 = \left(\frac{z - 1}{z}\right) \quad A$$

where z is the smoothing factor. By the second dot, the amplitude (A_2) will be reduced to:

$$A_2 = \left(\frac{z - 1}{z}\right)^2 A$$

In general,

$$A_n = A \left(\frac{z - 1}{z}\right)^{\frac{t}{\beta}} = A \left(\frac{z}{z - 1}\right)^{\frac{-t}{\beta}}$$

The envelope, f(t), of the dots can then be expressed in equivalent time.

$$f(t) = A \exp\left[-\left(\frac{t}{\beta}\right) \ln(y)\right]$$

The new parameter y is defined as follows.

$$y = \left(\frac{z}{z - 1}\right)$$

The minimum effective decay constant (K) is now determined.

$$K = \frac{\beta}{\ln(y)}$$

The maximum value of z is 3 for the 1S1 sampling unit. With this value, K becomes:

$$K = (2.5)\beta$$

The value of K determines the minimum lifetime (τ) which should be measured for a given dot density and sweep speed. This also gives the criteria for the necessary dot density. K should be less than one-tenth of τ. This then imposes on β the value:

$$= \left(\frac{0.1}{2.5}\right) (\tau) \qquad (59)$$

Combination of Eq. (58) and (59) then defines the necessary dot density

for the measurement of a given lifetime at a given sweep speed.

$$n = 25 \left(\frac{S}{\tau}\right)$$

For ease of determining the lifetime from the oscillogram, the factor S divided by τ should be about 1. Thus, the dot density should be maintained at more than 25 per centimeter.

Detection and Timing Device III: Delayed Coincidence

The two previously described detection and timing devices measured the envelope of the photoelectrons originating in the photomultiplier tube as a result of the emitted photons from the excited states under examination. (A complete description of this smoothing of discrete events is given by Holzberlein.[18]) Since the decay of excited states is a discrete occurence, a measuring system which utilizes this fact might be capable of measuring weaker light levels. Such was found to be the case. The delayed coincidence system, which operates on single photoelectron signals from the photomultiplier, was found to be capable of detecting lower light levels as well as measuring lifetimes of shorter duration than the other two systems. At the same time, when light levels are large enough and lifetimes long enough, the other two systems have certain advantages. Criteria for determining which system to use for a particular case will be discussed in more detail later.

The operation of the delayed coincidence system depended upon the measurement of the time between the occurence of two events: the cessation of electron excitation in the invertron and the production of a photoelectron in the photomultiplier tube. This measurement was per-

formed with a time to pulse height converter (Ortec model 437) and a pulse height analyzer. A start signal for the time to pulse height converter (TPHC) was derived by the differentiation of a small portion of the applied voltage to the invertron. A single, amplified photoelectron signal from a photomultiplier tube was used to generate the stop signal for the TPHC. A gate was applied to the TPHC in the coincidence mode to assure that a start signal could activate the TPHC only during the cutoff time of the excitation voltage applied to the invertron.

A brief discussion of the circuits used to develop the start pulse, the stop pulse and the gate pulse will now be presented. A detailed description of the circuits is given in the Appendix.

The start pulse for the TPHC was obtained with a simple differentiation of the invertron signal. Upon differentiation of this signal, a positive and a negative pulse were obtained. The negative pulse, which coincided with the cessation of the invertron excitation, was used as the start pulse to the TPHC. The width of the pulse was approximately equal to the product of capacitance and the total resistance in the circuit. This value was kept at about 0.1 nanosecond.

The stop pulse was obtained with two techniques. One technique utilized an Ortec Time Pickoff Control (TPC) and an Ortec Photomultiplier Timing Discriminator and Preamplifier (PTDP). The TPC controlled the bias level of the PTDP, which controlled the minimum necessary pulse signal from the photomultiplier required to trigger the PTDP. The pulse from the photomultiplier (the photomultiplier pulse has approximately a gaussian shape) was differentiated by the PTDP. The zero crossing point of this differentiated signal was used as the timing reference. Although

the pulse width and height from the photomultiplier fluctuates considerably, the jitter in the zero crossing point is less than 100 picoseconds as referenced to the time of production of a photoelectron. The output from the PTDP was a negative-going logic pulse; *ie*, a negative pulse of constant height and shape. This pulse was then applied to the TPHC via a terminated 50 ohm cable.

The envelope of the photomultiplier output, as was used in Detection and Timing Device I and II with high intensity light levels, has a minimum resolution time equal to the fall time of a photoelectron pulse.[18] For photomultiplier tubes, the fall times range from about two to 10 nanoseconds, which is about the minimum time resolution achievable when the light envelope is used. However, the minimum time resolution of the delayed coincidence system is limited by the jitter time of the zero crossing point. For this reason the delayed coincidence system has the capability of measuring shorter lifetimes. In addition, since it operates on a single photoelectron pulse, it is inherently more sensitive than the other two techniques.

The second device used to obtain the stop pulse was a Logic Pulse Generator (LPG). A tunnel diode was biased below its transition point. See Appendix for a more complete discussion.) The output pulse from the photomultiplier which had resulted from a single photoelectron was used to trigger the tunnel diode to its transition point. The resultant transition cycle of the tunnel diode produced a logic pulse which in turn was applied as a stop pulse to the TPHC. The minimum resolution time of this type circuit is less than the rise time of the photomultiplier pulse which in turn is less than the fall time of a photomultiplier pulse.

Thus the minimum resolution time, though probably not as good as that obtained from a zero level crossing circuit, is far superior to the envelope resolution time.

A single-photoelectron detection system has an additional advantage over the envelope type detection system. Noise which originates from any element in the photomultiplier can be discriminated against by adjustment of the bias level. Thus, the signal to noise ratio is improved.

The gate applied to the TPHC was generated with a Gate Pulse Generator (GPG). The GPG was triggered either by the Delayed Triggered Generator or the Timer. (For a discussion of the GPG, DTG and Timer, see the Appendix.) By appropriate adjustment of the timing sequences, the output of the GPG was brought into coincidence with the stop pulse derived from the Trigger Differentiator. The critical requirement was to assure that the gate did not coincide with the initiation of the exciation pulse to the invertron, since there was usually a negative component of the differentiated signal at this point.

A peculiarity of the TPHC will now be described. The specifications of the Ortec TPHC claimed that no negative pulse could trigger the circuit when operated in the coincidence mode except during the time that a gate was applied to the gate input. This is correct unless the negative pulse is immediately preceded by a positive pulse. When a large positive pulse precedes a negative pulse, the TPHC can be activated even if a gate is not applied in the coincidence mode. In applying the differentiated signal of the invertron excitation pulse, extreme care must be taken to assure that this does not occur. The only

way that was found to minimize this difficulty was to suppress the positive pulse as much as possible by setting the amplitude of the differentiated signal at a level where the negative pulse coinciding with the cessation of the invertron signal was barely of sufficient amplitude (approximately 0.25 volts) to trigger the start of the TPHC. Since this amplitude is dependent on the size and shape of the invertron excitation pulse, the adjustment of the Trigger Differentiator must be made each time the TPHC is to be used.

The output of the TPHC was a pulse of amplitude proportional to the time between the applied start and stop signals. This pulse was fed to a Pulse Height Analyzer (PHA). Each pulse was then recorded as a single event in a channel of the PHA determined by the height of the pulse from the TPHC. By many repetitions of the above described sequence, a signal was accumulated in the PHA. This signal decayed with an exponential factor identical to the exponential factor of decay of the envelope of the many-photon signal emitted after a single excitation pulse to the invertron observed for high radiation levels. The two exponential factors are the same because this decay constant describes the probability that a certain fraction of excited atoms will decay in a time interval between t and t + dt as well as the probability that a given atom will decay in a time interval between t and t + dt.

A modification to the above statement must be made. If a second photoelectron had originated in the photomultiplier tube after a single excitation to the invertron, this second stop pulse would not have registered in the TPHC. Thus, it would not have been measured. This, then, represented a distortion to the desired exponential decay. Quan-

titatively, it was obvious that this distortion would be greatest when the average number of photoelectrons was the largest. The theoretical distortion of the decay curve due to multiple photoelectron occurence was derived in Chapter II. Figure 1 displays this distorted curve for two values of M (1.0 and 0.3). For M equal to 0.1, the difference between the distorted curve and the undistorted curve could not be discerned in the figure. With a fine pencil, theoretical values of the distorted curve were plotted for two values of M and were then fit with a straight line. The resulting measured decay constants were 0.973 τ, 0.983 τ, and 0.997 τ for value of M equal to 0.12, 0.10, and 0.06, respectively. (τ is the lifetime used to determine the theoretical values of the decay curve.) Correction curves were plotted for the data presented in Chapter IV. All corrections made to the measured lifetimes were less than 2%.

To monitor the average number of pulses from the TPHC produced by the photoelectron pulses, a Classmaster Rate Meter (RM) (Model 1613A) was modified for use. A Rate Meter Amplifier (RMA) was used to produce uniform pulses to drive the RM. The RMA is necessary since the output pulses from the TPHC are of different amplitudes. The RMA was triggered by signals of about 400 millivolts. Thus, when the TPHC output was set at the maximum value of 10 volts, only pulses which would occur in the first 4% of the channels in the PHA would fail to be registered by the RM.

Combination Electronic Systems

The separate systems described above were combined with each other

in various manners. The combination systems are categorized as follows:

Combination System I: Direct View and Coaxial Cable

Combination System II: Direct View with Mercury Switch and Pulse Forming Network

Combination System III: Sampling Scope and Coaxial Cable

Combination System IV: Sampling Scope with Mercury Switch and Pulse Forming Network

Combination System V: Delayed Coincidence and Coaxial Cable

Combination System VI: Delayed Coincidence with Mercury Switch and Pulse Forming Network

Block diagrams of Combination System I and III, II and IV, V, and VI are given in Figures 4, 5, 6, and 7.

Combination Systems I and II are self explanatory. The separate components are discussed in Pulse Generating Device: I and II and Detection and Timing Device: I. The Trigger Differentiator was used to start the sweep circuits of the oscilloscope. Combination System II was used instead of Combination System I when longer excitation times were needed.

Combination Systems III and IV were used in place of I and II when one of two conditions necessitated their use: (1) the signal from the photomultiplier tube was too noisy to obtain a good measurement or; (2) the lifetimes to be measured were too fast for the response of the direct display oscilloscope amplifying circuits. Care must be taken when Combination System IV is used due to the jitter in the pulse width of the crowbarred excitation pulse. Since the sampling scope requires the signal to be repetitive except for the noise which is to be eliminated, the signal from the photomultiplier must be examined. This can be done by integrating the output from the photomultiplier to eliminate just the

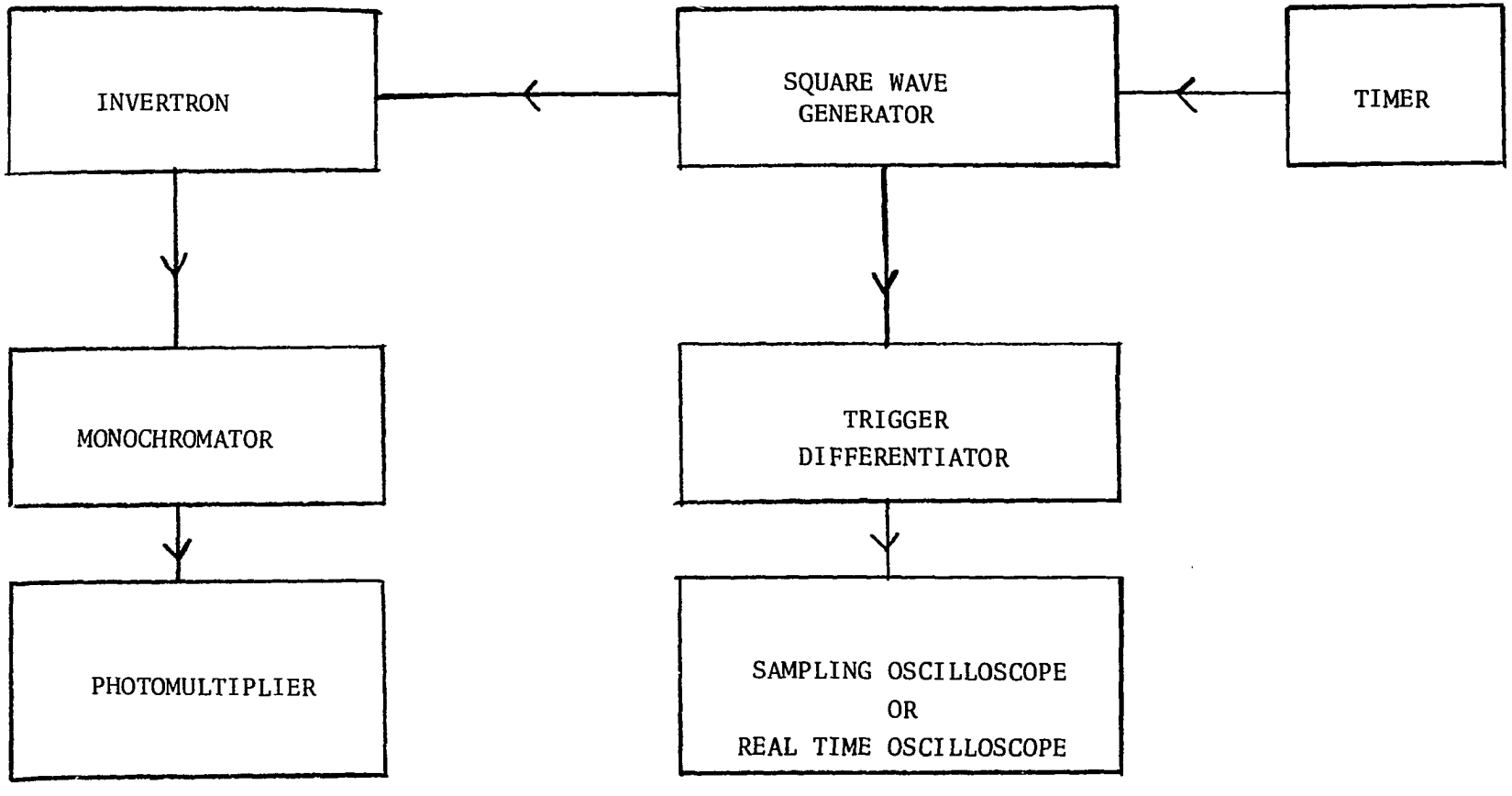

Figure 4. Combination System I or III: Direct View or Sampling Scope and Coaxial Cable.

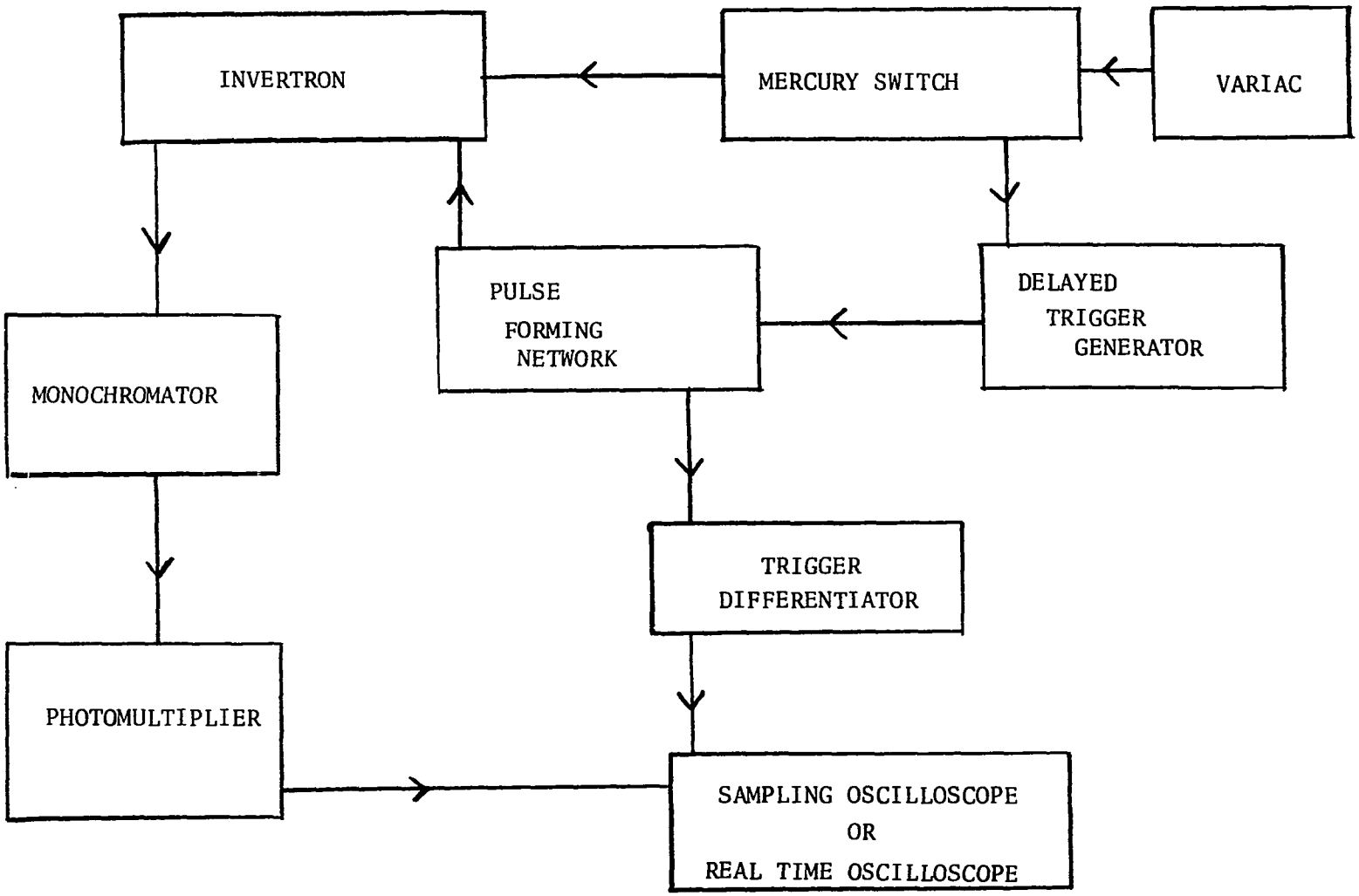

Figure 5. Combination System II or IV: Direct View or Sampling Scope with Mercury Switch.

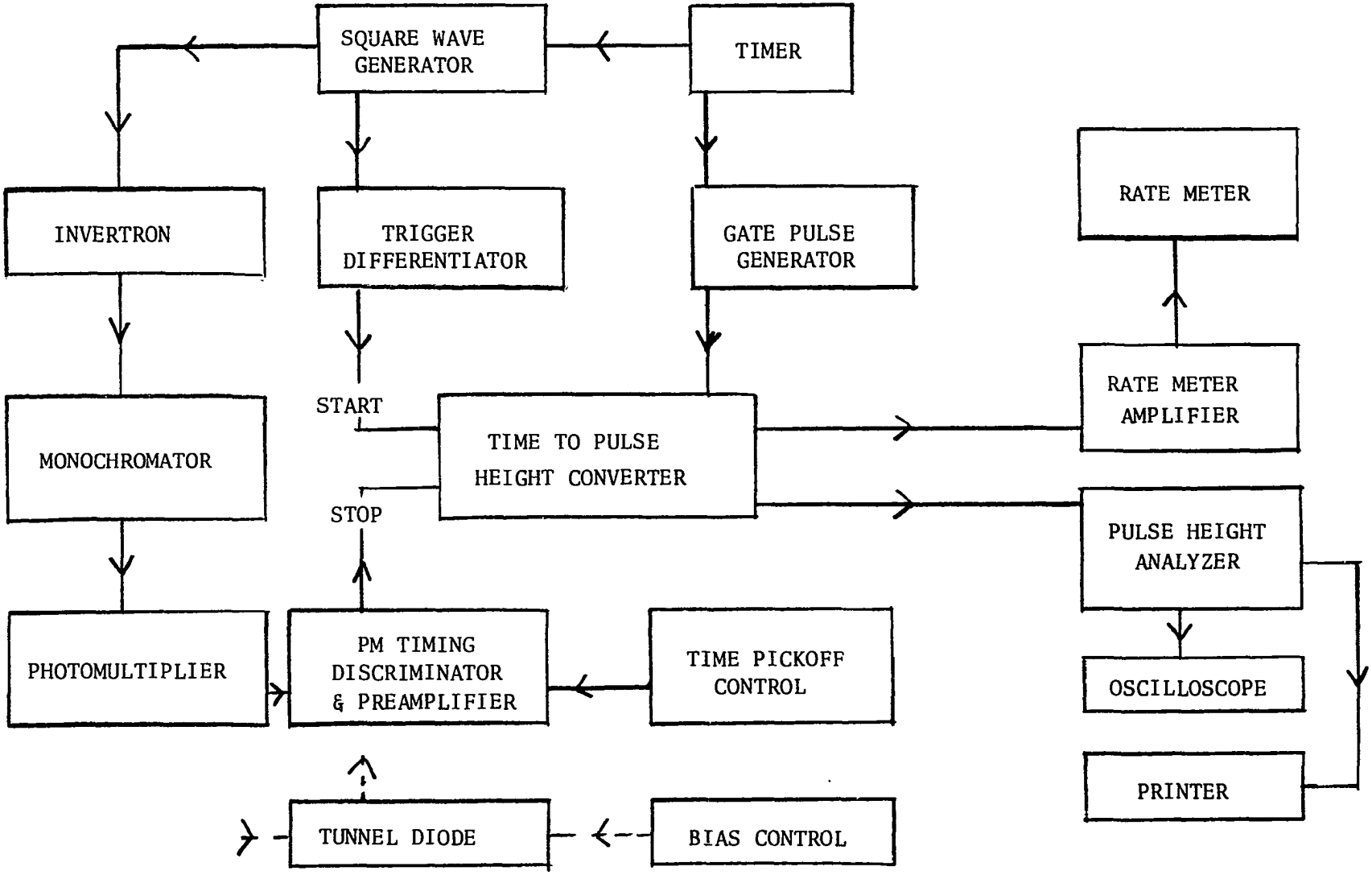

Figure 6. Combination System V: Delayed Coincidence and Coaxial Cable.

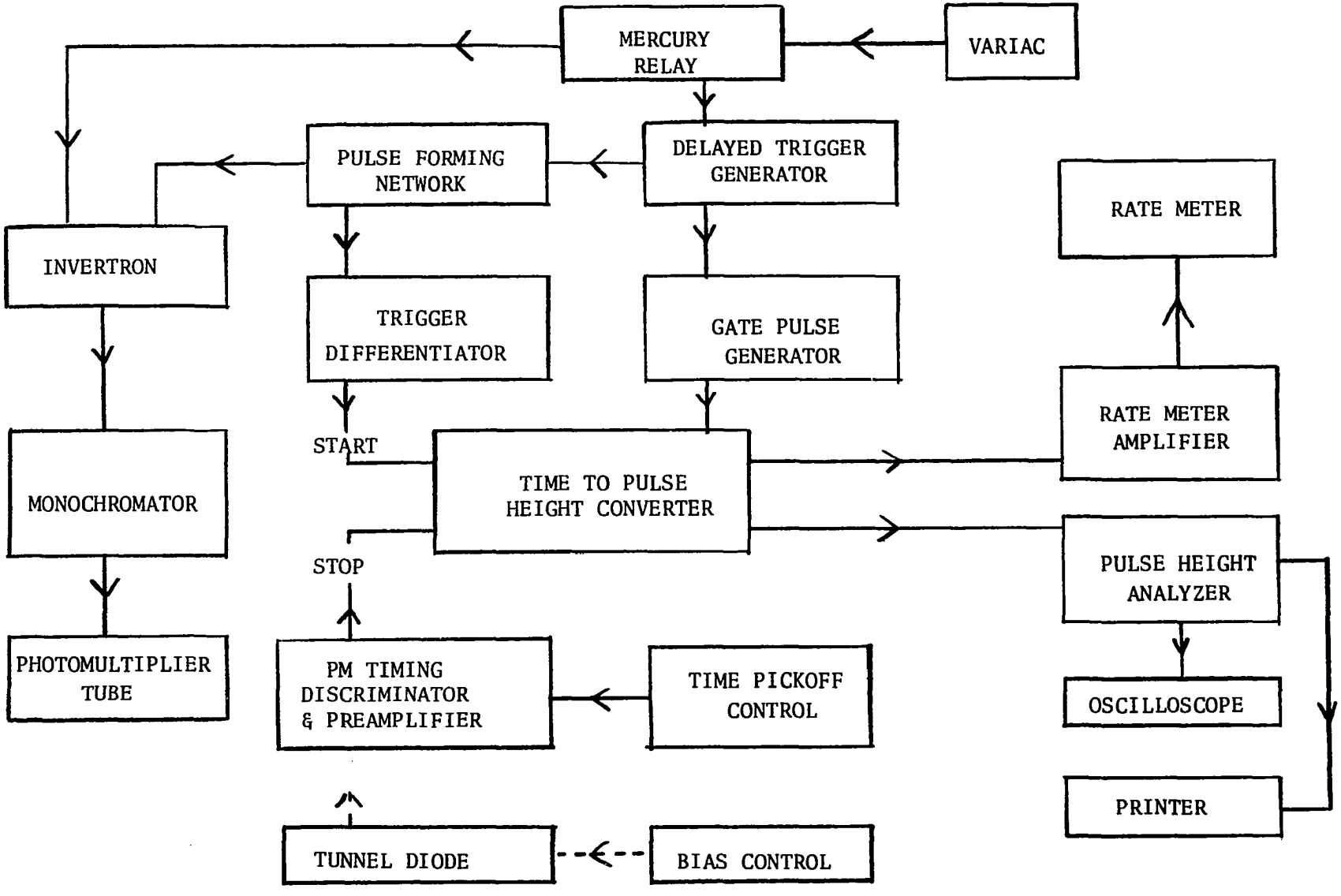

Figure 7. Combination System VI: Delayed Coincidence with Mercury Switch.

noise and applying the signal to a regular oscilloscope. The signal will be distorted, but this is of no concern. What is of interest is the uniformity of the repeating signals. Any observable non-uniformity will distort the decay constant measured from the sampling scope oscillogram. Uniformity of the signal must also be maintained when Complete System III is used, but this was usually no problem since the excitation pulse can be easily maintained constant in height and width.

Complete System V (Figure 6) was the combination of the Delayed Coincidence System and the real cable which have been previously described The Timer was used to initiate the Square Wave Generator (SWG) and the Gate Pulse Generator (GPG). A portion of the signal from the SWG was used in the Trigger Differentiator, as previously described, to start the Time to Pulse Height Converter. The GPG applied a gate to the TPHC in the coincidence mode. The stop pulse was derived from either the Ortec equipment or the Logic Pulse Generator. The Rate Meter Amplifier was connected to the 100 ohms impedance output of the TPHC. The other output of the TPHC (impedance 1 ohm) was applied to the PHA via terminated coaxial cable. An oscilloscope connected to the PHA was used for continuous monitoring of the accumulated signal as well as for the taking of the final oscillogram. A printer was also used to obtain the digital information from the PHA when desired.

Auxiliary Pulse Generating Device: Preionization

A preionization pulse is desirable for two reasons. First, the preionization of the gas allows the electrons of the excitation pulse to penetrate into the central region of the invertron at below or near ionization energies. In other words, the excitation pulse does not have

to produce the ionization. The second reason is to control the excitation time. Short excitation times preferentially excite the desired level more than longer lived levels which might cascade into the desired level.

The preionization pulse was obtained from essentially the same circuit as the one used with Pulse Generating Device II. The only difference was in the method of connecting the pulse to the invertron. The preionization pulse was physically connected into the excitation pulse chassis by a three inch coaxial connector. Under operation, the voltage developing resistor of the excitation pulse was also used as the voltage developing resistor of the ionization pulse.

The sequence and rate of activation of the preionization and excitation pulses was determined by the Timer. The actual delay time between the preionization pulse and the excitation pulse was chosen by observing the light output. The delay was continually increased until the excitation pulse would only barely penetrate into the excitation region of the invertron. The delay was then slightly decreased to allow stable operation but still minimize the interaction of the preionization pulse with the excitation pulse.

Timing Calibration of the Detection and Timing Devices

The Detection and Timing Devices I and II were calibrated with a Standard Signal Generator, Model 80, Measurement Corporation. The signal generator had been calibrated by the use of a Hewlett Packard Counter which was calibrated against special broadcast frequencies. The signal generator was found to drift an insignificant amount. By applying the

output of the signal generator to the input of the oscilloscope, a display of the oscillating signal was obtained on the CRT. For a given sweep speed, the frequency generator was adjusted so that at least five complete oscillations per centimeter appeared on the CRT. A count of the number of oscillations that occurred in ten centimeters then allowed the calculation of the sweep speed. The error was thus kept to less than 2%, since the measurement was good to a fraction of an oscillation out of 50 oscillations. Error of the calibration of the signal generator was certainly less than one part in a thousand.

Detection and Timing Device III required a different technique for calibration. Measured time lengths of coaxial cables were used. The coaxial cables were measured by applying the output signal from the Standard Signal Generator to one of the coaxial cables to be measured and to the input of the 454 Tektronix oscilloscope, simultaneously. The other end of the coaxial cable was connected to the other input of the oscilloscope. Adjustment was made on the oscilloscope so that the two input channels would add together to be displayed on the CRT. Mathematically, the combination of the sine waves is described as follows.

$$\sin wt + \sin w\ (t + d) = 2 \sin w\ (t + \frac{d}{2})\ \cos(\frac{wd}{2})$$

w is the frequency of oscillation from the signal generator and d is the delay time introduced by the coaxial cable. To determine the time length of the cable, the frequency of the signal generator was adjusted to produce a minimum amplitude of the signal on the CRT. The minimum occurs when:

$$\cos \frac{wd}{2} = 0$$

or

$$\frac{wd}{2} = (n + 1/2)\ \pi$$

The frequency necessary to produce a minimum was determined for two adjacent values. Thus:

$$(w_1 - w_2)\frac{d}{2} = (n_1 - n_2)\pi = \pi$$

where w_1 and w_2 are the adjacent frequencies. Thus:

$$d = \frac{2\pi}{(w_1 - w_2)} = \frac{1}{(f_1 - f_2)}$$

f is the frequency of oscillations in units of Hertz.

For convenience, the cables used for these calibrations were divided into two groups. One group (Group I) was composed of three lengths of cable of the approximate size of RG 59/U. The cable was actually triaxial cable but the outer conductor was not used. The other group (Group II) was composed of the cables used to generate the excitation pulses. For timing calibration, the two groups were not mixed with each other. The results of measuring the lengths of cable are given in Table 2.

The three lengths of coaxial cable in Group I were used to calibrate the Time to Pulse Height Converter (TPHC) and the Pulse Height Analyzer (PHA). A trigger signal was applied to the start input of the TPHC and one of the measured coaxial cables simultaneously. The other end of the coaxial cable was connected to the stop input of the TPHC. Thus, a known delay time between the start and the stop pulse occurred. The output of the TPHC was connected to the PHA, and a number of counts were obtained in the PHA. The other timed coaxial cables were used in the same way. Counts were thus accumulated in three channels. The known times and the known channel numbers then allowed the calculation of the equivalent time per channel.

Table 2. Time Lengths of Coaxial Cable Used for Timing Calibration

Group I	
Cable	Length
Short	27.85±0.2 nanoseconds
Medium	44.00±0.2 nanoseconds
Long	88.20±0.8 nanoseconds

Group II	
Cable	Length
A	63.2±1.2 nanoseconds
B + E	256.5±4.0 nanoseconds
D	46.5±1.0 nanoseconds
A + D	90.9±1.0 nanoseconds
Extra Long	380.4±2.8 nanoseconds

The linearity of the TPHC was tested, also. To do this, the coaxial cables were connected in various combinations to the TPHC to obtain as many points as possible. A plot of the pulse amplitude out of the TPHC versus the time between the start and stop pulses then determined if the TPHC was linear. If the points were on a straight line, the TPHC was linear. The 100, 200 and 400 nanosecond range settings were found to be linear. The 50 nanosecond range scale was found to be non-linear and, consequently, was not used to measure lifetimes.

Techniques for Obtaining Decay Constants

The decay constants of the examined levels were extracted from the data two ways. One way was used exclusively with the digital data output from the PHA. This was to graph the digital printer information on semilog paper. An exponential curve forms a straight line when plotted on semilog paper. By drawing a straight line through the plotted data, the decay constant was obtained from the slope of the curve.

One other technique was used to obtain the decay constant. This technique utilized a Comparator and an Exponential Function Synthesizer (EFS), which was designed specifically for the analysis of the data obtained from the invertron. (A description of the circuit of the EFS appears in Appendix.) The EFS was capable of producing three exponentially decaying signals with variable decay constants. In addition, the amplitudes of the three signals could be independently adjusted.

The EFS was used in the following manner. First a picture was taken of the displayed information on the CRT. This information represented the signal obtained directly from the photomultiplier output, the sampling scope display or the display of the number of the counts per channel from the PHA. The oscillogram was then placed in the Comparator. The comparator contained a beam-splitting mirror which allowed the observer to focus his eyes on the oscillogram and the face of an oscilloscope (Tektronix 545) simultaneously. The output from the EFS was then applied to the viewed oscilloscope. By proper adjustment of the EFS output, the signal on the oscillogram and the signal displayed on the CRT resulting from the EFS could be brought into coincidence. The calibrated dials on the EFS then supplied the amplitude and time constant of the radiation decay from the excited atoms as recorded on the oscillogram. The time constants as obtained above were in units of centimeters. To transform into unit of time, the sweep speed (in units of seconds per centimeter) of the oscilloscope used to make the oscillograms was multiplied by the time constant obtained from the EFS. This then gave the lifetime of the observed level of the atom as well as the levels which cascade into the observed level. When the time constants of the various exponential decays of a single oscillogram differed by a factor of two or more, they could be reasonably well separated if no more than three decay constants were present. For differences of factors of less than two, the correctness of the results became doubtful.

CHAPTER IV

RESULTS OF MEASUREMENTS

Helium

As an overall test of the Combination System V, a few levels of helium were measured for comparison with other measurements and with theory. The data was obtained at low pressures (less than 0.05 Torr) for levels with lifetimes short enough to not be appreciably affected by collisional depopulation. Table 3 tabulates the results of this work. Also tabulated in the table are results obtained by other measurements and by theory. The results of this work for helium agree well enough with previously obtained values to justify the use of the overall system.

$B^3\Pi_g$ State of N_2

The lifetimes of six vibrational levels of the $B^3\Pi_g$ electronic state were measured at various values of gas pressure. This state decays by spontaneous emission to the $A^3\Sigma_u^+$ state to produce the first positive band system, which is very prominent in the nitrogen afterglow and the aurora. In Fig. 8, these levels are displayed in an energy level diagram. The wavelengths chosen to monitor the radiation decay of the vibrational levels are given in Table 4. Listed under $B^3\Pi_g$ and $A^3\Sigma_u^+$ are the vibrational quantum numbers of the upper and lower levels, respectively.

Table 3. Lifetimes of Electronic Levels of Helium

Level	Worker	τ(nanoseconds)
4^1S	Pendelton and Hughes (24)	87±9
	Bennett *et al.* (25)	84±9
	This Work	89±3
	Theory: Gabriel and Heddle (26)	90
4^1D	Fowler *et al.* (27)	35±4
	Pendelton and Hughes (24)	47±5
	Bennett *et al.* (25)	34.5 ±4
	This Work	41±3
	Theory: Gabriel and Heddle (26)	38
3^3P	Heron *et al.* (28)	115±5
	Fowler *et al.* (27)	91±8
	Pendelton and Hughes (24)	115±2
	Bennett *et al.* (25)	105±5
	Jeunehomme and Duncan (29)	127±10
	This Work	122±5
	Theory: Gabriel and Heddle (26)	97
4^3S	Heron *et al.* (28)	67.5 ±1
	Bennett and Dalby (4)	77.5 ±4
	Fowler *et al.* (27)	59±6
	Pendelton and Hughes (24)	68±1
	Bennett *et al.* (25)	64.5 ±4
	This Work	62±3
	Theory: Gabriel and Heddle (26)	64

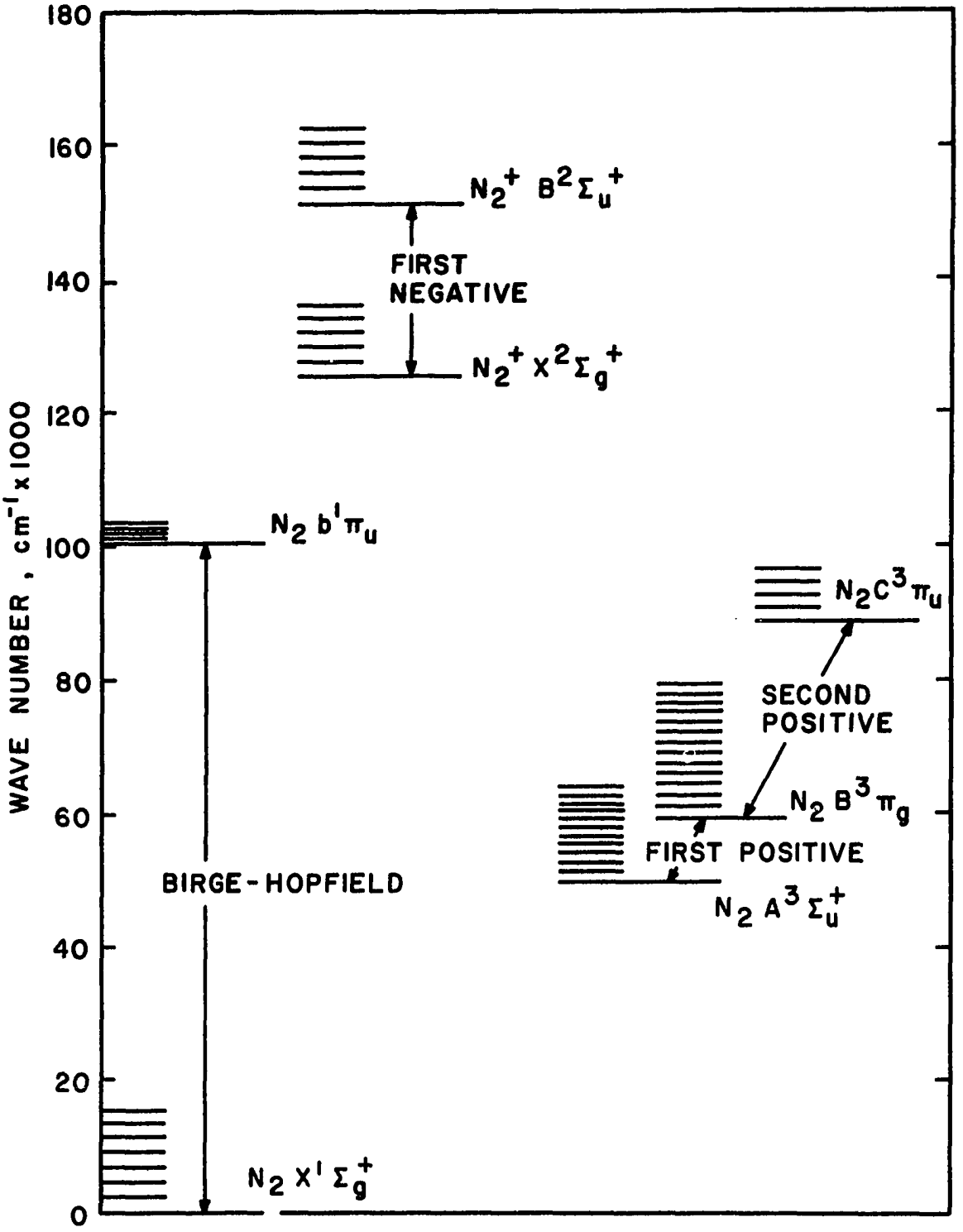

Figure 8. Energy Level Diagram of the Nitrogen Molecule.

Table 4. Wavelengths of the First Positive Band System.

$B^3\pi_g$	$A^3\Sigma_u$	λ (Å)
3	1	7626
4	1	6788
4	2	7504
5	2	6705
6	3	6624
7	4	6545
8	5	6469

In Fig. 9, a spectrogram is given of the first positive system which results from a change in vibrational quantum number of three. The three main peaks noticeable in each band are characteristic of a triplet state. Since the upper state is a $^3\Pi$ state, the additional structure, which is discenable in the spectrogram, is much more complicated with greater wavelength resolution.

Combination System I was used to obtain the oscillograms representative of the light decay. A simple resistor, capacitor integrating device was used to smooth the output from an EMI 9558 photomultiplier tube. The decay constant of the integrator was always less than one-tenth the decay constant of the excited level under observation. A ¼-meter Jarrell-Ash monochromator was used for spectral isolation of the desired radiation. The time constants and resulting lifetimes were measured from the oscillograms with the Exponential Function Synthesizer and the Comparator.

Since the lifetimes of these levels are relatively long (greater than 2 microseconds), the analysis developed in Chapter I for the case of wall quenching and volume collisional depopulation must be used to determine the spontaneous emission lifetime. A description of some of the consideration needed to analyze the data will be given before the results are presented.

Consideration must be given to the collision frequency term contained in the mathematical analysis of Chapter I. For the analysis of the data herein to be presented, this collision frequency term was assumed to be proportional only to the concentration of the particles

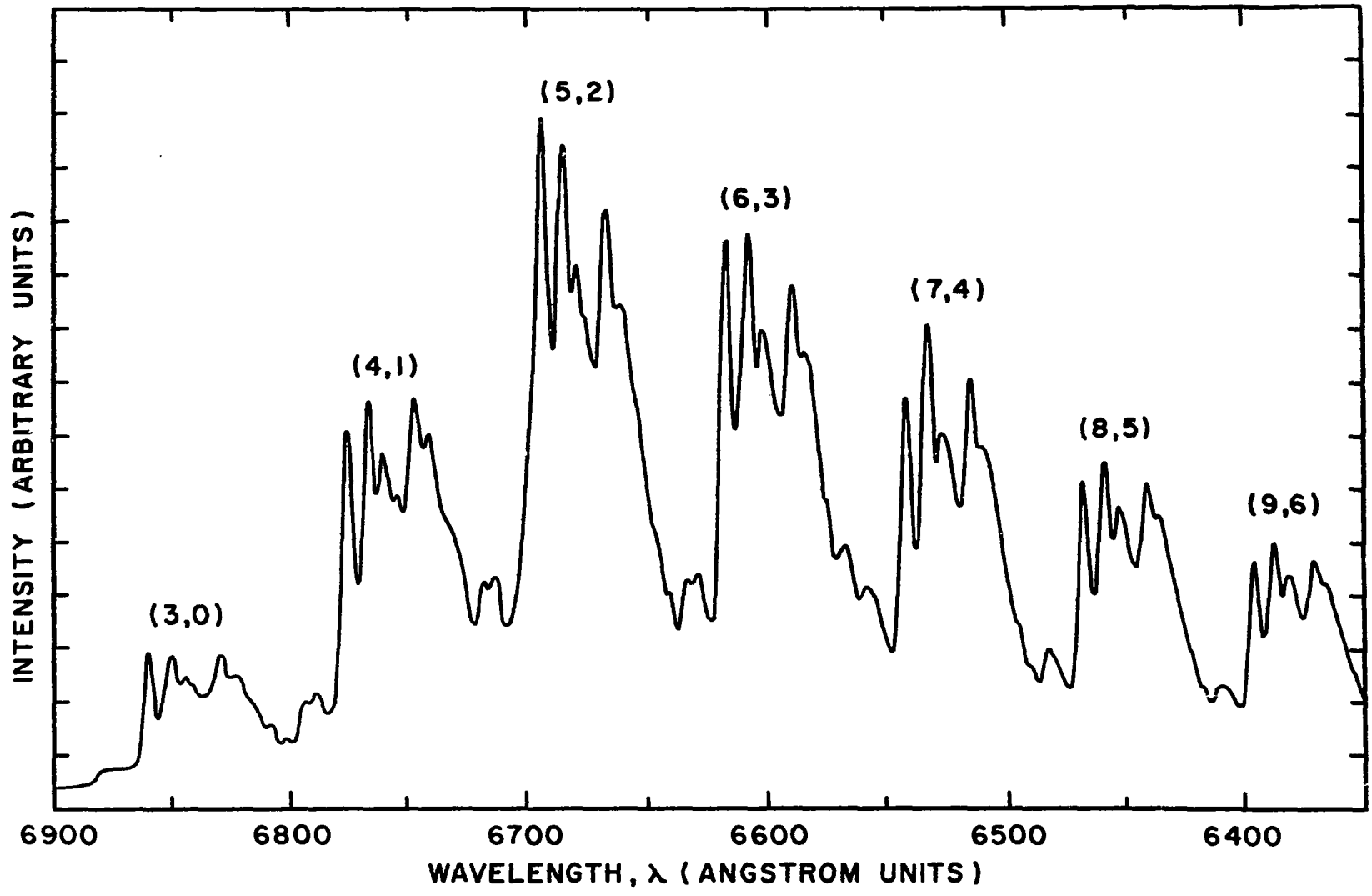

Figure 9. Spectrum of First Positive Bands of $N_2(\Delta V = 3)$.

contained in the invertron. This assumption is reasonable if the temperature of the gas is kept constant for all pressures. The temperature of the cathode was measured with an optical pyrometer. (Since the collision frequency is proportional only to the square root of the temperature, the error this measurement produces is relatively small.) The gas temperature was then taken to be the temperature of the cathode. A comparison of the Boltzmann temperature of the excited states with the measured cathode temperature is presented elsewhere. The agreement between the Boltzmann temperature and the measured cathode temperature lends creditability to the assumption that the gas kinetic temperature is also the same.

The concentrations of the nitrogen gas particles were determined from a measurement of the pressure with a mercury, McLeod gauge. The concentration or number density (N_o) was then determined with the following relation.

$$N_o = N_M \frac{T_M}{T}$$

N_M is the density of the particles determined from the McCloud gauge at the ambient temperature T_M. T is the temperature of the gas inside the invertron.

From Eq. (36) in Chapter II, the effective transition probability may be expressed as follows.

$$\bar{A} = A + N_o(\sigma v) + \frac{0.52}{N_o} \qquad (60)$$

$\bar{A}$ is the reciprocal of the measured lifetime. Measured lifetimes were determined for a number of different pressures with Combination System I.

A least squares fit was imposed upon the data to match the form of Eq. (60). The two parameters, A and (σv), were determined by the following equations, which resulted from the least squares fit.

$$A = \frac{n \Sigma_i A_i N_i - \Sigma_i \frac{0.52}{N_i} - (\Sigma_i N_i)(\Sigma_i A_i) - \Sigma_i \frac{0.52}{N_i}}{n \Sigma_i (N_i)^2 - (\Sigma_i N_i)^2}$$

$$\sigma v = \frac{\Sigma_i A_i - \Sigma_i \frac{0.52}{N_i} - A\Sigma_i N_i}{n}$$

A_i and N_i are the measured reciprocal lifetimes and number densities, respectively. (A_i and N_i are designated $\bar{A}$ and N_o, respectively, in Eq. (60).) n represents the number of measurements. In the least squares fit, only the A_i's were assumed to vary.

As can be seen in Eq. (60), $\bar{A}$ becomes very large as N_o becomes small, due to the third term on the right hand side of the equation. Thus $\bar{A}$ has a minimum value as implied by Eq. (60) and becomes infinite as N_o goes to zero. In fact, this does not happen. The difficulty is with the diffusion term used in the analysis of Chapter II. For small number densities where the mean free path becomes comparable with the size of the containing vessel (in this case the invertron), diffusion is no longer a valid concept.

The technique used to analyze the data was to find the minimum point of the curve and then let this value (A_{min}) of the reciprocal lifetime hold for all smaller values of N_o.

Figures 10 to 12 display the measured values and estimated errors of the effective transition probability and the derived curve fit (solid line). Table 5 gives the derived value of the spontaneous emission reciprocal lifetime (A), the spontaneous emission lifetime (τ), the product term (σv), and the minimum point of the measured reciprocal lifetime (A_{min}). The estimated error for A is 15 per cent and for σv, 10 per cent. Also, in the same table is given the derived value of the effective cross section for the depopulation mechanism, σ. The value of the velocity (v) was taken to be the average velocity of a nitrogen molecule at the measured temperature (1050° K) of the invertron, 10^5 cm per second.

The Knudsen relation describes the number of particles which strike the walls of a vessel of area B and volume V at a given temperature. Thus, an effective transition probability (hereafter referred to as the Knudsen transition probability, A_K) can be determined for the case where the diffusion concept is no longer applicable and volume collisional depopulation is no longer important.

$$A_K = A + \frac{\bar{v}}{4}\frac{B}{V}$$

B is the area of the containing vessel and V is the volume of the vessel. The second term on the right hand side of the above equation is the Knudsen term. For the dimensions of the invertron and the measured temperature, 1050° K, this second term has the value of 0.6×10^5 per second. For each vibrational level, the values of A_K are given in Table

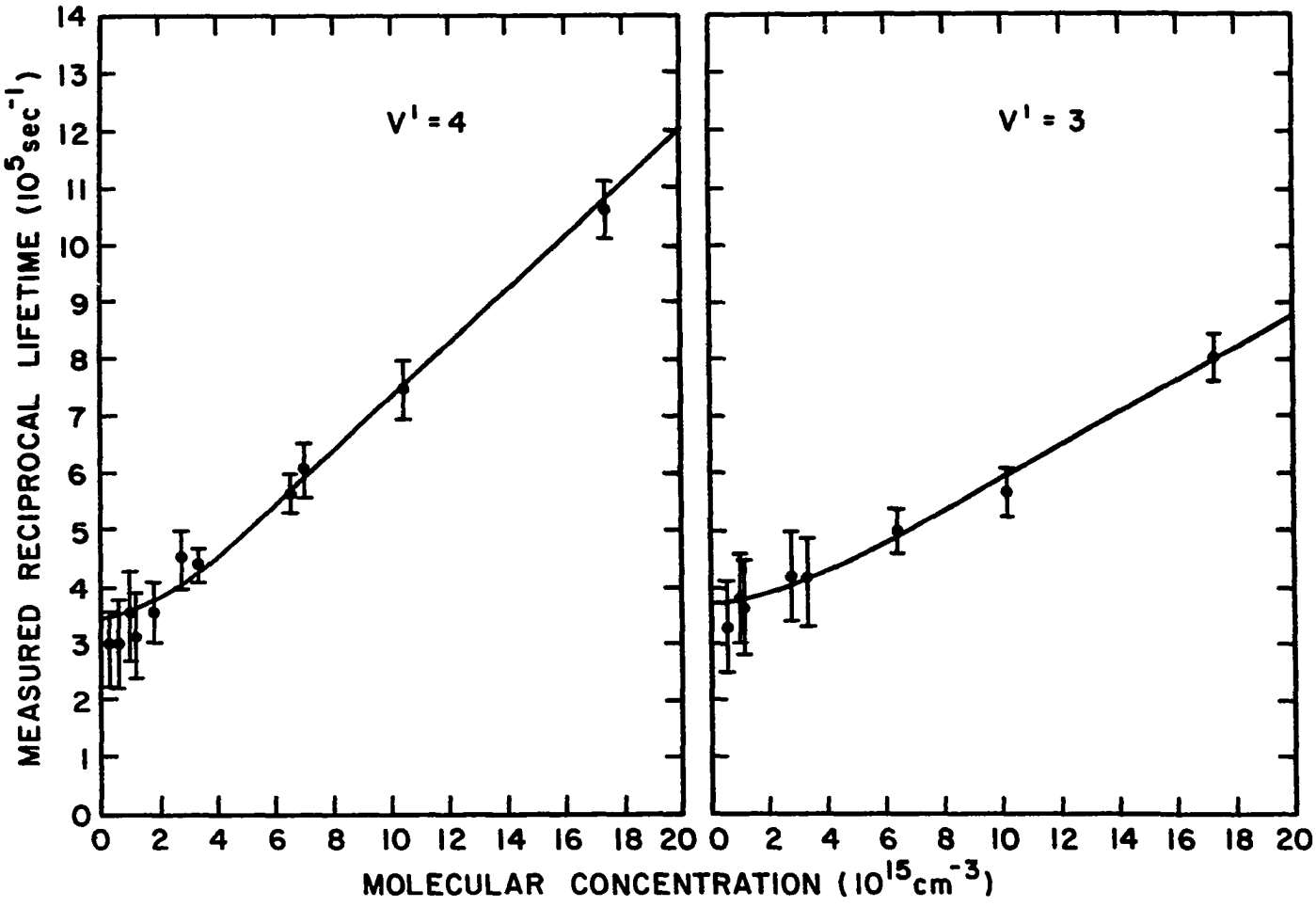

Figure 10. Pressure Dependence of the Measured Reciprocal Lifetimes of Vibrational Levels (v' = 3 and 4) of the $B^3\Pi_g$ States of N_2.

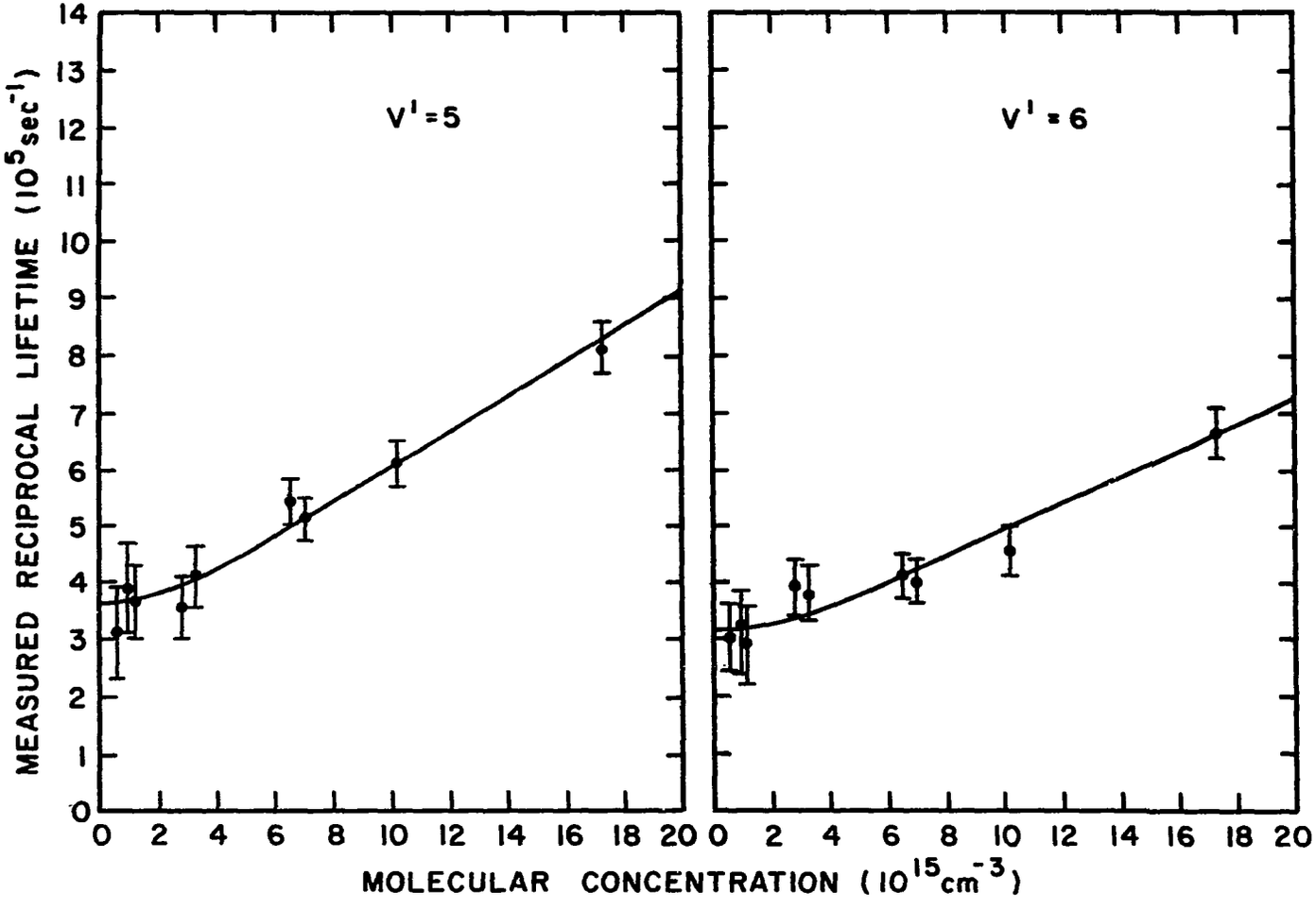

Figure 11. Pressure Dependence of the Measured Reciprocal Lifetimes of the Vibrational Levels (v' = 5 and 6) of the $B^3\Pi_g$ States of N_2.

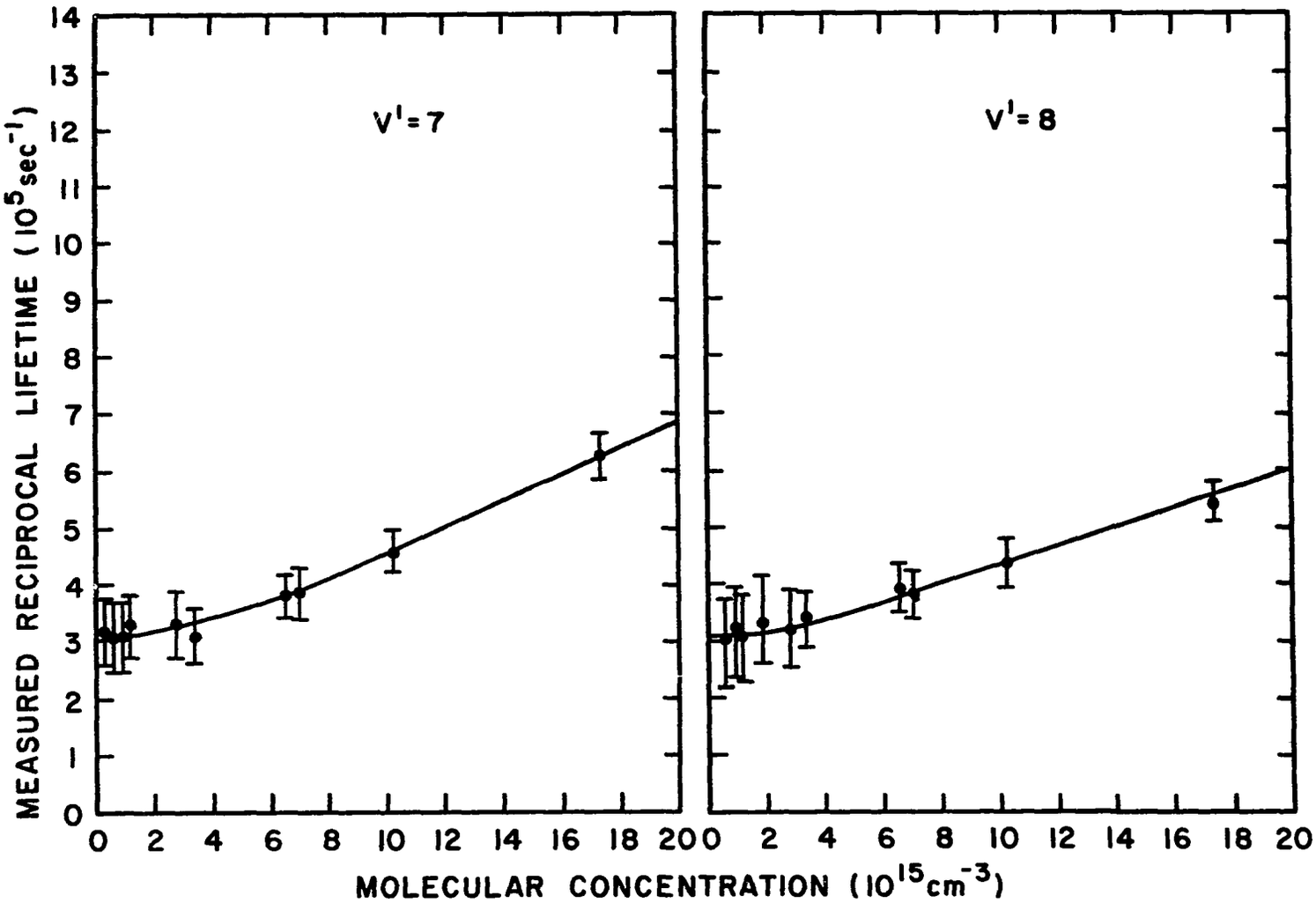

Figure 12. Pressure Dependence of the Measured Reciprocal Lifetimes of Vibrational Levels ($v' = 7$ and 8) of the $B^3\Pi_g$ States of N_2.

Table 5. Reciprocal Lifetimes (A), Lifetimes (τ), Cross-Sections (σ), and other Associated Parameters Concerned with the Vibrational Levels of the $B^3\Pi_g$ Level of N_2

v'	3	4	5	6	7	8	units
A	3.0	2.5	2.8	2.5	2.3	2.5	$10^5 sec^{-1}$
τ	3.3	4.0	3.5	4.0	4.3	4.0	$10^{-6} sec$
σv	3.0	4.8	3.2	2.4	2.3	1.8	$10^{-11} sec^{-1} cm^3$
σ	3.0	4.8	3.2	2.4	2.3	1.8	$10^{-16} cm^2$
A_{min}	3.7	3.5	3.6	3.4	3.0	3.1	$10^5 sec^{-1}$
A_K	3.6	3.1	3.4	3.1	2.9	3.1	$10^5 sec^{-1}$
$\tau(J)$*	6.8	6.5	6.2	6.0	5.3	4.8	$10^{-6} sec$

*M. Jeunehomme[1]

5. A_K and A_{min} should be equal if the assumptions of this analysis are correct. Table 5 demonstrates the reasonable agreement between A_{min} and A_K.

The results indicate that the collisional depopulation cross-section peaks for the v' = 4 vibrational level. The potential energy curves of N_2 determined by Gilmore[30] indicate a near asymptotic crossing of the $B^3\Pi_g$ and $A^3\Sigma_u^+$ potential energy levels between v' = 4 and v' = 5 of the $B^3\Pi_g$ state. The resonance energy, collisional perturbation of the $A^3\Sigma_u^+$ level may account for the increased collisional depopulation cross-section about the $B^3\Pi_g$ (v' = 4) level.

The results of Jeunehomme[1] are also given in Table 5 listed by $\tau(J)$. Jeunehomme extrapolated to zero pressure the reciprocal lifetime to obtain the values given. He excited N_2 mixed with NO to reduce the diffusion losses, although no attempt was made to correct for the diffusion losses. Correction for diffusion losses tends to lower the measured lifetimes. No comparison was made between Jeunehomme's measured cross-sections and those given in Table 5 since the main particle producing collisional depopulation in his vessel was NO.

Wuster measured the absorption oscillator strength of the $B^3\Pi_g(v'=0)$ to $A^3\Sigma_u^+(v'=0)$ in a shock heated nitrogen gas. The value, 0.0028, which he obtained corresponds to a lifetime of 3.64 microseconds for the upper vibrational level if the branching ratio of 0.34 predicted by the Franck-Condon factors as calculated by Halmann and Laulicht is used. In the calculation of this lifetime, the electronic transition moment was assumed constant. Wuster's result agrees well with the results of this work but differs from Jeunehomme's results by a factor of two.

$C^3\Pi_u$ Vibrational Level of N_2

The second positive band system of nitrogen results from vibrational transitions from the $C^3\Pi_u$ to $B^3\Pi_g$ states. (See energy level diagram in Fig. 8) The lifetimes of four of the vibrational levels of the $C^3\Pi_u$ states ($v' = 0,1,2,3$) were measured with Combination System V. Spectral resolution of the desired lines was obtained with a ½-meter Jarrell-Ash monochromator. The band pass of the monochromator was adjusted so that only the radiation from the band heads to two angstrom units behind the band heads of the vibrational levels was admitted onto the face of the photomultiplier. Since the $C^3\Pi_u$ level is composed of two only slightly non-degenerate electronic states, the two states were measured as one. All that follows treats these near degenerate electronic states and the rotational levels as one level.

The transitions chosen to monitor the number densities of the respective vibrational levels are listed in Table 6. Under $C^3\Pi_u$ are listed the upper level vibrational quantum numbers, under $B^3\Pi_g$ are listed the lower level vibrational quantum numbers, and under λ is listed the wavelength in angstroms characteristic of the transition.

The electron cross section for the production of the $C^3\Pi_u$ state from the ground state has the triplet shape. The cross section is very large near onset excitation energies and then decreases rapidly as the electron energy increases. In Figure 13 are two spectrograms which graphically demonstrate this effect. The radiation from the $B^3\Sigma_u^+$ states increases slowly in the energy range of 28 - 100 eV.[5] The radiation

Table 6. Lifetimes (τ_P and τ_E) of Vibrational Levels of the $C^3\Pi_u$ State and the Wavelength (λ) used for the Measurements.

$C^3\Pi_u$	$B^3\Pi_g$	λ	τ_P (nanoseconds)	$\#_P$	τ_E (nanoseconds)	$\#_E$
v' = 0	v'' = 0	3371Å	38.4±2.0	7	39.7±2	4
1	0	3159Å	39.2±2.0	8	39.7±2	4
2	1	3136Å	37.8±3.0	6	39.6±3	4
3	2	3117Å	38.0±3.0	5	39.6±3	4

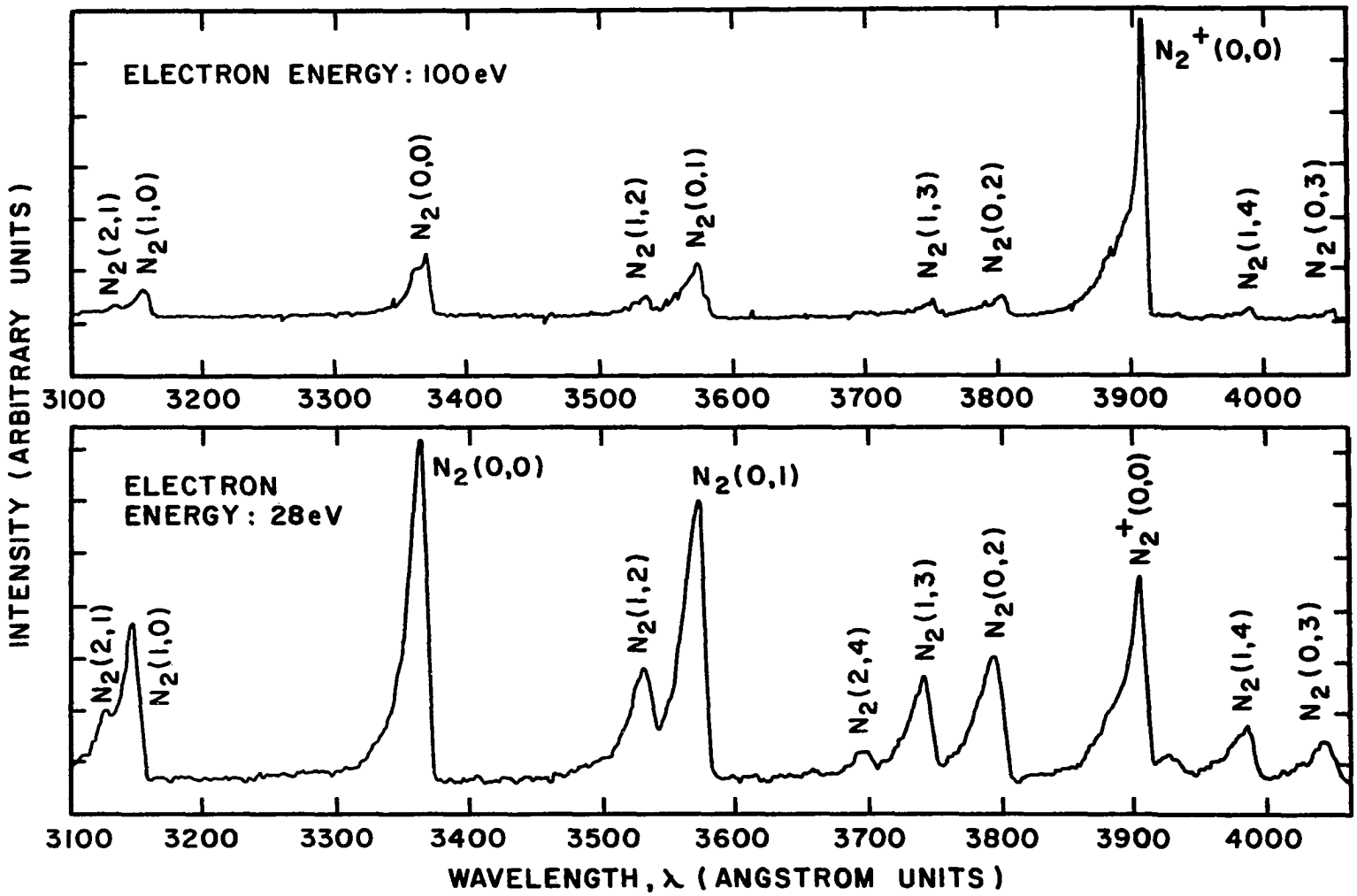

Figure 13. Spectrograms of the Second Positive and First Negative Systems of Nitrogen for Two Different Electron Energies.

from the $C^3\Pi_u$ states decreases dramatically, however, from 28 eV excitation energy to 100 eV excitation energy.

Due to considerable confusion resulting from previous measurements of the lifetime of this level, a pressure dependent and energy dependent examination of the vibrational levels was undertaken. The pressure dependent examination will be described first.

If spontaneous emission and volume collisional depopulation are the only population or depopulation mechanisms of a level, the intensity (I) of the emitted radiation has the following time dependence.

$$I = I_o \exp[-(A + N_o\sigma v)t] \tag{61}$$

I_o is the initial intensity, A is the sum of all possible transition probabilities, N_o is the total number of particles, σ is the effective collisional depopulation cross-section and v the velocity of the particles. The measured reciprocal lifetime (A_M) may be defined from Eq. (61).

$$A_M = A + N_o\sigma v$$

The lifetimes of four vibrational levels of the $C^3\Pi_u$ states were measured over a pressure range of 0.03 to 1.4 Torr. For a gas temperature of 1000° K, this corresponds to a number density of 0.028 to 1.3×10^{16} per cubic centimeter. The excitation voltage applied to the invertron was 60 volts. No detectable dependence of the lifetime on number density was observed. Since the spontaneous emission lifetimes for this level are so short, the lack of dependency on number density was not unexpected.

However, the data did set an upper limit on the collisional depopulation cross-section at 4 x 10^{-15}cm^2 for v' = 0 and v' = 1 and 6 x 10^{-15}cm^2 for v' = 2 and v' = 3.

In Table 6, the average of the measured values of the lifetimes of the 0, 1, 2 and 3 vibrational levels of the $C^3\Pi_u$ state are listed under τ_p. The estimated error is also given. This estimated error is the total estimated absolute error. The fluctuation in the measured values is less than the reported absolute error. Under the symbol $\#_p$ is given the number of measurements which were averaged to give the reported value.

A possible dependency of the lifetimes of the $C^3\Pi_u$ states on electron energy was also considered experimentally. Previous measurements[5] indicated that the lifetimes increased by about a factor of two to over 70 nanoseconds with a change in the exciting electron energy from 40 eV to 100 eV. In principle, the spontaneous emission lifetime of a given level should be a parameter characteristic only of the level. To test the validity of the principle, the lifetimes of the $C^3\Pi_u$(v'=0,1,2,3) levels were measured over a range of electron excitation energies of 40 to 125 eV. The pressure was held at 0.06 Torr for all these electron energy dependent measurements. This pressure corresponds to a number density of 5.6 x 10^{+13} per cubic centimeter. Collisional depopulation effects account for much less than 1 per cent of the measured values at these pressures.

When the invertron is operated with 40 volts applied to the accelerating grid at pressures as low as 0.06 Torr, the pre-ionization pulse must be used to get stable, reproducible excitation. For these measurements, a 30 volt amplitude preionization pulse of about 8 microseconds width was applied 20 microseconds before the application of the excitation pulse. The intensity of the radiation, which was emitted from the observed $C^3\Pi_u$ levels and produced by the preionization pulse, had decayed to a value which was less than 10^{-4} times the value of the intensity produced by the excitation pulse. Thus, there was a negligible residual background radiation for the lifetime measurements.

The excitation pulse width was 130 nanoseconds. The width was set at this value to reduce the population of long lived species which might cascade into the observed levels. Thus, the decay curves resulting from the observed light decay were composed of only one exponential decay plus a small constant background.

The measured values of the lifetimes varied by less than 1.5 nanosecond for the $v' = 0, 1, 2, 3$ levels of the $C^3\Pi_u$ state with a change in the electron accelerating voltage from 40 volts to 125 volts.

In Table 6 is listed the average of these measurements under τ_E. As can be seen, τ_E and τ_P agree to well within the estimated error. Since the pressure dependent study and the electron dependent study were performed under different absolute calibration conditions, the agreement was expected to be no better than it is. Under the column labelled $\#_E$ in Table 6 is listed the number of measurements made for the electron energy dependent study.

Figures 14, 15 and 16 contain the plot of the raw data (circles) from the multichannel analyzer for three decay curves. Note the absence of a long cascade component. Only a constant noise level had to be subtracted from the counts. The squares in the figures represent the raw data with the noise level subtracted. This corrected data has been plotted with a shift to the left side for clarity. The solid straight line is the fit to the data and was used to obtain the decay constants and corresponding lifetimes.

An average of all the lifetime measurements given in Table 6 for the $C^3\Pi_u$ level is 39 nanoseconds. In Table 7 is listed the results of all known investigators to date who have measured the lifetime of the $C^3\Pi_u$ state of N_2.

The measured value of this work for the $C^3\Pi_u$ level agrees to within the reported experimental error of Bennett and Dalby.[4] Fink and Welge[5] reported a value for the lifetime of this level, which does not fit the extrapolation to onset energy of their data. A reanalysis of their data yields a value for the lifetime given in Table 7 in parenthesis, which agrees much better with the results of this work. Jeunehomme's[8] reported value does not agree with the results of this work to within the reported possible error. However, in his paper, Jeunehomme "suggests" a value of 47±8 nanoseconds. Due to the peculiar technique Jeunehomme used to obtain his reported value from his pressure dependent lifetime measurements, the "suggested" value is probably the better value. Nichols and Wilson[10] did not measure the lifetimes they reported below a pressure of 50 Torr. A very small error in the measured

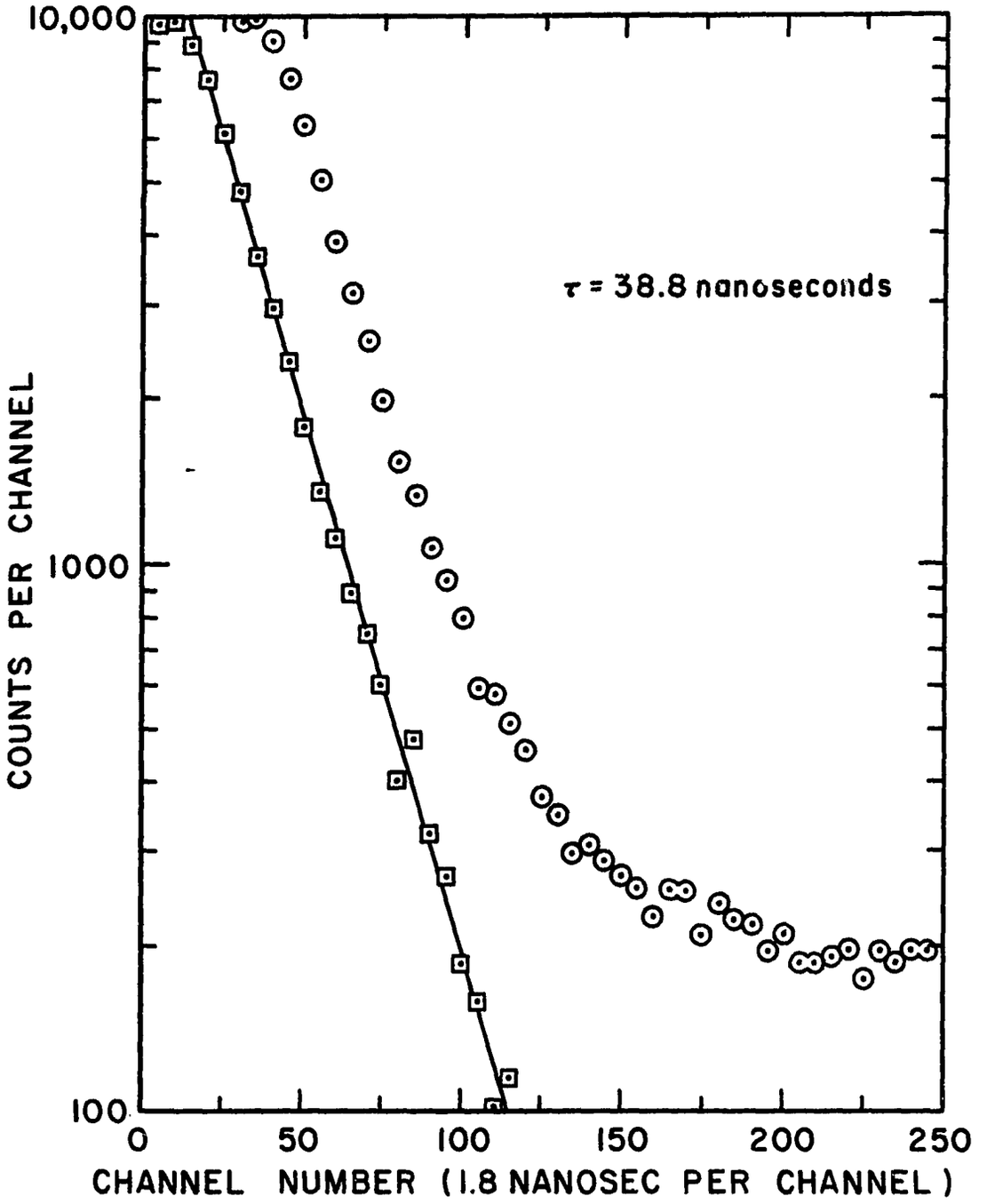

Figure 14. Decay Curve for the $C^3\Pi_u(v' = 0)$ Level of N_2.

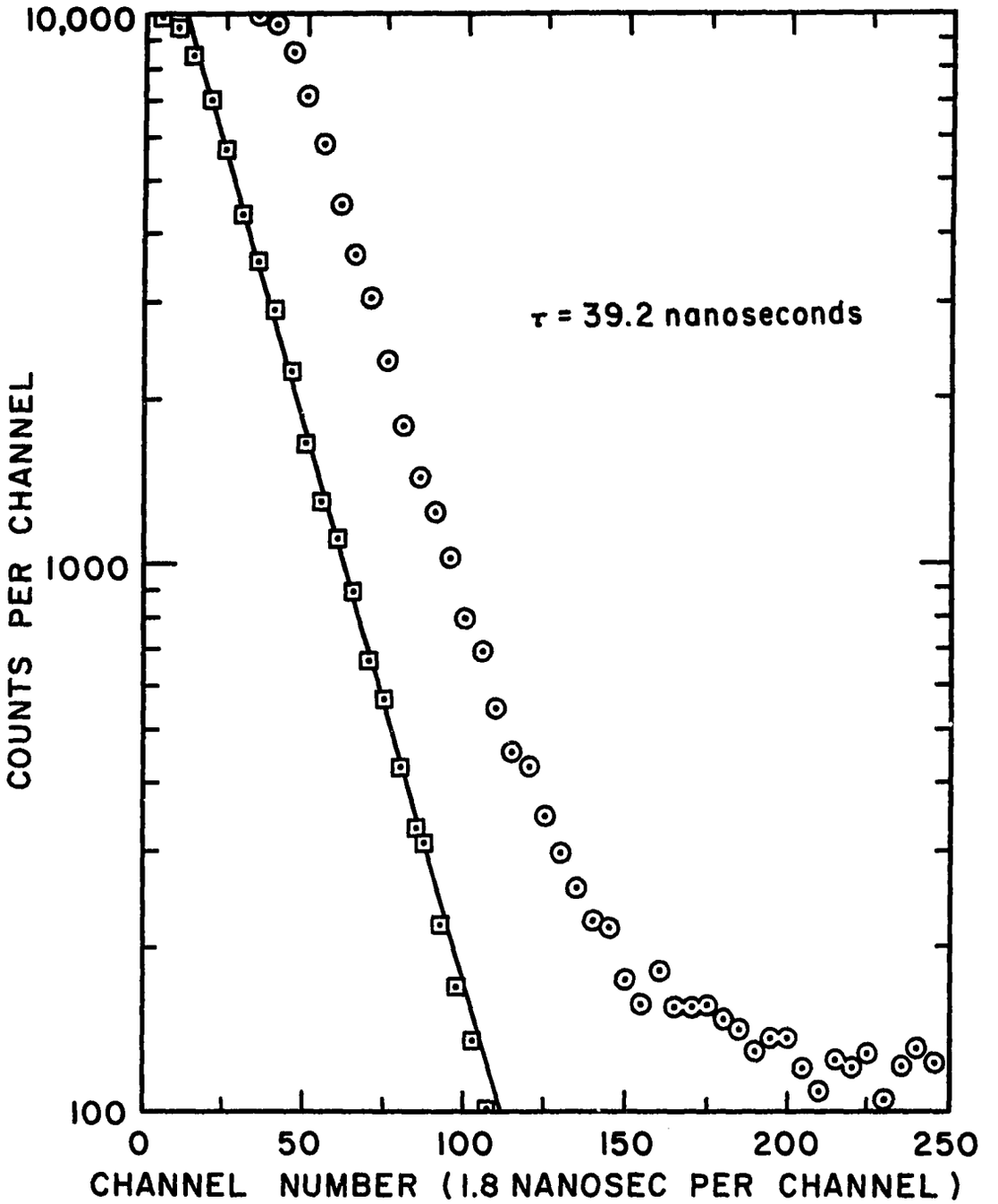

Figure 15. Decay Curve for the $C^3\Pi_u(v' = 1)$ Level of N_2.

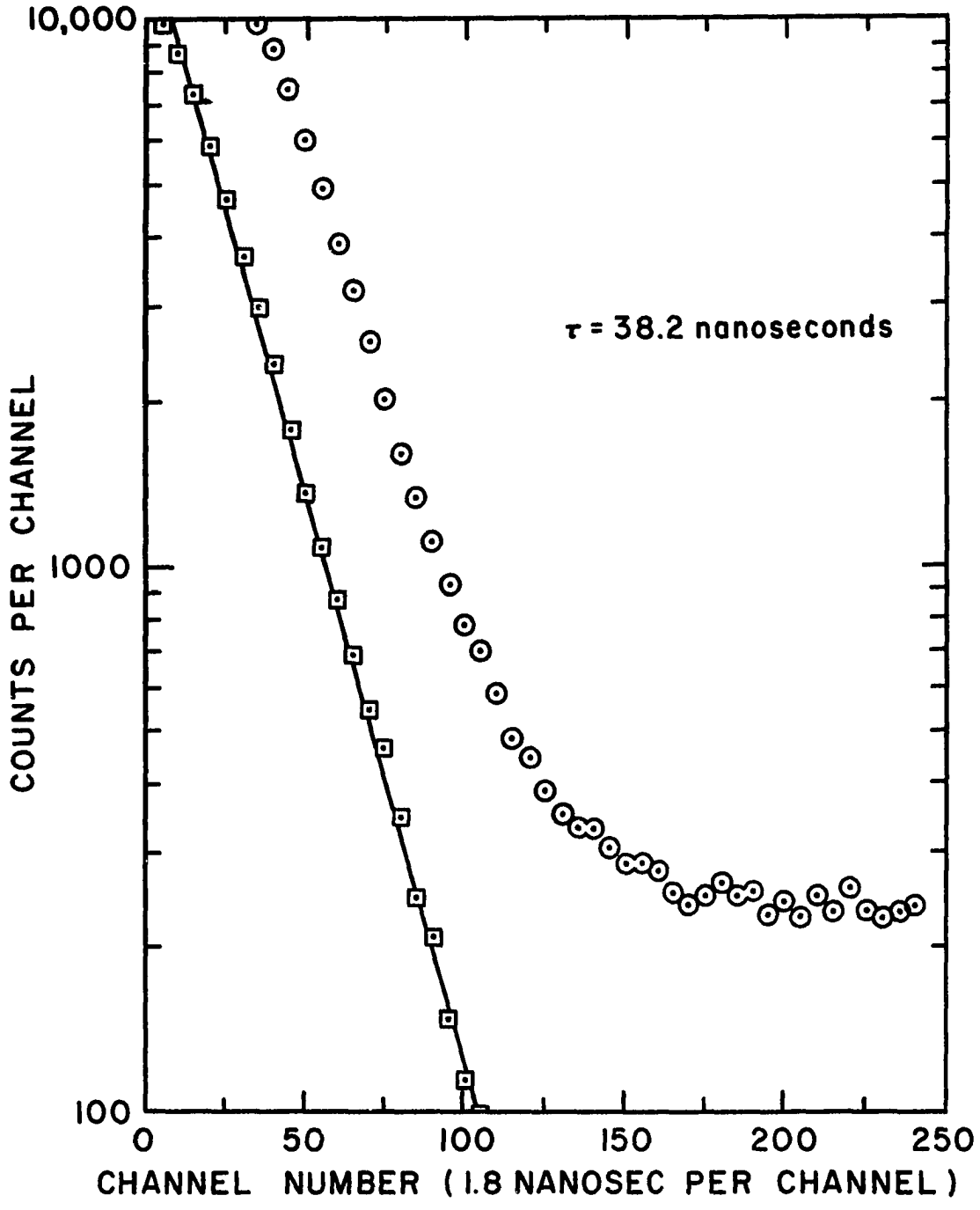

Figure 16. Decay Curve for the $C^3\Pi_u(v' = 2)$ Level of N_2.

Table 7. Measured Lifetimes of the $C^3\Pi_u$ States of N_2

Experimentalist	Lifetime (nanoseconds)
Bennett and Dalby[4]	44.5±6
Fink and Welge[5]	27 ±5 (39)*
Jeunehomme[8]	49 ±5 (47±8)**
Nichols and Wilson[10]	45.4 (v' = 0) 31.2 (v' = 1)
This Work	39 ±2.5

*A better extrapolation of Fink and Welge's electron energy dependent curve is 39 nanoseconds.

**Value suggested by Jeunehomme.

pressure dependent lifetime or in the measured pressure would dramatically affect the extrapolated zero pressure value of the lifetime from pressures as high as they operated. In addition, a discrepancy exists between the large difference (50 per cent) in the lifetime of the two vibrational levels reported by Nichols and Wilson[10] and the relatively small dependence (10 per cent) of the electronic transition moment of the $C^3\Pi_u$ to $B^3\Pi_g$ transition.[31]

Collisional depopulation cross sections for these levels calculated from the pressure dependent lifetimes measured by Nichols and Wilson should be more accurate than the zero pressure lifetimes. If the temperature of the gas in their vessel was 300° K, their results indicate an effective collisional depopulation cross section of $1.7\times10^{-16}cm^2$ and $4.2\times10^{-16}cm^2$ for v' = 0 and v' = 1, respectively. These values are well below the upper limit of $4\times10^{-15}cm^2$ set by the results of this work.

The transition probabilities for the various vibrational transitions of the second positive system may be calculated from the lifetimes of Table 6 and relative intensity measurements. The measured relative intensities reported by Tyte[32] were used to calculate the transition probabilities given in Table 8 with the use of Eq. (5). The sum term listed in the table was obtained by normalization of the Franck-Condon factors calculated by Zare *et al.*[33] to the measured values of Tyte. Since the sum term adds a small correction, the error introduced into the other transition probabilities by the error in the correction will be very small.

Table 8. Transition Probabilities for the $C^3\Pi_u$ - $B^3\Pi_g$ Transitions and Lifetimes for the $C^3\Pi_u$ State of the Nitrogen Molecule.

v''	v' = 0		v' = 1		v' = 2	
	λ (Å)	$A(0,v'')\times10^6 sec^{-1}$	λ (Å)	$A(1,v'')\times10^6 sec^{-1}$	λ (Å)	$A(2,v'')\times10^6 sec^{-1}$
0	3371.3	12.4	3159.3	11.1	2976.8	4.6
1	3576.9	8.8	3339.0	0.62	3136.0	10.9
2	3804.9	3.1	3536.7	5.3	3309.0	0.72
3	4059.4	1.0	3755.4	4.7	3500.5	1.9
4	4343.6	0.29	3998.5	2.4	3710.5	3.3
5					3943.0	2.4
6		$\sum_{v''=5}^{8} = 0.15$		$\sum_{v''=5}^{8} = 1.6$	4200.5	1.4
7					4490.2	0.42
						$\sum_{v''=8}^{8} = 0.49$
τ		38.3×10^{-9} sec		39.3×10^{-9} sec		38.5×10^{-9} sec

$B^2\Sigma_u^+$ of N_2^+

The radiation produced by the $B^2\Sigma_u^+$ to $X^2\Sigma_g^+$ transition of the nitrogen molecular ion is referred to as the first negative system. See energy level diagram in Fig. 8. The lifetime of the zero vibrational level of the $B^2\Sigma_u^+$ state is probably capable of being measured more accurately than any other molecular vibrational level. The reasons that this is so are many. The electron production cross-section for this level from the neutral nitrogen molecule is large. Since the transition occurs in the nitrogen molecular ion, resonance absorption of the radiation occurs only from the produced ion. With short excitation pulses the ion number density may be kept low. Cascading levels into this level are very weak and have relatively very long lifetimes. The lifetime of the $B^2\Sigma_u^+(v' = 0)$ level is long enough to be easily measured by the apparatus yet short enough so that collisional effects can be made small.

Due to the possibility of precise measurements of the lifetime of this vibrational level, it was chosen for the study of any dependence of the lifetime on the rotational level. The $B^2\Sigma_u^+(v' = 0)$ to $X^2\Sigma_g^+(v'' = 0)$ is the strongest transition from the upper level and results in the emission of radiation with the bandhead at 391.4 nanometers. The band system was resolved into 35 rotational components of the R branch. Figure 17 is a spectrogram showing these components. (Since the spin splitting of the rotational levels was not observable with the apparatus used, this transition will be discussed as if it were a $^1\Sigma$ to $^1\Sigma$ transition.) In order to ascertain the pressure at which the lifetimes should be measured

$B^2\Sigma_u^+$ of N_2^+

The radiation produced by the $B^2\Sigma_u^+$ to $X^2\Sigma_g^+$ transition of the nitrogen molecular ion is referred to as the first negative system. See energy level diagram in Fig. 8. The lifetime of the zero vibrational level of the $B^2\Sigma_u^+$ state is probably capable of being measured more accurately than any other molecular vibrational level. The reasons that this is so are many. The electron production cross-section for this level from the neutral nitrogen molecule is large. Since the transition occurs in the nitrogen molecular ion, resonance absorption of the radiation occurs only from the produced ion. With short excitation pulses the ion number density may be kept low. Cascading levels into this level are very weak and have relatively very long lifetimes. The lifetime of the $B^2\Sigma_u^+(v' = 0)$ level is long enough to be easily measured by the apparatus yet short enough so that collisional effects can be made small.

Due to the possibility of precise measurements of the lifetime of this vibrational level, it was chosen for the study of any dependence of the lifetime on the rotational level. The $B^2\Sigma_u^+(v' = 0)$ to $X^2\Sigma_g^+(v'' = 0)$ is the strongest transition from the upper level and results in the emission of radiation with the bandhead at 391.4 nanometers. The band system was resolved into 35 rotational components of the R branch. Figure 17 is a spectrogram showing these components. (Since the spin splitting of the rotational levels was not observable with the apparatus used, this transition will be discussed as if it were a $^1\Sigma$ to $^1\Sigma$ transition.) In order to ascertain the pressure at which the lifetimes should be measured

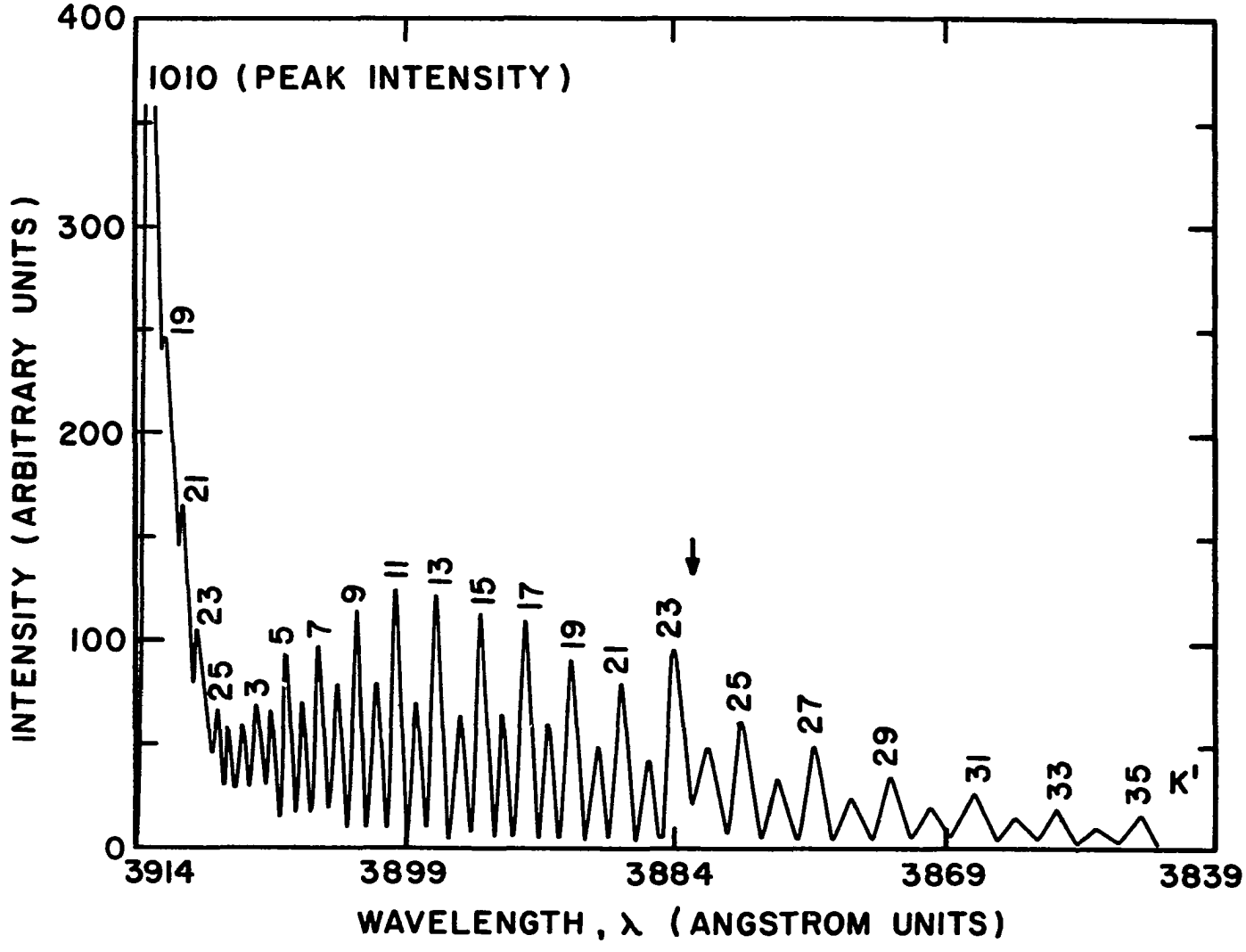

Figure 17. Spectrogram of the Rotational Structure of the $B^2\Sigma_u^+(v' = 0)$ to $X^2\Sigma_g^+(v' = 0)$ Transition.

so that collisional terms would be negligible, the pressure dependency of the lifetimes was examined. A more extensive, low pressure examination of the lifetimes was then performed.

Pressure Dependency

The pressure dependencies of the lifetimes of the three rotational levels (K' = 11, 19, 31) of the (v' = 0) vibrational level and of the lifetime of the (v' = 1) vibrational level of the $B^2\Sigma_u^+$ state were measured. Combination System V was used to perform the measurements. Four lifetimes for each referred to level were measured at a pressure of 0.12, 0.24, 0.5 and 1.0 Torr, which correspond to a number density of 0.10, 0.21, 0.43 and 0.87 x $10^{16}cm^{-3}$, respectively, at the measured cathode temperature of 1100 K. Figures 18, 19, 20 and 21 are graphs of the measured reciprocal lifetimes versus the number density. The solid straight line is the estimated best fit to the data points. The error bars represent the maximum estimated error in the precision of the measurements. These measurements are estimated to be accurate to within ± 6 per cent of the given value.

Two decay curves are illustrated in Figs. 22 and 23 to demonstrate the pressure dependence. Both are of the $B^2\Sigma_u^+(v' = 1)$ level. Figure 21 was obtained at 0.12 Torr and Fig. 22 at 0.24 Torr. The measured lifetimes were 56.2 and 54.6 nanoseconds, respectively.

The values of the lifetimes, τ, at zero pressure are given in Table 9 which were obtained from Figs. 18, 19, 20 and 21. The quoted errors are the precision errors. The accuracy error is ± 6 per cent.

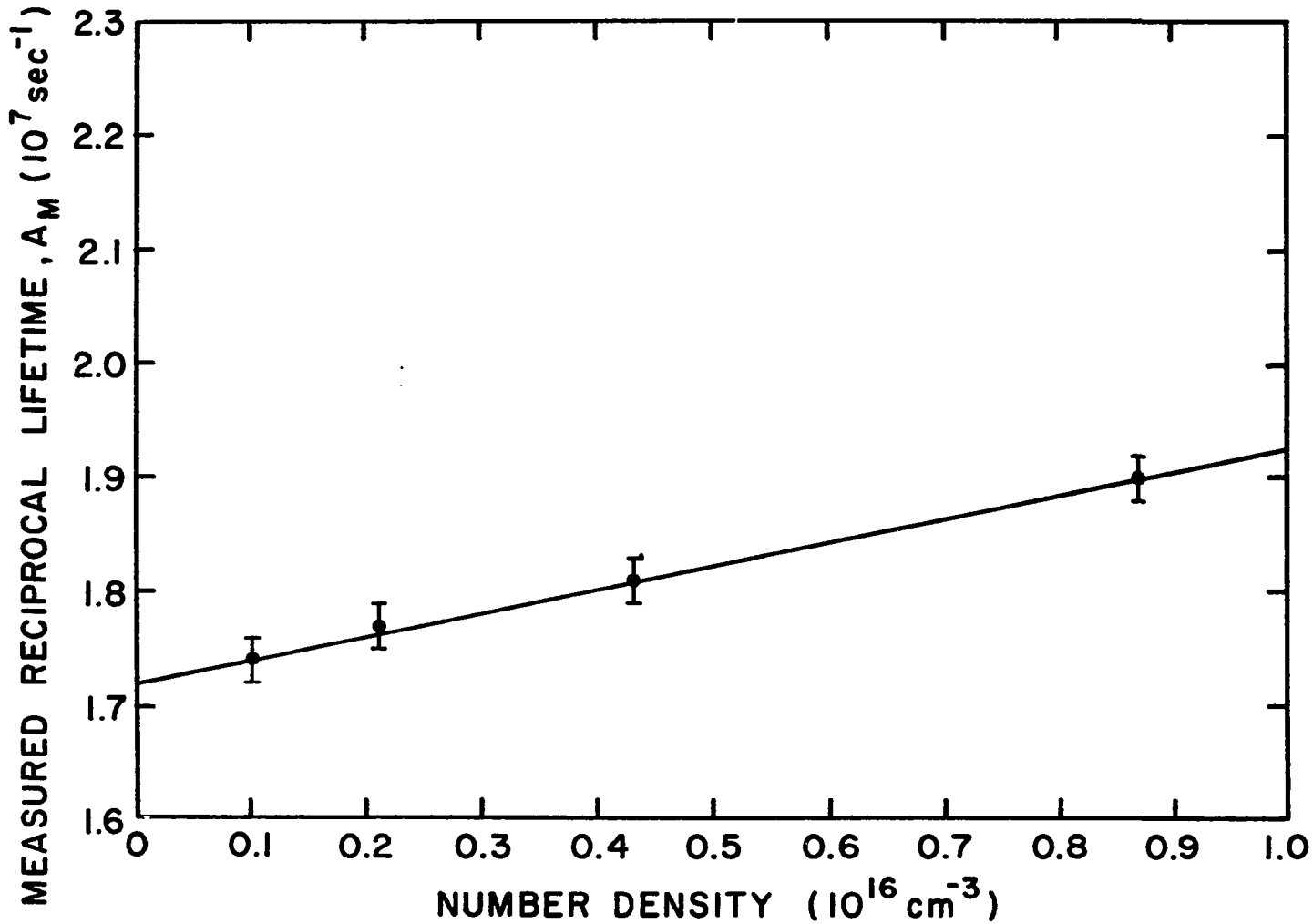

Figure 18. Pressure Dependence of the Reciprocal Lifetimes of the $B^2\Sigma_u^+(v' = 0, K' = 11)$ Level of N_2^+.

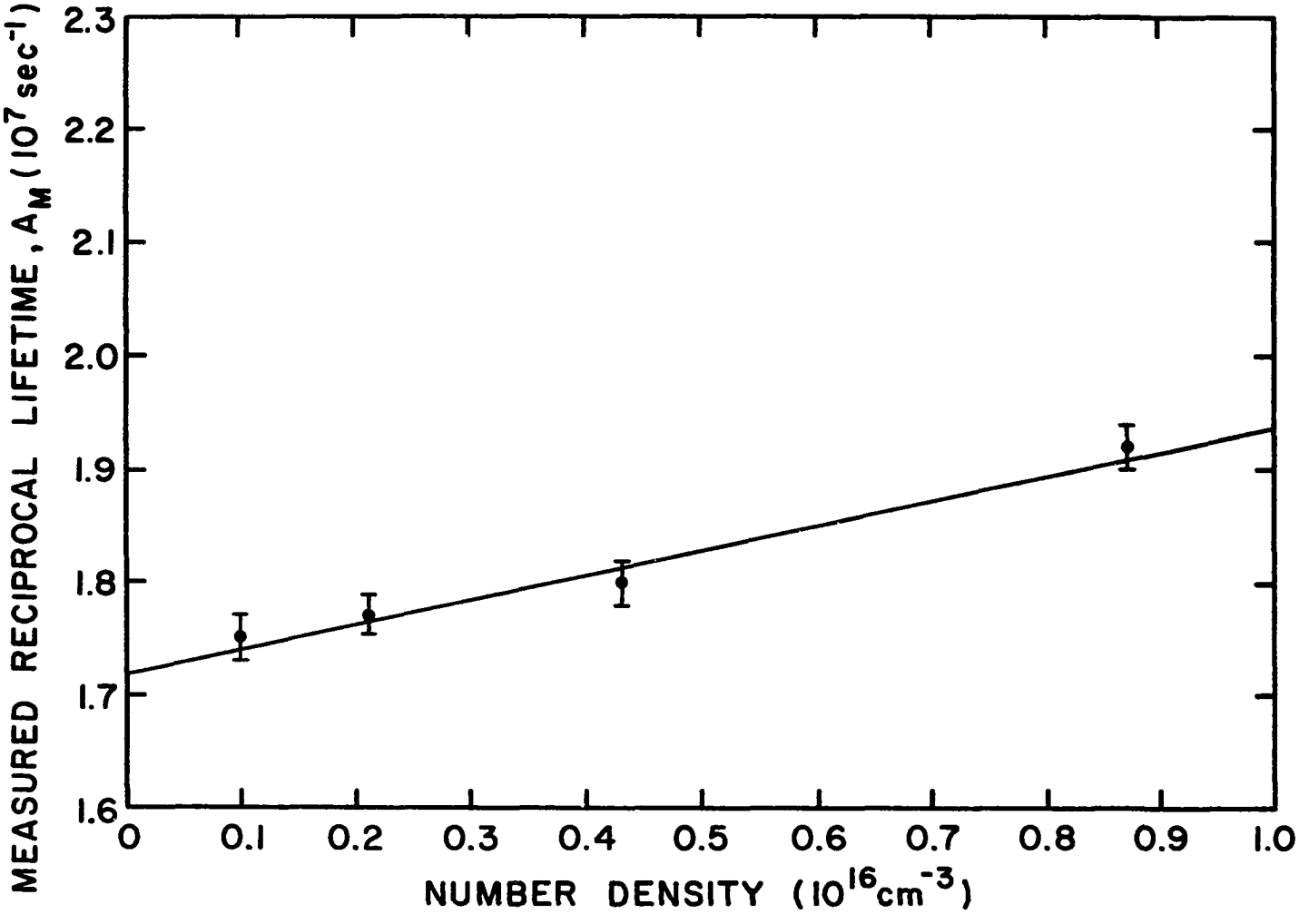

Figure 19. Pressure Dependence of the Reciprocal Lifetimes of the $B^2\Sigma_u^+(v' = 0, K' = 19)$ Level of N_2^+.

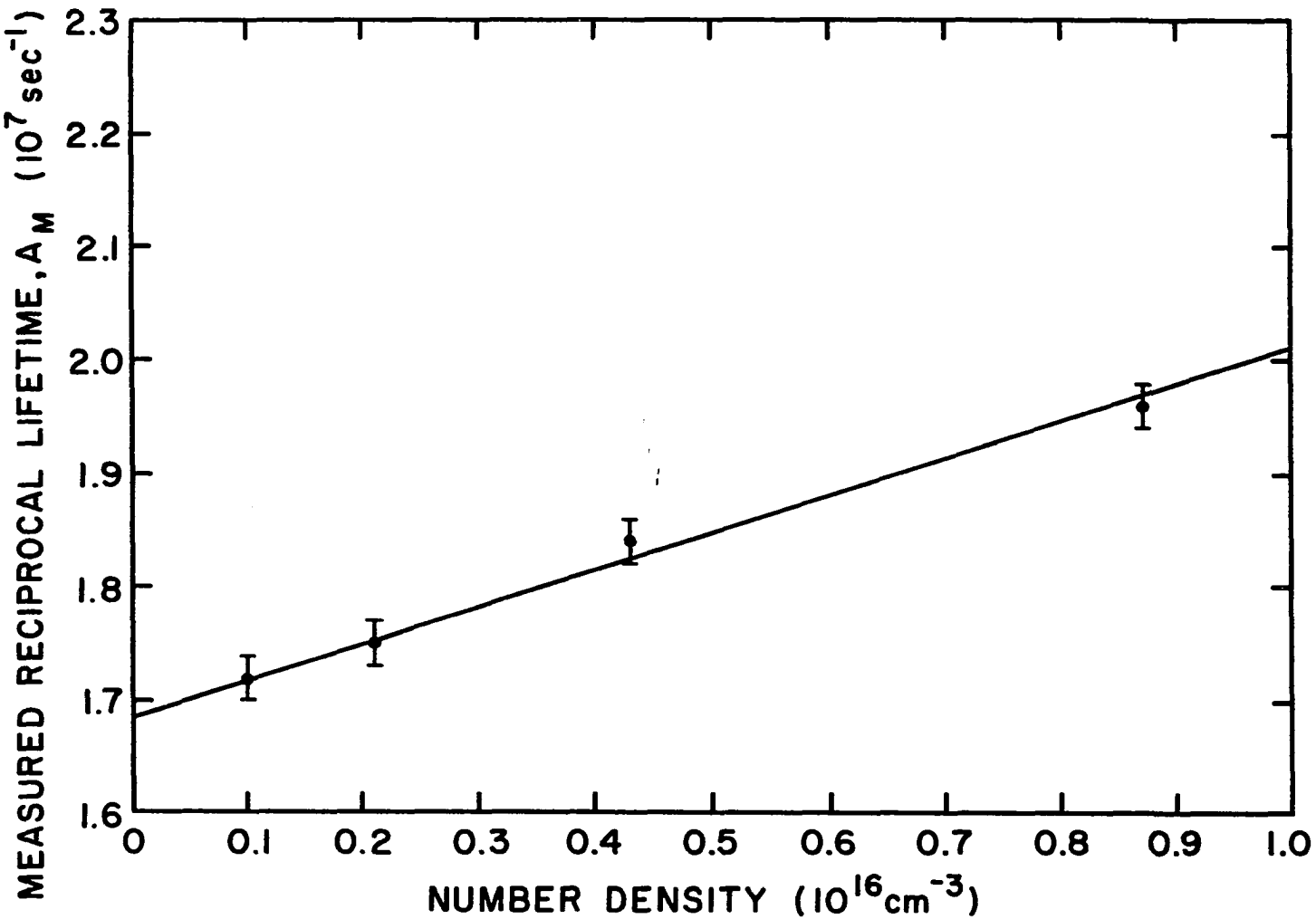

Figure 20. Pressure Dependence of the Reciprocal Lifetimes of the $B^2\Sigma_u^+(v' = 0, K' = 31)$ Level of N_2^+.

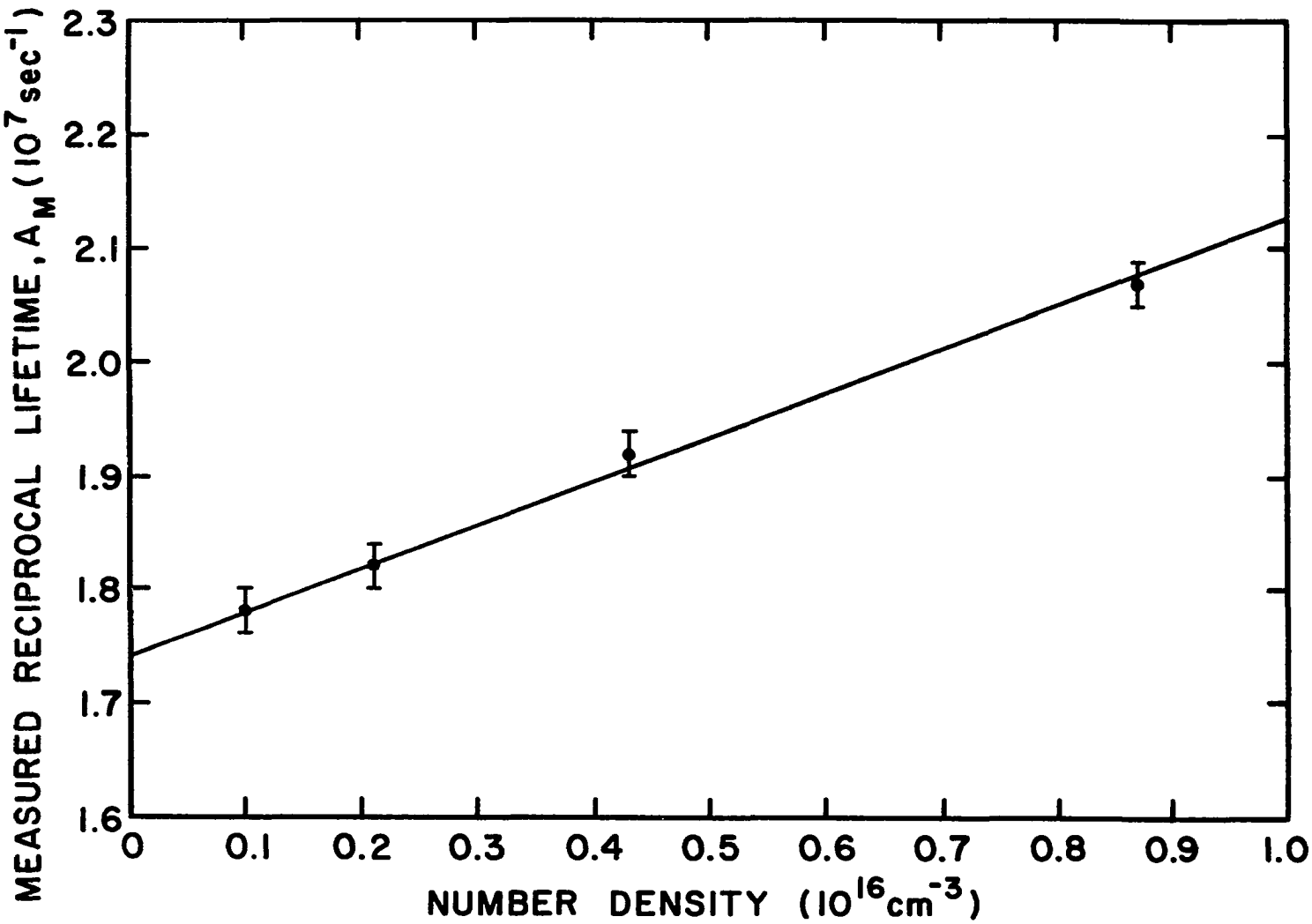

Figure 21. Pressure Dependence of the Reciprocal Lifetimes of the $B^2\Sigma_u^+(v' = 1)$ Level of N_2^+.

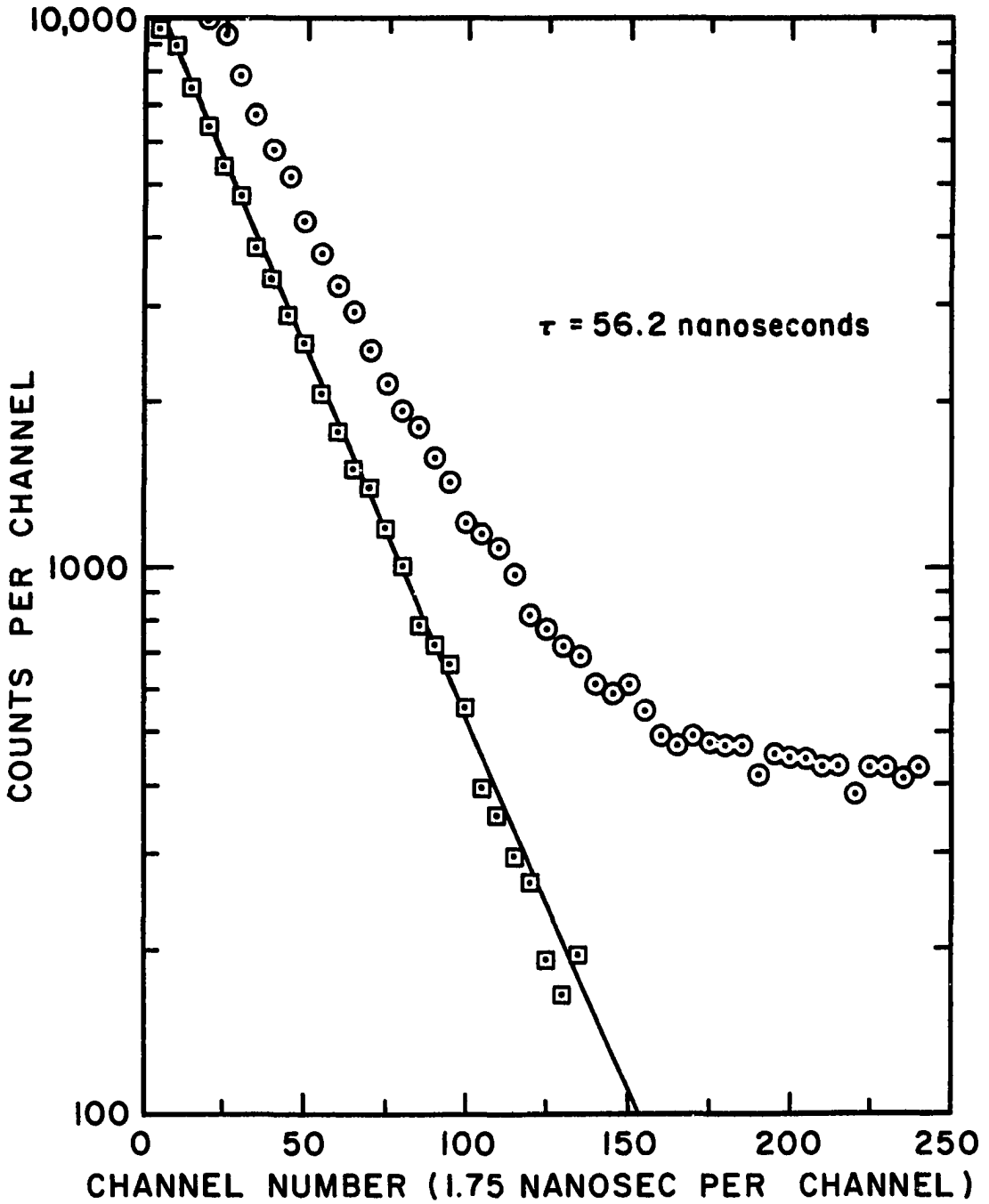

Figure 22. Decay Curve of the $B^2\Sigma_u^+(v' = 1)$ Level at 0.12 Torr.

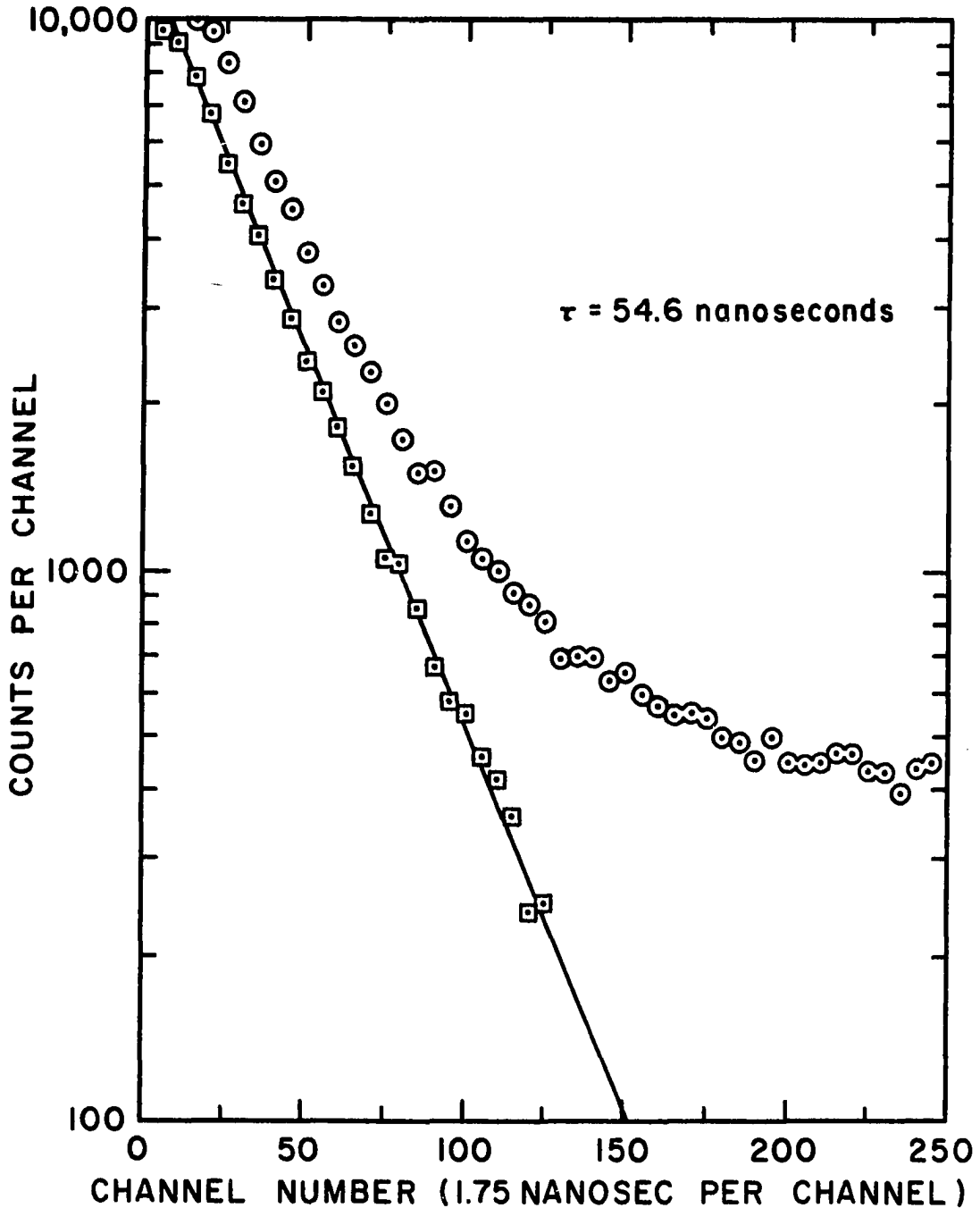

Figure 23. Decay Curve of the $B^2\Sigma_u^+(v' = 1)$ Level at 0.24 Torr.

Table 9. Zero Pressure Lifetimes and Depopulation Cross Sections of the $B^2\Sigma_u^+$ ($v' = 0$, $k' = 11$, 19 and 31) and $B^2\Sigma_u^+(v' = 1)$ Levels of N_2.

	$v' = 0$			$v' = 1$	units
	$K' = 11$	19	31		
τ	59.1±1.4*	59.2±1.4*	59.3±1.4*	58.5	10^{-9}sec
σ	2.07	2.22	3.28	3.94	$10^{-15}cm^2$

*Estimated precision.

Also included in Table 9 are the measured effective depopulation cross-sections, σ, calculated from the same figures. The measured depopulation cross sections σ given in Table 9 are nearly the same as the diffusion cross section of nitrogen ($3.42 \times 10^{-15} cm^2$) as tabulated in the Landolt-Bornstein Tables.[34]

From Figs. 18, 19 and 20 the approximate error in a measured lifetime due to collisional depopulation can be determined. At a temperature of 1100 K and pressures of 0.05 Torr or less, the error is less than 0.3 nanosecond for the K' = 11, 19 and 31 rotational levels of the $B^2\Sigma_u^+(v' = 0)$ level.

A compilation of the direct measurements of the lifetimes of the $B^2\Sigma_u^+(v' = 0)$ level is given in Table 10. The first direct measurements were performed by Bennett and Dalby.[4] They used interference filters to resolve the emitted radiation from the excited gas. The electron energy dependence of the lifetime which they observed was probably due to the mixing of the radiation from the second positive system in their photomultiplier tube. Consequently, they probably underestimated their error. Nevertheless, their result and the result of this work do agree within the experimental error. Fink and Welge[5] quote a value of 45±4 nanoseconds as the lifetime of this level. However, a straight-forward extrapolation of their data to zero pressure gives a value of 59 nanoseconds. They also probably had a spectral resolution problem. The electron energy dependent lifetime which they measured for the $B^2\Sigma_u^+$ state approaches the lifetime of the $C^3\Pi_u$ state. A persual of their nitrogen spectrum for different energy values leads to the conclusion

Table 10. Measured Lifetimes for the $B^2\Sigma_u^+(v' = 0)$ Level.

Experimentalist	τ(nanoseconds)
Bennett and Dalby[4]	65.8±3.5
Fink and Welge[5]	45 ±4 (59)*
Sebacher[6]	65 ±2
Fowler and Holzberlein[7]	70 ±15
Jeunehomme[8]	71.5±5
Hesser and Dressler[9]	59 ±6
Nichols and Wilson[10]	65.9±1
This work	59.2±4

*Value obtained by extrapolation to zero pressure from their data.

that for lower energies the radiation from the $C^3\Pi_u$ state could indeed have dominated the spectral range in which the $B^2\Sigma_u^+$ radiation occurs. Thus, they should have regarded the dependency of the lifetime on electron energy as instrumental. Their pressure dependent lifetime of 59 nanoseconds agrees well with the results of this work.

Sebacher's[6] result for the $B^2\Sigma_u^+$ level barely agrees to within the quoted error with the results of this work. He used a 10 KeV pulsed electron gun as the excitation source. However, there was not enough information in the published article to comment on the measurement. The result of Fowler and Holzberlein[7] agrees with the result of this work. Jeunehomme's[8] result does not agree with the results of this work. One possible difficulty he might have had was a large cascade component in the radiation. The excitation pulse he used was a r-f discharge which acted for a relatively long time before termination. Consequently, the long lifetime cascade components had time to become significant in the decay curve, thus complicating the analysis. A more severe problem was the long cut-off time (quoted at 25 nanoseconds) of his excitation pulse. Early measurements made in this work on the $B^2\Sigma_u^+$ levels with Combination System I indicated that the lifetimes were about 70 nanoseconds. This value was the result of a band pass in the electronic equipment equivalent to only 20 nanoseconds. A cut-off time of 25 nanoseconds could easily produce a measured lifetime for this level as large as 71.5 nanoseconds, which is Jeunehomme's reported value. The result of Hesser and Dressler[9] agrees well with the result of this work. They used a phase shift technique to measure this lifetime. This level is particularly

well suited for measurement by a phase shift technique for the same reasons given at the beginning of this chapter.

The listed result in Table 10 by Nichols and Wilson[10] is added only for completeness. In their article, they reported only this result with no description of the analysis necessary to obtain this result. Consequently, no comment is possible.

Rotational Level Dependency

No previous test has been made on the possible dependency of molecular lifetimes on the rotational levels of a given vibration level. The theory predicts (see Chapter II) that the rotational lifetimes should remain nearly constant, with a possible small change due to the frequency term in the transition probabilities. The rotational lifetimes of the $B^2\Sigma_u^+(v' = 0)$ level were examined to test the validity of these assumptions by monitoring the radiation decay of the $B^2\Sigma_u^+(v' = 0) \rightarrow X^2\Sigma_g^+(v'' = 0)$ transition.

In Fig. 17, a spectrogram of the 3914Å band is reproduced to demonstrate the rotational structure of the $B^2\Sigma_u^+(v' = 0)$ level. This spectrogram was obtained by monitoring the emitted radiation only within -25 and +50 nanoseconds of the time of cessation of the excitation in the invertron. For this reason, it is referred to as a time dependent spectrum. The original data was corrected for the double photon effect with the use of Eq. (52) and (56). Figure 17 is the plot of the corrected results. The rotational level which produces the lines are labeled. The P branch is only partly resolved, so that branch is not all labeled. All the lifetime measurements were made on the R branch. The arrow notes a change in the

slit width of the monochromator. The alternating intensity structure demonstrated in this figure is characteristic of Σ states of homonuclear molecules. The envelope of the maximum peaks (with the exception of $K' = 23$) is a simple result of the gas temperature and the level statistical weight. The $K' = 23$ level is overlapped by the bandhead (3884.3Å) of the $B^2\Sigma_u^+(v' = 1) - X^2\Sigma_g^+(v'' = 1)$. The existence of this level was fortuitous. It was difficult and tedious to adjust the monochromator on a particular line. However, the reference offered by the 3884.3Å transition plus the alternating intensity pattern of the lines greatly facilitated the monochromator adjustment.

The pressure dependent results previously described of the $B^2\Sigma_u^+$ level indicated that collisional depopulation effects would change these lifetimes by less than 0.3 nanoseconds at pressures of 0.05 Torr or less. All of the results now to be described were obtained from data taken at pressures lower than this value.

Thirty-nine measurements of the lifetimes of various rotational levels from $K' = 7$ to $K' = 35$ were made. Figures 24 to 28 are plots of the multichannel analyzer output of some of these measurements. (All measurements were made with Combination System V.) A short excitation pulse was used to minimize any possible long cascade components. As can be seen in the figures, only a small part of the curve is due to anything other than the one exponential decay.

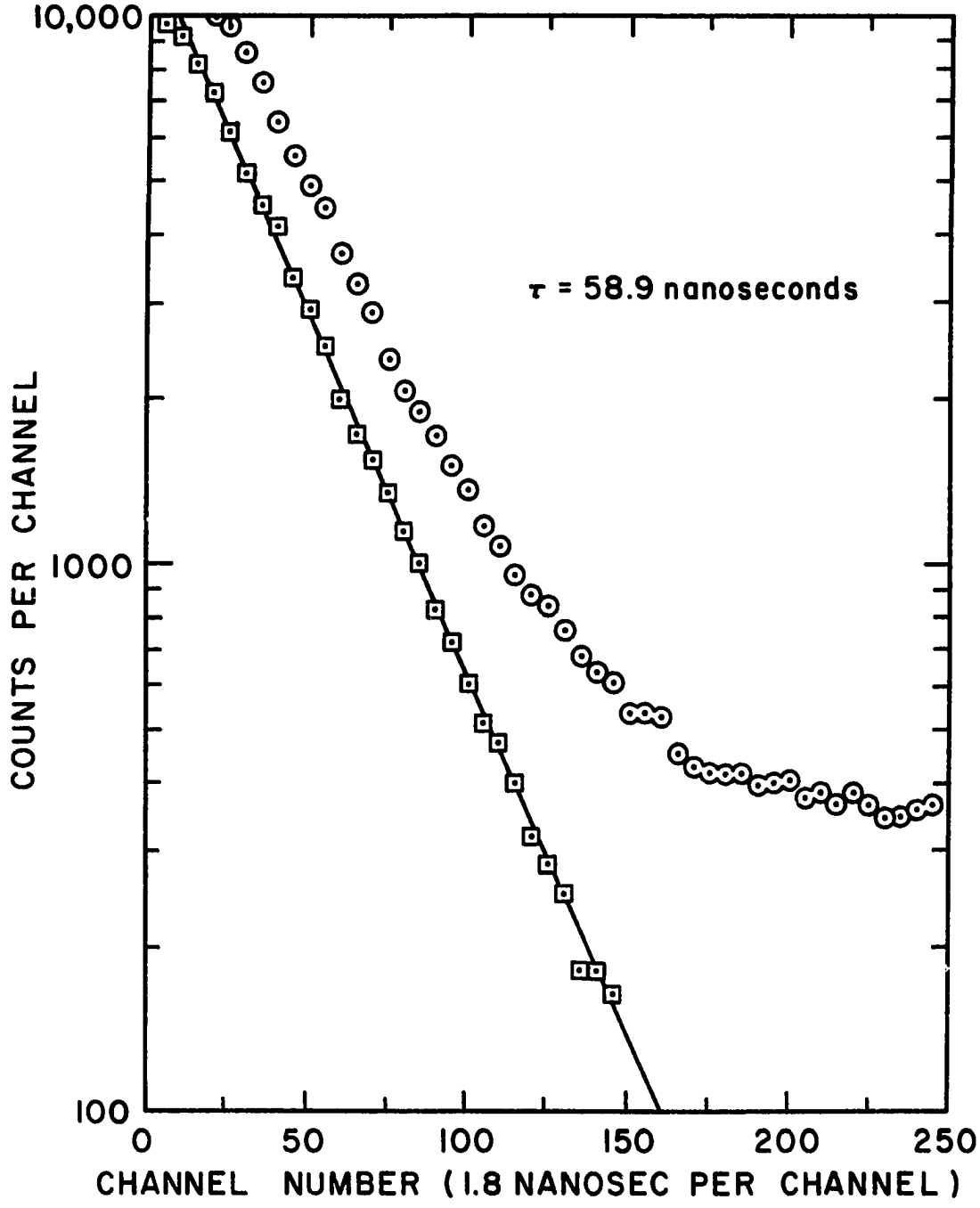

Figure 24. Decay Curve of the $B^2\Sigma_u^+(v' = 0, K' = 7)$ Level.

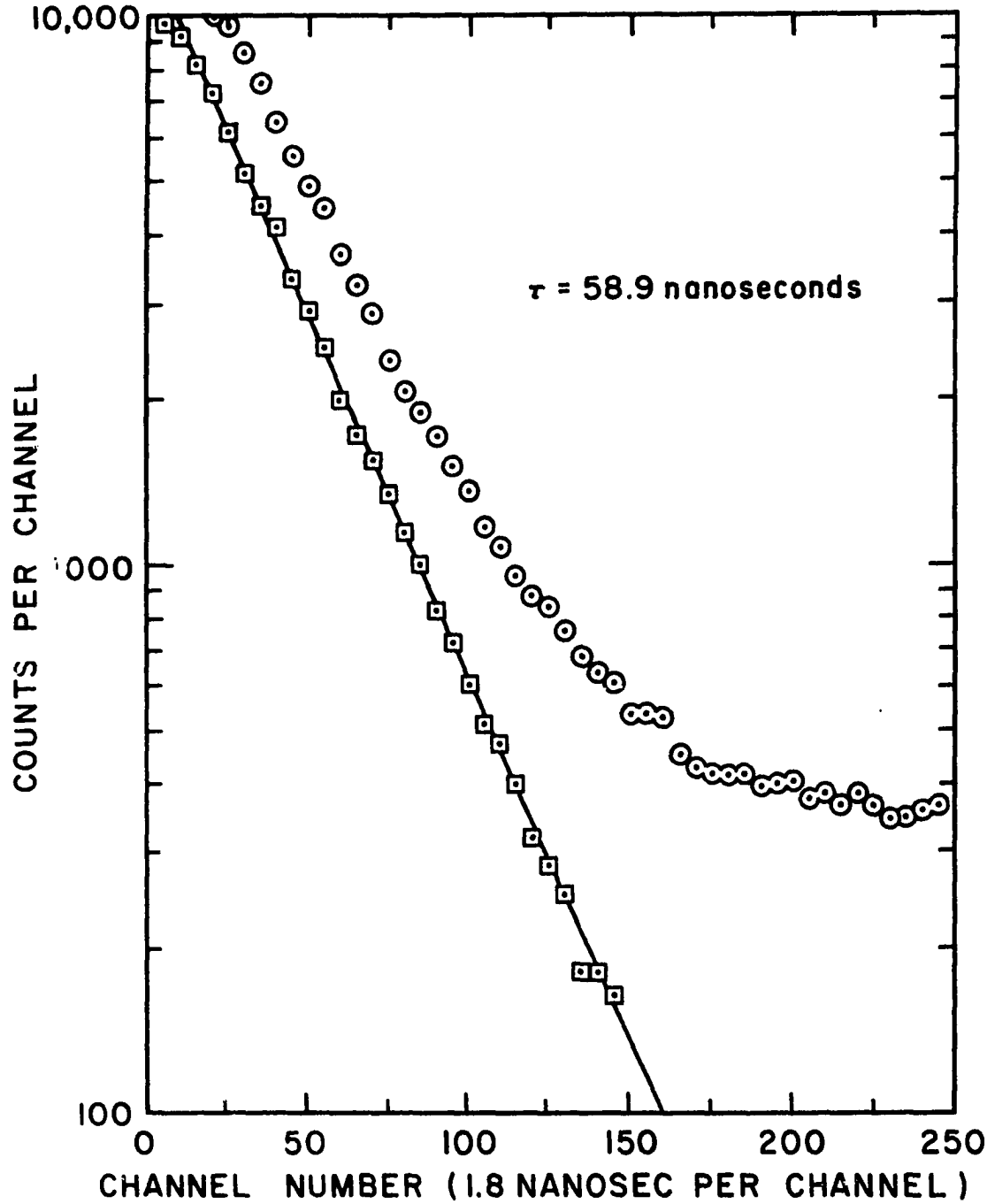

Figure 24. Decay Curve of the $B^2\Sigma_u^+(v' = 0, K' = 7)$ Level.

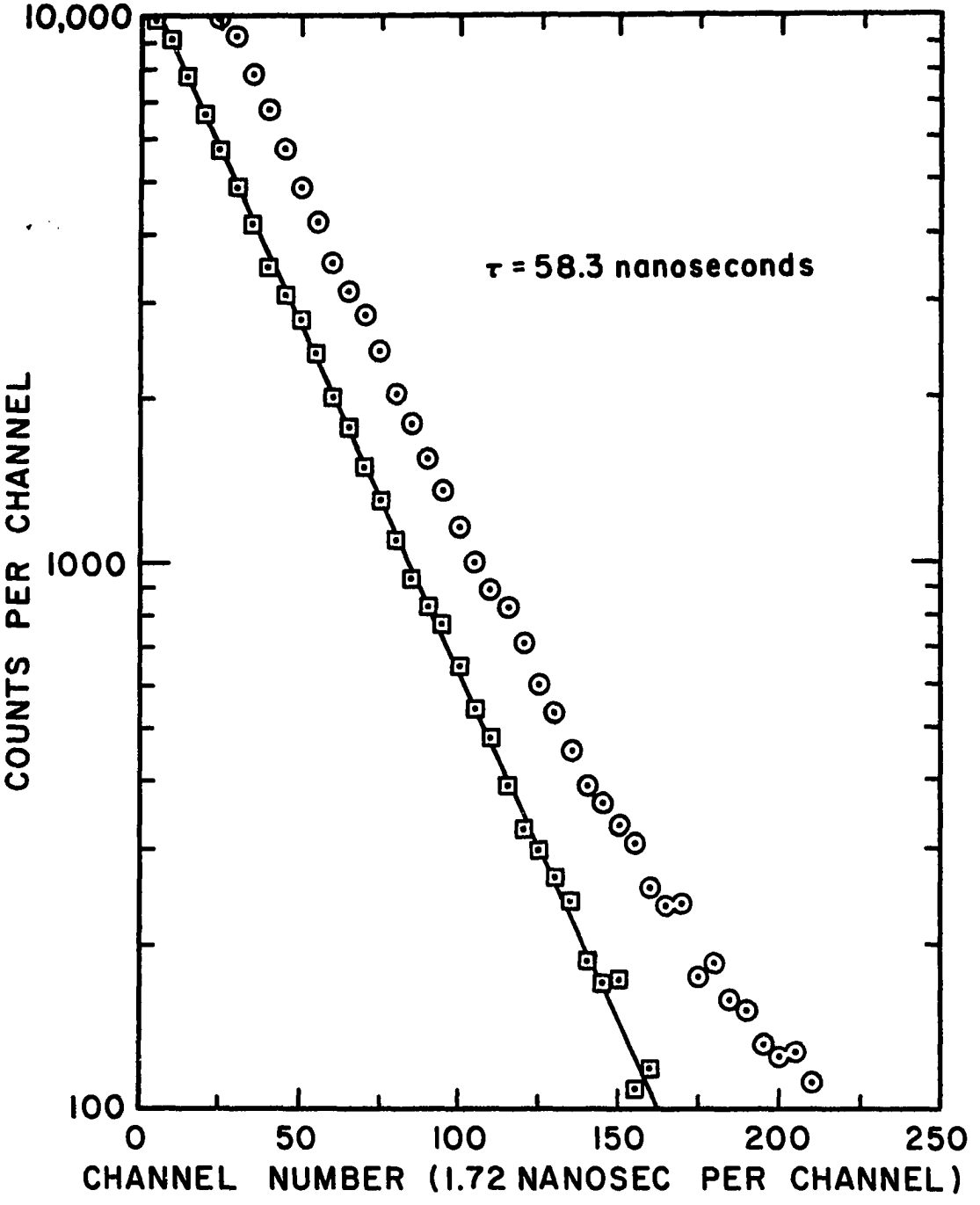

Figure 25. Decay Curve of the $B^2\Sigma_u^+(v' = 0, K' = 15)$ Level.

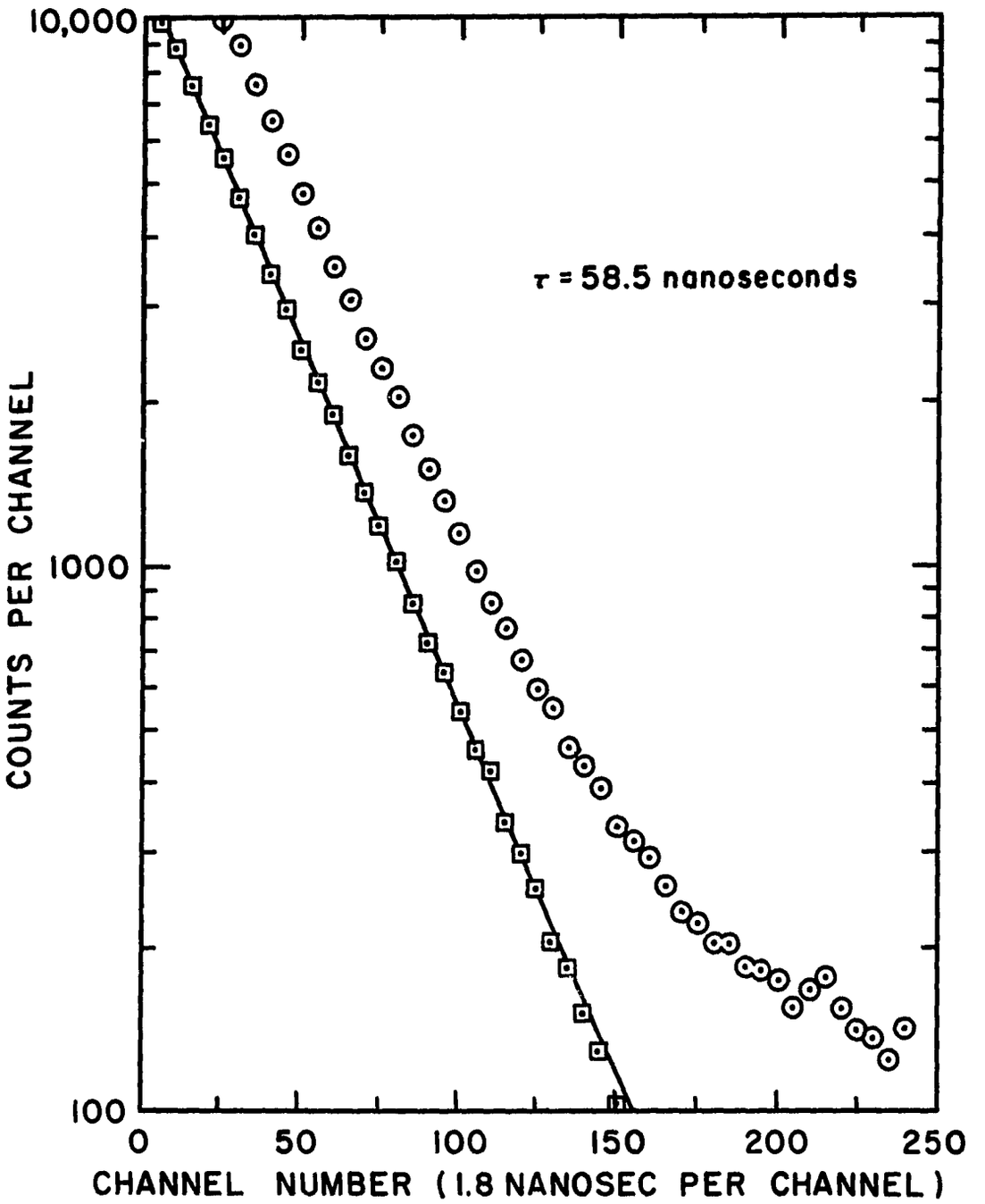

Figure 26. Decay Curve of the $B^2\Sigma_u^+(v' = 0, K' = 17)$ Level.

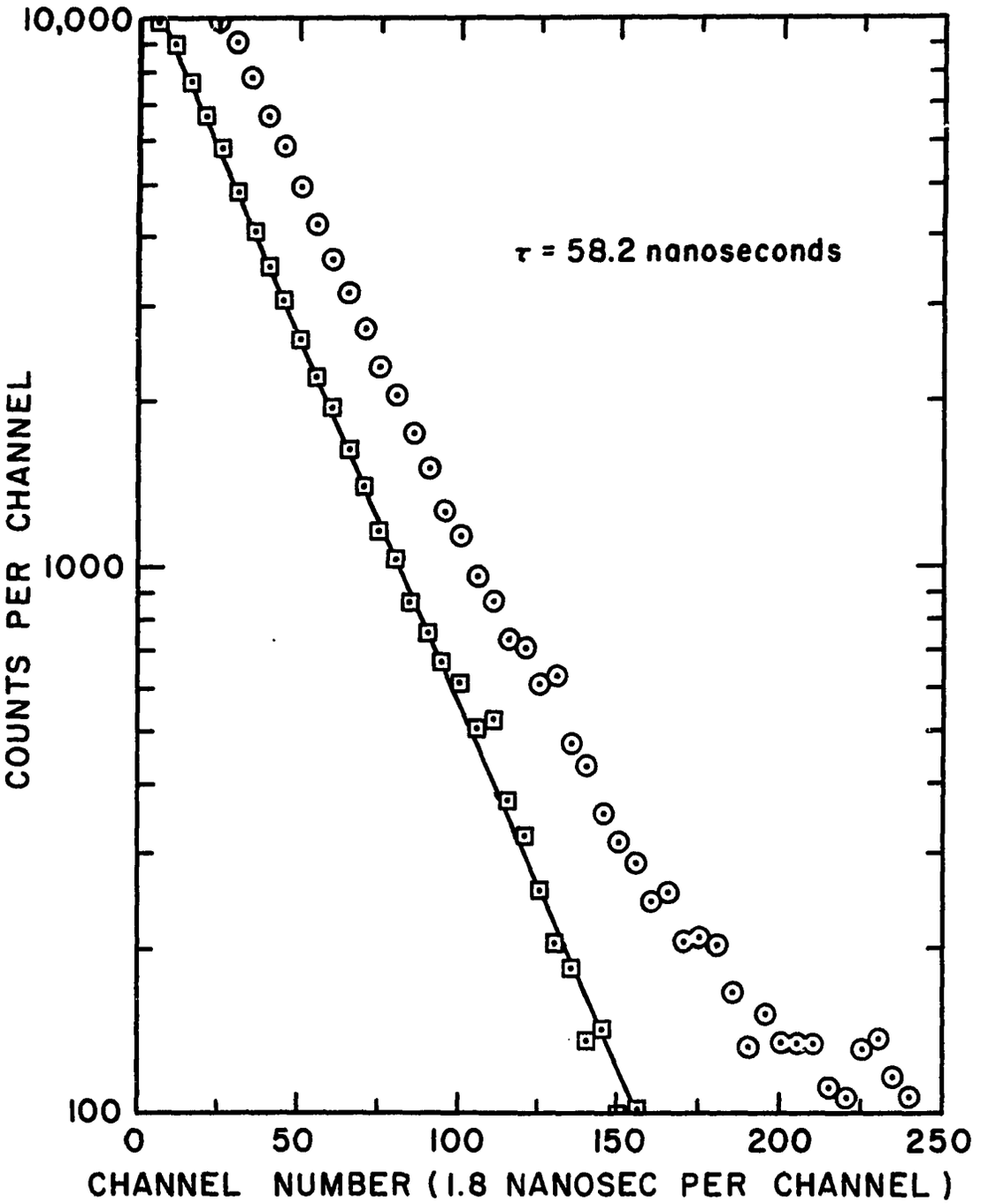

Figure 27. Decay Curve of the $B^2\Sigma_u^+(v' = 0, K' = 19)$ Level.

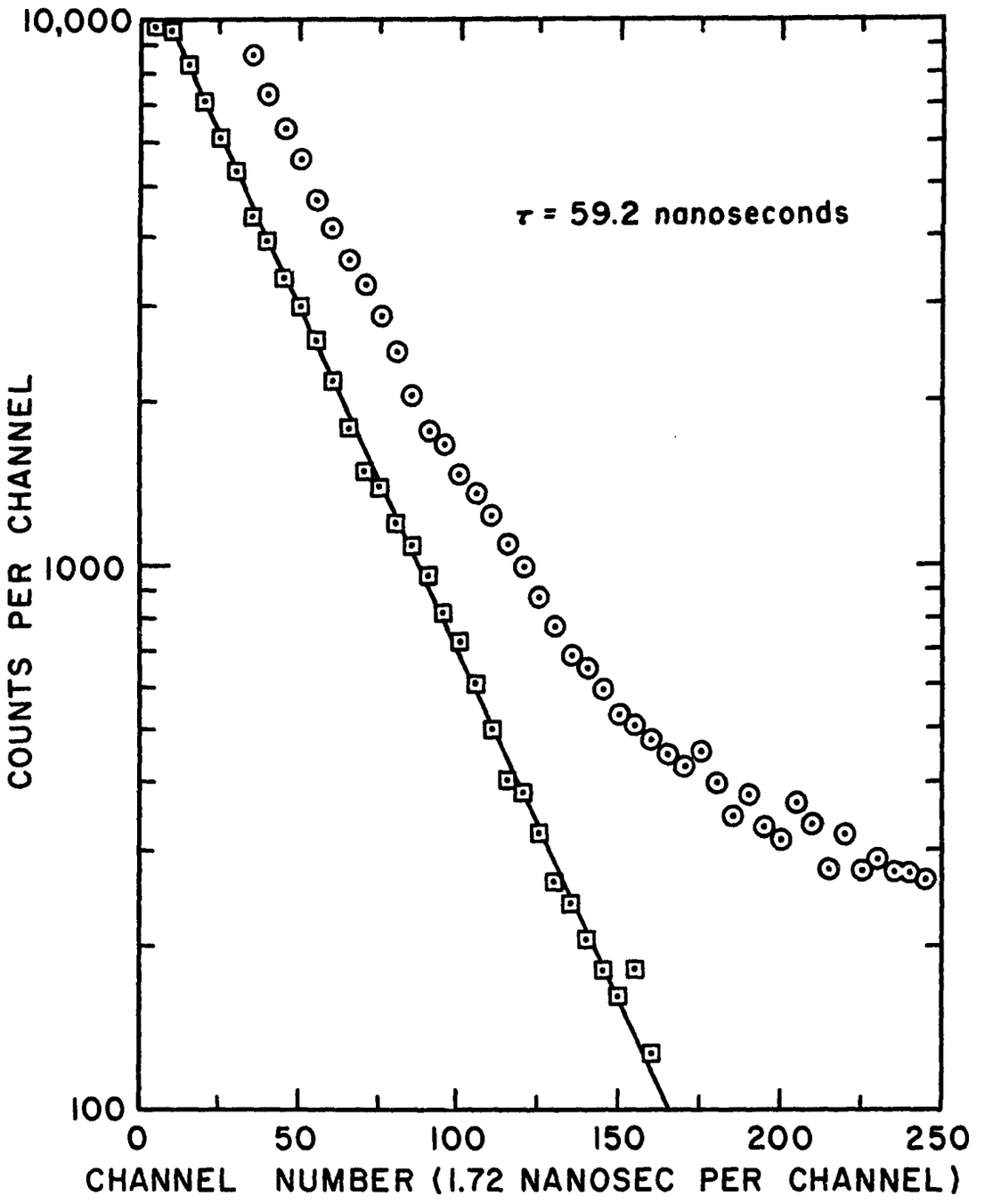

Figure 28. Decay Curve of the $B^2\Sigma_u^+(v' = 0, K' = 33)$ Level.

Since the measurements extended over a few days, the system was recalibrated six times with respect to the effective number of nanoseconds per channel. Table 11 gives the average values of the measured lifetimes for the listed ranges of K'. The quoted error is one standard deviation. (<2.5 per cent) The number of measurements for each range of K' is also given in Table 11.

Within the error of the measurements, the results indicate no dependency of lifetime on rotational level. Since the measurements were made with different time calibrations, the reproducibility of the experiment is apparently good.

In an attempt to analyze the data for very small dependencies of the lifetimes on the rotational levels, a different comparison was made. Only the two ranges, K' = 15 - 20 and K' = 30 - 35, were compared. The values in one range were compared to the values in the other range only for measurements made with the same absolute calibration. The total average difference (D_A) was then calculated from the differences (Di) in the values for a given absolute calibration condition.

$$D_A = \frac{\Sigma_i D_i}{n}$$

The total number of differences was n. The calculated result is as follows.

$$D_A = 0.35 \pm 0.71 \text{ nanosecond.} \qquad (62)$$

Table 11. Rotational Lifetimes of the $B^2\Sigma_u(v' = 0)$ Level of N_2.

K'	less 14	15-20	21-25	30-35
τ(nanosec)	59.6±1.4	58.5±0.8	59.5±0.3	59.5±0.9
#	6	16	4	13

Table 12. Vibrational Transition Probabilities of the $B^2\Sigma_u^+(v') - X^2\Sigma_g^+(v'')$ Transitions.

v'' \ v'	0	1
0	$A = 11.76 \times 10^6 sec^{-1}$	$6.39 \times 10^6 sec^{-1}$
1	4.07	3.90
2	.830	4.41
3	.158	1.73
4	$\sum_{v''=4}^{\infty} = .067$	.041
		$\sum_{v''=5}^{\infty} = .026$
τ	59.2 nanoseconds	58.5 nanoseconds

One standard derivation of the differences is 0.71. In Eq. (62) a plus value indicates a longer lifetime for the larger vibrational quantum number. From the calculated ratios of the lifetimes tabulated in Table 1, the value of D_A should be -0.95 nanosecond, which disagrees with the results in Eq. (62) by more than one standard derivation.

The results displayed by Eq. (62) indicate that the lifetime does not depend upon the rotational level, in agreement with the approximations used to obtain Eq. (16). The frequency corrections tabulated in Table 1 do not agree with the results displayed by Eq. (62). A small coupling of the vibrational and rotational motion probably accounts for the discrepancy. From a practical point of view, this small effect will be of negligible importance in energy transport calculations, since the experimental errors of all absolute values of lifetimes obtained from direct measurements are much larger than this relatively small frequency effect. Consequently, a lifetime obtained by monitoring the radiation in the bandhead is a useful parameter to use as the lifetime of all the rotational levels in the vibrational level under observation.

The transition probabilities (A) for the $v' = 0$ and 1 levels of $B^2\Sigma_u^+$ are given in Table 12. The relative intensities used in Eq. (5) to calculate the transition probabilities of Table 12 were taken from recent electron beam measurements.[35] The sum term listed in Table 12 was determined from the Franck-Condon factors given by Nichols.[36] The lifetimes used for these calculations are given in Table 12 beside τ.

Rotational Temperature of 3914Å Band of N_2^+

To test for the correlation between the temperature of the cathode and the temperature of the gas, measurements were made on the rotational temperature of the 3914Å Band of N_2^+, which results from the $B^2\Sigma_u^+(v' = 0)$ to $X^2\Sigma_g^+(v'' = 0)$ transition. Implicit in the following discussion is the assumption that the rotational Boltzmann distribution corresponds to a temperature which is equal to the kinetic temperature of the gas.

Figure 17 is a spectrogram of the 3914Å Band emitted from the pulsed invertron. The results were corrected for double photon distortion. Since the spectrum was taken within 100 nanoseconds of the invertron cutoff pulse, the emitted light intensity is due almost entirely to direct electron excitation of the excited level.

The number of particles in a given rotational band depends upon the temperature of the gas. For thermodynamic equilibrium, Herzberg has derived the following equation. The rotational temperature of the R branch of the 3914Å transition may be measured from the following equation.[15]

$$\log\left(\frac{I_{K'}{}^{R}}{2K'}\right) = A - \frac{B_{v'}K'(K'+1)hc}{kT_R} \quad . \tag{63}$$

$I_{K'}{}^{R}$ is the photon intensity in the R branch which originates from the K' rotational level, A is a constant, $B_{v'}$ is the vibrational spectroscopic parameter, T_R is the rotational temperature, c is the speed of light, and h and k are Planck's and Boltzmann's constants, respectively. Figure 29 is a plot $\frac{I_{K'}{}^{R}}{2K'}$ versus K'(K' + 1) of both the maximum and minimum peaks of

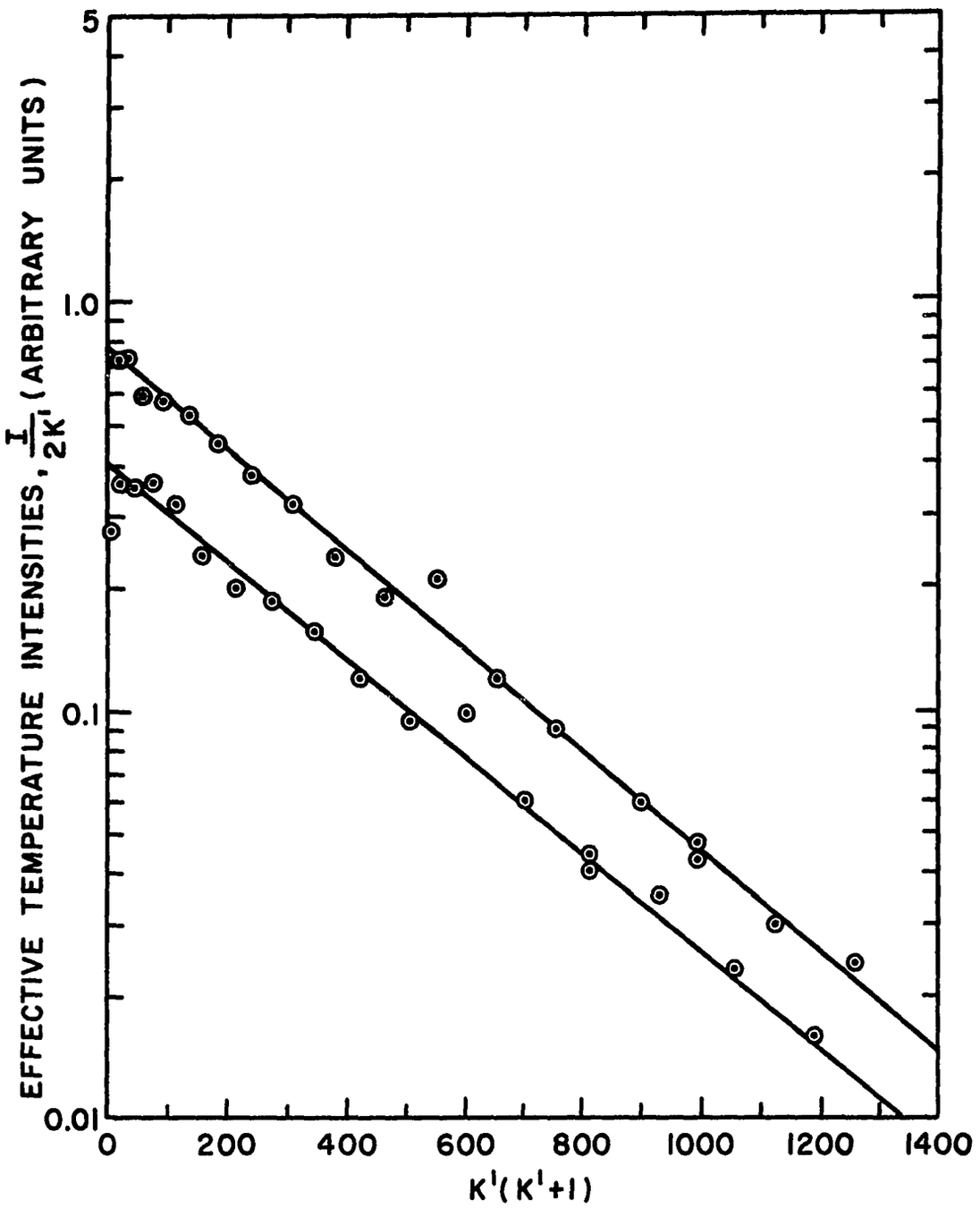

Figure 29. Rotational Intensity Dependence of the 3914 Å Band of N_2^+ (0.04 Torr).

the spectrum in Fig. 17. A plot of the same parameters of only the maximum peaks is given in Fig. 30 under another set of conditions. The anomalous peaks at K'(K' + 1) equal to 552 and 600 are due to the 3884.3Å bandhead of the $B^2\Sigma_u^+(v' = 1)$ to $X^2\Sigma_g^+(v' = 1)$ transition in N_2^+.

Table 13 gives the experimental conditions and the results obtained from Figs. 29 and 30. P is the pressure in the invertron. T_B is the brightness temperature of the invertron as measured with an optical pyrometer which had been calibrated against a tungsten lamp. T_R is the rotational temperature obtained from the slope of the lines in Figs. 29 and 30. The reasonable agreement between the rotational temperature and the measured temperature agrees with the assumption that the cathode brightness temperature and gas kinetic temperature are the same. If one assumes that the emissivity of the cathode is unity, then the above measurements indicate that the rotational temperature is the true temperature of the gas. Conversely, if one assumes that T_R of Eq. (63) is the true temperature, then this indicates that the emissivity of the cathode is one. Since the brightness temperature of the cathode was measured on the inside part of the invertron, the cavity effect of the cylindrical cathode approximates a black body. The difference between the brightness temperature and true temperature of a radiating body with an emissivity of only 0.3 is about 50° K at 1100° K. Since the emissivity of the invertron cathode is probably more than 0.3, these measurements indicate that the rotational temperature of the 3914Å Band is about 5 per cent less than the true temperature.

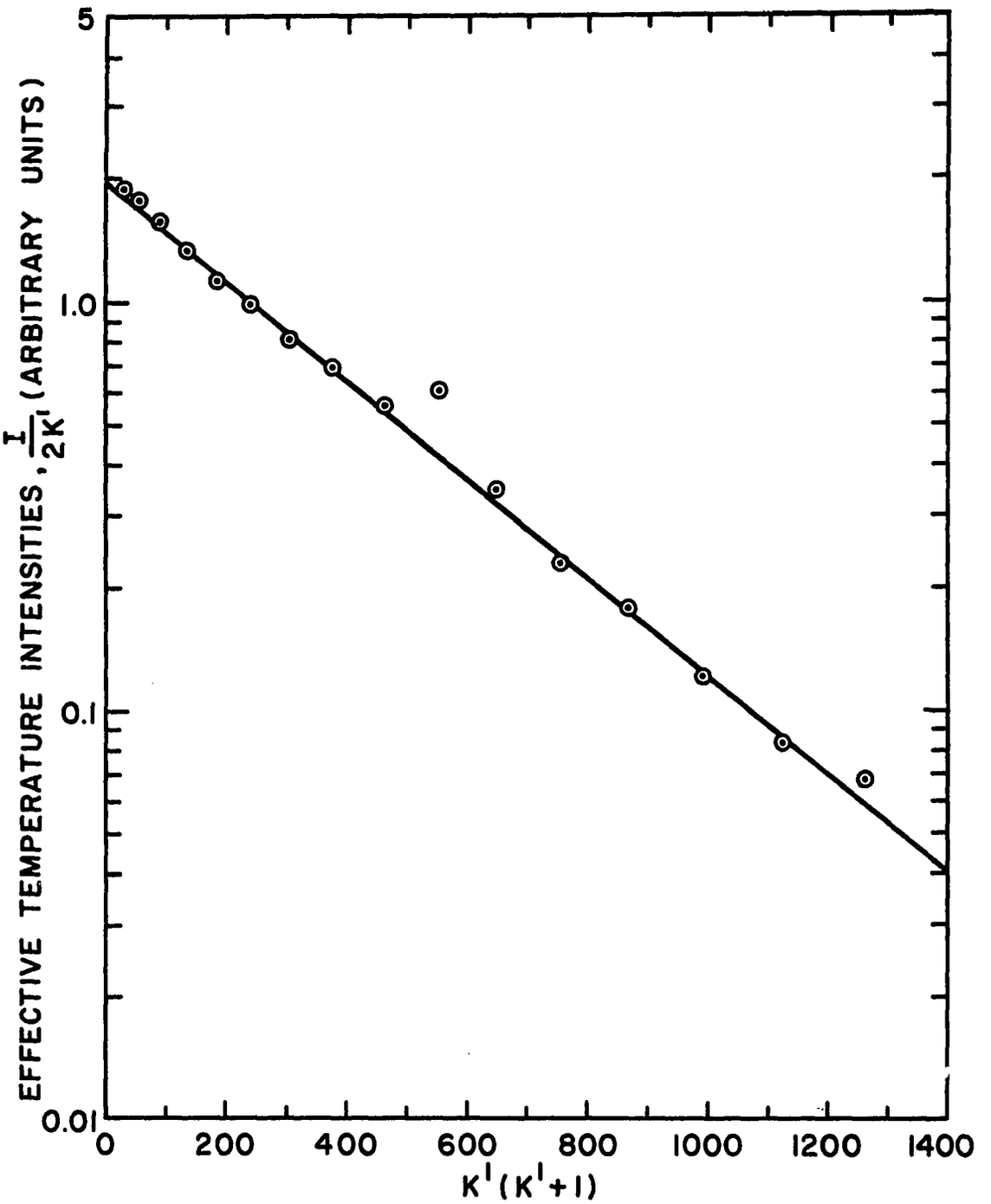

Figure 30. Rotational Intensity Dependence of the 3914 Å Band of N_2^+ (0.4 Torr).

Table 13. Comparison of Rotational Temperature (T_R) and Brightness Temperature (T_B)

	P Torr	T_R °K	T_B °K
Figure 29	0.05	1052	1078
Figure 30	0.4	1068	1123

Predissociation of $b^1\Pi_u(v' = 0)$ Level of N_2

The initial goal of these measurements was to determine the importance of those radiations, which are called the Birge-Hopfield bands, in energy transport in nitrogen. The lifetimes of the upper levels of the Birge-Hopfield bands are parameters which are necessary to describe the energy transport. Since the Birge-Hopfield bands which originate on the $b^1\Pi_u(v' = 1)$ level are in the vacuum u-v (1050 - 1438Å), the invertron was connected to a vacuum u-v monochromator. (See energy level diagram in Fig. 8.) The lifetimes of these levels was expected to be about one nanosecond. Thus the very rapid cut-off pulse of Combination System VI was believed necessary for these measurements. (Indeed, the system was originally designed to make these measurements.)

The invertron was first connected to the vacuum ultraviolet monochromator with a standard double slit arrangement. The first slit was used as a pump slit and the second slit was used as the entrance slit to the spectrograph. The region between the two slits was pumped to maintain a difference of pressure in the monochromator and the invertron. The excitation voltage to the invertron was generated with a mercury switch system.

First, the emission spectrum of hydrogen was observed between 1500-1000Å. Lyman-α and Lyman-β, plus the multiline family of the hydrogen molecule, were readily observed when hydrogen was admitted to the invertron. When nitrogen was admitted to the invertron, only the nitrogen atomic spectrum was detectable in this region. In order to assure that the $b^1\Pi_u$ emission spectrum was not absorbed in the space between the invertron and the slits, or in the monochromator, several things were done. The spectrograph was cleaned, new seals were put in place, the pump oil was replaced, and a new grating was obtained. A LiF window was used instead of the differential pump slit to allow the shortening of the length between the invertron and entrance slit. The excitation pulse was changed to one generated by a real coaxial cable. (Combination System V). This allowed for shorter pulse widths to eliminate the possibility of build up of the higher vibrational levels, which might then absorb the radiation from the $b^1\Pi_u$ states. In addition, a gas flow system was employed to assure that the gas in the invertron would be replaced between excitation pulses.

With these changes, a survey of the radiation from the invertron was again undertaken. First, the dark current of the photomultiplier was measured and was found to correspond to an effective 0.005 counts per excitation pulse to the invertron. The counts here refer to the number of single electrons originating at the photocathode of the photomultiplier during the time increment of 100 nanoseconds. This time increment was located from 20 nanoseconds before to 80 nanoseconds after the excitation pulse to the invertron was stopped. In the case of the dark current measurements, each pulse may correspond to more than one electron at the photocathode. In the measurement of the count rates due to photoelectrons, the probability of a double electron pulse can be disregarded for the conditions to be cited.

At a resolution of 3.5 Å on the vacuum ultraviolet monochromator, the radiation from the $2p^2(^3P)3s \rightarrow 2p^3$ transition array of the $^4P \rightarrow {}^4S^0$ multiplet ($\simeq$ 1200 Å) of nitrogen gave a measured output of greater than 0.1 counts per pulse. The gas pressure in the invertron was 0.01 Torr. The accelerating voltage applied to the invertron was 200 V.

Under the same conditions, the spectral range from 1200 Å to 1300 Å was carefully observed. An additional atomic transition was observed and identified at 1243 Å. At all other points in this spectral range, the output count rate was nearly constant and about twice the dark current rate. The monochromator was set at 1258 Å, a point of an expected transition from the $b^1\Pi_u$ state. A decay curve was obtained at this wavelength. Although the curve had considerable noise superimposed on it, a lifetime of roughly 60 nanoseconds was obtained.

The uniform count rate observed between 1200 Å and 1300 Å was probably due to a very low level of scattering in the monochromator of the 1st Negative system of N_2^+ and the 2nd Positive system of N_2 which have a measured lifetime of 59 and 39 nanoseconds, respectively.

A similar examination was undertaken in the spectral range 1000 to 1100 Å with similar results: no detectable emission from the $b^1\Pi_u$.

Explanation of Results

For short electron excitation pulse widths, the number of excited states at time t is given by:

$$N_{b1} = N_{XO} \frac{i}{eB} \frac{\sigma(XO\text{-}b1)}{\Sigma_j A(b1 - Xj)} [1-\exp(-t/T_1)] \quad . \tag{64}$$

i is the current in the beam, e is the charge of the electron, B is the area of the beam, (T_1) is the lifetime of the b1 level, σ(XO-b1) is the cross section for electron excitation from the XO level to the b1 level, N_{XO} is the number density of the molecules in the XO level, and A(b1-Xj) is the transition probability from the b1 to the Xj level. Notice that

$$1/(T)_1 = \Sigma_j A(b1\text{-}Xj) \quad .$$

The emitted radiation, I(b1-Xj), for a particular transition is

$$I(b1\text{-}Xj) = A(b1\text{-}Xj)N_{b1} \quad . \tag{65}$$

For times longer than T_1, the radiation Eq.(65) becomes approximately,

$$I(b1\text{-}Xj) \quad N_{XO} \frac{i}{eB} \frac{A(b1\text{-}Xj)}{\Sigma_k A(b1\text{-}Xk)} \sigma(XO\text{-}b1) \quad . \tag{66}$$

Let b1 be the $b^1\Pi_u(v' = 1)$ level[37] and Xj be the $X^1\Sigma_g^+(v'' = j)$ level of N_2. From Eq. (64), it is seen that the parameters applicable to a particular state are the cross section for production and the ratio of the transition probability of the particular transition to the sum of the transition probabilities of all the possible transitions. (This transition probability ratio will be referred to as the branching ratio). For the $b^1\Pi_u(v' = 1)$ level, there are two obvious contributing factors to the inherent weakness of a particular transition. First, the largest branching ratio is not more than 0.1;[38] and second, the cross section for production is relatively small.[39]

Specific information may be obtained from a comparison of the expected intensity I(b1-X10) of the $b^1\Pi_u \rightarrow X^1\Sigma_u^+$ transitions with the expected intensity I(1200 Å) of the atomic nitrogen transition which occurs at approximately 1200 Å. Equation (66) leads to the following ratio, after cancelation of the common terms:

$$R(1) = \frac{I(b1\text{-}X10)}{I(1200\ A)} = \frac{A(b1\text{-}X10)}{\Sigma_i\ A(b1\text{-}Xi)}\ \frac{\sigma(XO\text{-}b1)}{\sigma[XO\text{-}N(1200\ A)]}\ \frac{\Sigma_j A(2p^2 3s\text{-}j)}{A(1200\ A)} \tag{67}$$

A(1200 Å) is the transition probability of the nitrogen transition which gives rise to the ≃1200 Å lines, $\Sigma_j A(2p^2 3s\text{-}j)$ is the sum of the transition probabilities of all the transitions from the atomic level under discussion, σ[XO-N(1200 Å)] is the cross section for the production of

the aforementioned atomic level from the lowest vibrational level of the nitrogen molecule. The other terms have been previously explained.

The branching ratio for the b1-X10 transition is estimated to be 0.1.[38] The cross section, σ(XO-b1), was taken from the electron absorption spectroscopy studies of Lassettre[40] *et al.*, and Meyer[39] *et al.* From Ref. 40 the total oscillator strength for a broad energy range is given as 0.945. From Ref. 39 the fractional part of the oscillator strength due to excitation to b1 is estimated as 0.012. For electrons with energy of 200 eV, the fractional part of the oscillator strength corresponds to a cross section, via the Born approximation:[41]

$$\sigma(\text{XO-b1}) = 8.1*10^{-18}\text{cm}^2 \ .$$

As a check, the ratio of the $C^3\Pi_u(v' = 0)$ cross section to the b1 cross section is taken from Skerbele[42] *et al.* With this ratio and recently measured cross sections for the $C^3\Pi_u(v' = 0)$ level,[43] the cross section is calculated with the Born Approximation to be at 200 eV,

$$\sigma(\text{XO-B1}) = 7.5*10^{-18}\text{cm}^2 \ .$$

The individual terms in Eq. (67) relative to atomic nitrogen are not obtainable, but a measureable ratio can be formed from Eq. (66) to obtain the product of the atomic nitrogen terms.

$$R(2) = \frac{I(1200\ \text{Å})}{I[H(2P\text{-}IS)]}$$

$$= \frac{A(1200\ \text{Å})}{\Sigma_j A(2p^2 3s\text{-}j)} \ \frac{\sigma[\text{XO-N}(1200)]}{\sigma[H_2\text{-}H(2P)]} \ \frac{N_{XO}}{N_{H_2}} \ \frac{A(2P\text{-}1S)}{\Sigma_k A(2P\text{-}k)} \ . \tag{68}$$

$I[H(2P-1S)]$ is the intensity of the atomic hydrogen transition 2P-1S, $\sigma[H_2\text{-}H(2P)]$ is the cross section for production of the excited atomic level 2P from molecular hydrogen, N_{H_2} is the number density of molecular hydrogen in the invertron, $A(2P-1S)/\Sigma_k A(2P-k)$ is the branching ratio for the atomic hydrogen transition, and the other terms are the same as previously defined. Notice that only the relative number density of molecular nitrogen to the number density of molecular hydrogen is needed.

It is possible to write a ratio similar to Eq. (67) and (68) between the molecular nitrogen transition and the atomic hydrogen transition. This was not done because of experimental necessity. The molecular hydrogen radiation is strong in the region where the molecular nitrogen transitions radiate. Only the atomic nitrogen radiation was strong enough to be distinguished easily from the hydrogen radiation. The three terms relating to atomic nitrogen may be eliminated from Eq. (67) and (68) and a predicted value for R(1) obtained. The cross section for the reaction

$$H_2 + e \rightarrow H + H^*(2P) + e,$$

is taken from the results of Fite and Brackman[44] to be $8.0\times10^{-18}cm^2$ at 200 eV. With the above mentioned value of the parameters, plus the observed ratio of atomic hydrogen and atomic nitrogen, in the invertron, R(1) has a predicted value of greater than 1.0. But the observed value of R(1) was less than 0.1. An incorrect value for the branching ratio of the b1-X10 transition is the most likely explanation for this discrepancy. The vibrational levels of the $b^1\Pi_u$ state above 1 definitely are

known to predissociate either into the ground level of atomic nitrogen or into the first excited level. Energy considerations allow the v' = 1 level to dissociate also into the same above mentioned atomic nitrogen levels, although evidently not to as high a degree as is the case with v' greater than 1.

Therefore, the conclusion is that the branching ratio

$$\frac{A(b1\text{-}X10)}{\Sigma_i A(b1\text{-}Xi)}$$

used in Eq. (67) does not in fact correctly describe the b1 level. The sum in the denominator of the branching ratio must also include the dissociation transition probability. The results indicate that the probability of dissociation of the $b^1\Pi_u(v' = 1)$ level is over ten times as large as the probability of spontaneous emission of the same level. This is another way of saying that the branching ratio for spontaneous emission of this level is never greater than 0.01 for any given band.

The lifetime of the $b^1\Pi_u$ state is not the correct parameter to use to calculate the absorption coefficient of the ground state nitrogen molecule. The work of Meyer[39] *et al.* and Huffman[45] *et al.* point out clearly that the major absorption coefficients are due to the vibrational levels of the $b^1\Pi_u$ state above v' = 1. It is only the v' = 1 level which has ever been observed in emission; thus the lifetime of only the v' = 1 level can be measured, at best. Since this level also predissociates preferentially, its lifetime cannot lead to a correct value for the absorption coefficient from the ground level of N_2.

The absorption oscillator strengths for the $b^1\Pi_u$ state have been measured by Lawrence[46] *et al.* for photon absorption, and by Lassettre *et al.*[39,40,41] for electron energy absorption. The results are given in Table 14. The zero vibrational level of $X^1\Sigma_u^+$ is the lower level for every transition. In Table 14, a v' = 0 is listed. This level was originally designated as the $j^1\Sigma_u^+(v' = 0)$ by Worley. With the new vibrational assignment of Ogawa *et al.*[37] there is additional reason to believe that the $j^1\Sigma_u^+(v' = 0)$ level is the result of a strong interaction between the v' = 0 of the $b^1\pi_u$ and another level. For completeness, a v' = 5 and v' = 6 is listed. Again these levels are most likely the result of electron state interaction.[47] The notation $\ell^1\Pi_u$ given after the vibration numbers is that used originally by Worley.[48] For comparison, the $p'^1\Sigma_u^+(v' = 0)$ level is also in Table 14. This is the strongest absorbing level of the nitrogen molecule which has been observed.

The oscillator strength listed under f_e are obtained from the work of Lassettre *et al.*[39,40,42] except for v' = 5 and v' = 6. For v' = 5, the oscillator strength was obtained from the relative values reported by Lawrence[46] *et al.* to have been obtained from J. Geiger and B. Schröder as private communication. This relative value was then normalized to Lassettre's value by comparison to v' = 4. For v' = 6, only a rough estimate is obtainable from the published results of Lassettre *et al.*[39,40,42] and Geiger and Stickel[49]. The value given in Table 14 of v' = 6 is good as an upper limit. All of the values listed in

Table 14. Oscillator Strengths and Electron Excitation Cross Sections for the $b^1\Pi_u$ States of N_2.

	λ	$f^{(a)}$	f_e (b)		(b)
$v'=0(j^1\Sigma_u^+)$	991.85 Å	-	.003	2.	$x10^{-18}cm^2$
$v'=1$	985.65 Å	-	.012	8.1	
$v'=2$	978.87 Å	-	.025	20.	
$v'=3$	972.1 Å	0.02	.05	40.	
$v'=4$	965.63 Å	0.055	.09	73.	
$v'=5(\ell^1\Pi_u)$	960.21 Å	0.04	.06 (c)	-	
$v'=6(\ell^1\Pi_u)$	955.08 Å	-	(0.03) (c)	-	
. . . . .					
$v'=0(p'^1\Sigma_u^+)$	958.17 Å	0.14	0.2	162.	

(a) Ref. 46.

(b) Ref. 39, 40, and 42.

(c) See text for discussion.

Table 14 under f_e as measured by Lassettre *et al.*[39,40,42] are in agreement with the relative results of Geiger and Stickel.[47]

Lawrence *et al.*[46] were able to show that in the earlier work of Huffman *et al.*[44] the product of absorption path and pressure was too large. An additional problem inherent in using any radiation source other than a black body in photon absorption studies is the possibility that the source is also an emitter of monochromatic energies. When the absorption line width is narrower than the resolution of the spectrograph, significant errors can result from a source which is not a continuum. For the $b^1\Pi_u(v' = 3)$ to $x^1\Sigma_u^+(v'' = 0)$ transition, the resolution of Lawrence *et al.* appears to be better than the line width. One of the difficulties in understanding their results, though, is that the $v' = 3$ level of $b^1\Pi_u$ is more diffuse than the $v' = 4$ level. That these levels are diffuse clearly indicates predissociation, but the degree of diffuseness is reversed from that expected.

The cross section results of Lassettre *et al.* are in good agreement with the cross section results of Stanton.[43] This lends credibility to the absolute value of the cross sections of Lassettre *et al* . However, the attempt to use the resulting generalized oscillator strength at zero momentum change as the oscillator strength for photon absorption rests on a somewhat tenuous foundation. Indeed, the only final justification for doing so would be good agreement with absorption measurements.

Criticism

The work of Lawrence *et al.* sets a lower limit on the value of the oscillator strength due to line absorption saturation. This is a result of the effective slit width of the monochromator being wider than the absorption line width. It is then possible to use, unintentionally, an absorption path length which is too long or a pressure which is too high. The result is a measured oscillator strength which is smaller than the true oscillator strength.

The values of the oscillator strengths listed in Table 14 which were taken from the work of Lassettre *et al.* represents an upper limit. When Stanton's result was previously compared to Lassettre's result, there was very close agreement, but Stanton measured the absolute value of the apparent electron cross section. The value of the true (cascade free) cross section has as its upper limit the value of the apparent cross section. Thus, with Stanton's work used as a reference, the oscillator strengths taken from Lassettre's work are an upper limit to the correct value.

Observations on the $b'^1\Sigma_u^+$ State of N_2

Since the $b'^1\Sigma_u^+$ state radiates in the same spectral range as the $b^1\Pi_u$ state, it was also looked for, but was not found either. For short pulse conditions, this now appears as a reasonable result. Indeed, the vibration levels 0, 2, and 3 of the b' state have not been observed in photon absorption[37,45] or electron energy loss[39,46] spectra from the ground vibrational level of the $X^1\Sigma_g^+$ state. It is possible that the

v = 1 level of the b' state has been observed in a photon absorption spectra,[37] but it was very weak. The large offset of the b' minimum[30] of potential energy from the ground state minimum produces such small Franck-Condon factors as to limit severely the probability of transition between the lower vibrational levels. From Ref. 49, a maximum value for the oscillator strength of the vibrational levels of the b' state may be obtained. (None of the presently published data on photon absorption for the band system of the b' state should be used to obtain relative oscillator strengths due to the saturation effects previously mentioned in the discussion of the $b^1\pi_u$ state of N_2.) Only the v = 7 level of the b' state is detectable in the electron energy loss spectrum of Ref. 49. An oscillator strength of about 0.01 may be assigned to this transition, $b'^1\Sigma_u^+(b' = 7) \leftarrow X^1\Sigma_g^+(v'' = 0)$. For all other transitions from the ground level $X^1\Sigma_g^+(v'' = 0)$ to the vibrational levels $b'^1\Sigma_u^+(v' = 0,1,2,3,4,5,6)$ an oscillator strength of less than 0.003 is indicated. There are no indications of any vibrational levels of the b' state above v = 7.

Speculations

The following statements are almost completely speculative. Since the $b'^1\Sigma_u^+$ state of the nitrogen molecule is observed in emission only in very energetic or unique discharges and since no absorption to the lower vibrational levels has been observed, the excitation process is probably a two or more step process. The number densities of the triplet states (especially $B^3\pi_g$ and $A^3\Sigma_u^+$) and of the higher vibrational levels of the ground state increase in the discharge. Excitation will occur more

favorably from these triplet and higher vibrational levels to the lower vibrational levels of the $b'^1\Sigma_u^+$ state, since these levels have a more favorable Franck-Condon factor with the levels of the $b'^1\Sigma_u^+$ state than the zero vibrational level of the ground state does.[40] Thus, the number density of the molecules in the excited b' level and, consequently, the intensity of radiation from the b' level, in those cases in which it has been observed, is probably due, almost entirely, to one or both of these two stage excitation processes.

LIST OF REFERENCES

1. M. Jeunehomme, J. Chem. Phys. 45, 1805 (1966).
2. W. Brennen, J. Chem. Phys. 44, 1793 (1966).
3. W. H. Wurster, J. Chem. Phys. 36, 2111 (1962).
4. R. G. Bennett and F. W. Dalby, J. Chem. Phys. 31, 434 (1959).
5. Von E. Fink and K. H. Welge, Z. Naturforschg 19a, 1193 (1964).
6. D. I. Sebacher, J. Chem. Phys. 42, 1368 (1965).
7. R. G. Fowler and T. M. Holzberlein, J. Chem. Phys. 43, 1124 (1966).
8. M. Jeunehomme, J. Chem. Phys. 44, 2672 (1966).
9. J. E. Hesser and K. Dressler, J. Chem. Phys. 45, 3149 (1966).
10. L. L. Nichols and W. E. Wilson, Applied Optics 7, 167 (1968).
11. E. U. Condon and G. H. Shortley, The Theory of Atomic Spectra (Cambridge: Cambridge Press, 1953).
12. M. Kotani, K. Ohno and K. Kayama, Handbuch der Physik (Berlin: Springer - Verlag, 1961) V I. XXXVII/2.
13. R. de L. Kronig, Band Spectra and Molecular Structure (Cambridge: Cambridge Press, 1930).
14. F. Reiche and H. Rademacher, Z. Physik 39, 444 (1926); 41, 453 (1927).
15. G. Herzberg, Molecular Spectra and Molecular Structure (Princeton: D. Van Nostrand Company, Inc., 1950).
16. R. S. Mulliken, Rev. Mod. Phys. 3, 89 (1931).
17. W.H.J. Childs, Proc. Roy. Soc. (London) 137A, 641 (1932).
18. T. M. Holzberlein, Ph.D. Dissertation, University of Oklahoma. Norman, Oklahoma (1963).

References (Contd.)

19. E.R.S. Winter, Trans. Faraday Soc. 47, 342 (1951).

20. E. B. Winn, Phys. Rev. 80, 1024 (1950).

21. T. M. Holzberlein, Rev. Sci. Instr. 35, 1041 (1964).

22. G. Russell and T. M. Holzberlein, to be published in Phys. Fluids.

23. Stanley Robertson, Master's Thesis, University of Oklahoma. Norman, Oklahoma (1966).

24. W. R. Pendelton and R. H. Hughes, Phys. Rev. 138, A683 (1965).

25. W. R. Bennett, Jr., P. J. Kindlman and G. M. Mercer, Appl. Opt. Suppl. 2, 341 (1965).

26. A. H. Gabriel and D.W.O. Heddle, Proc. Roy. Soc. (London) 258, 24 (1960).

27. R. G. Fowler, T. M. Holzberlein, C. H. Jacobson and S.J.B. Corrigan, Proc. Phys. Soc. 84, 539 (1964).

28. S. Heron, R.W.P. McWhirter, E. H. Rhoderick, Proc. Phys. Soc. (London) A234, 565 (1956).

29. M. Jeunehomme and A.B.F. Duncan, J. Chem. Phys. 41, 1692 (1964).

30. F. R. Gilmore, J. Quant. Spect. and Rad. Trans. 5, 369 (1965).

31. D. C. Jain and R. C. Sahni, J. Quant. Spect. and Rad. Trans. 7, 475 (1967).

32. D. C. Tyte, Proc. Phys. Soc. 80, 1347, 1354 (1962).

33. R. N. Zare, E. O. Larson and R. A. Berg, J. Mole. Spec. 15, 117 (1965).

34. Arnold Eucken, Landolt Bornstein Tables (Berlin: Springer-Verlag, 1951).

References (Contd.)

35. Paul N. Stanton, Ph.D. Dissertation at the University of Oklahoma. Norman, Oklahoma (1968).

36. R. W. Nocholls, J. of Research (N.B.S.) 65A, 451 (1961).

37. M. Ogawa, Y. Tanaka, A. S. Jursa, Canadian J. Phys. 42, 1716 (1964).

38. Astrophysical Journal Supplement Series, 6, 467 (1962).

39. V. D. Meyer, A. Skerbele, E. N. Lassettre, J. Chem. Phys. 43, 3769 (1965).

40. E. N. Lassettre, F. M. Glaser, V. D. Meyer, A. Skerbele, J. Chem. Phys. 42, 3430 (1965).

41. N. F. Mott, H.S.W. Massey, The Theory of Atomic Collisions, Oxford University Press (1965).

42. A. Skerbele, M. A. Dillon, E. N. La-settre, J. Chem. Phys. 46, 4161 (1967).

43. Private communication, Paul N. Stanton.

44. W. L. Fite, R. T. Brackman, Phys. Rev. 112, 1151 (1957).

45. R. E. Huffman, Y. Tanaka, J. C. Larrabee, J. Chem. Phys. 39, 910 (1963).

46. G. M. Lawrence, D. L. Mickey, K. Dressler, J. Chem. Phys. 48, 1989 (1968).

47. K. Dressler, Proc. Interna'tl. Conf. Spectry, Bombay, 1, 104 (1967).

48. R. E. Worley, Phys. Rev. 64, 207 (1943).

49. J. Geiger and W. Stickel, J. Chem. Phys. 43, 4535 (1965).

APPENDIX

Square Wave Generator

The square wave generator was the main component of Pulse Generating Device I. When the characteristic impedance is connected to a charged coaxial cable, a square wave is generated across the resistance by the discharging of the cable. This property of a coaxial cable was used to generate the voltage pulse to be applied to the invertron. (See Fig. 31.)

The coaxial cable was a 3/4 inch, foam dielectric, Phelps Dodge cable. The outer conductor was aluminium and the inner conductor was copper. The characteristic impedance of the cable was 50 ohms. The center conductor was connected to a positive power supply (B^+) with approximately a 100 kilohms resistor.

A negative bias (B^-) was applied to the first grid of the gas thyratron (2D21) to prevent premature conduction. A positive pulse from the Timer activated the 2D21 when desired. A part of the output voltage of the cathode circuit was used as the excitation pulse to the invertron.

The termination impedance was the sum of the cathode resistors plus the impedance of the 2D21. The approximate value of the 2D21 impedance was 20 ohms. A cathode resistance of 30 ohms therefore developed the proper 50 ohms impedance for the cable. The actual value of the effective terminating resistor (2D21 plus cathode resistors) was less than 50 ohms. An under terminated coaxial cable will produce a series of

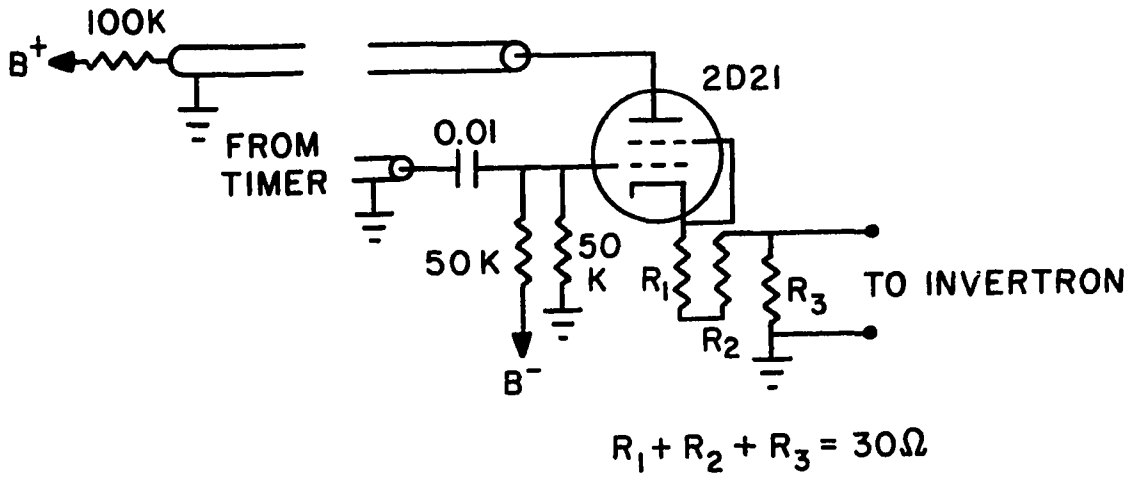

Figure 31. Square Wave Generator.

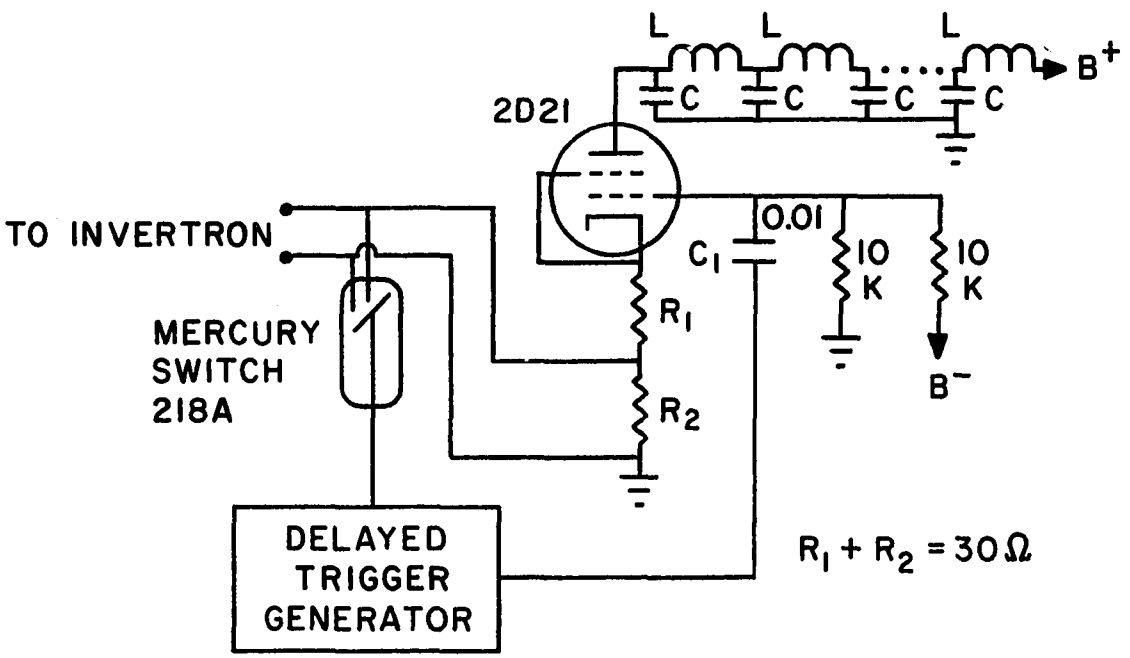

Figure 32. Mercury Switch and Pulse Forming Network.

alternating polarity square waves. However, the 2D21 will not start to conduct again. The advantage of the under termination of the coaxial cable was to decrease the cutoff time of the pulse applied to the invertron.

To maintain a fast rise and fall of the excitation pulse, the physical geometry of the connections to the coaxial cable, the 2D21 and the invertron must be considered. The area of all the conducting loops should be as small as possible.

Mercury Switch and Pulse Forming Network

The mercury switch and pulse forming network were used to generate long excitation pulses with very fast cutoff times. A Delayed Trigger Generator activated the pulse forming network in delayed coincidence with the contacting of the center rod of the mercury switch to the ground side of the invertron. (See Fig. 32) From 0.5 to 8 microseconds after the pulse forming network had applied the excitation voltage to the invertron, the mercury switch shorted across the invertron, thus stopping the excitation pulse.

The 2D21 used in the pulse forming network was biased and connected as the one in the Square Wave Generator. The L and C of the pulse forming network were 0.6 microhenries and 0.01 microfarads, respectively. The pulse time per section was 0.6 microseconds and the effective characteristic impedance was 60 ohms.

The most critical connections were from the invertron to the mercury switch and from the cathode resistor, R_2, to the mercury switch

and invertron. The two leads from the mercury switch were connected directly to the two connections of the invertron. (Extreme care should be exercised when one solders to the leads of the mercury switch. The gas envelope of the switch seals in a high pressure of hydrogen.) R_2 was connected to the two leads of the mercury switch by a 3 inch length of coaxial cable.

Trigger Differentiator

To obtain a pulse to start the Time to Pulse Height Convertor, a small part of the applied excitation signal was used. A simple R-C circuit differentiated the square wave to produce a negative and a positive going spikes. The negative signal triggered either the sweep on an oscilloscope, or the start of the time to pulse height converter.

Gate Pulse Generator

This circuit produces a delayed, rectangular voltage pulse when triggered by a pulse from the Delayed Trigger Generator. It is used to control the gate on the Ortec Time to Height Converter. When set in the coincidence mode, the TPHC will accept input start pulses only when such pulses are coincident with a pulse from the Gate Pulse Generator. This system prevents the TPHC from responding to false start pulses or noise.

The Gate Pulse Generator produces a 30 volt positive pulse with a variable width (1.5 to 60 microseconds) and a variable delay (1.5 to 100 microseconds). Output impedance is 680 ohms, and the circuit is designed to feed directly into the Ortec 1000 ohm gate circuit. Input impedance when used in conjunction with the Delayed Trigger Generator is

about 20 to 30 kilohms. Input pulse width should be no less than 0.5 microseconds. The minimum trigger voltage is about 4 volts positive, adjustable by means of the sensitivity control. The maximum input voltage should not exceed 70 volts positive.

Within a limited range of delay time, output pulses as short as 100 to 200 nanoseconds are attainable, with rise times of 20 to 40 nanoseconds.

In order to ensure stable operation, the sensitivity control should be set at the minimum value which will allow the circuit to be triggered. Initially set the sensitivity completely counter clockwise; then gradually turn clockwise until the circuit begins to operate. Increase the sensitivity slightly beyond that point.

The input circuit is protected against negative signals of up to about 7 volts; negative signals greater than 7 volts may cause damage, especially if the sensitivity is set at maximum.

The minimum input impedance (maximum sensitivity) is about 1000 ohms. A 50,000 ohms potentiometer is in series with this impedance and serves to attenuate large input signals.

The circuit (Fig. 33) consists basically of two, one-shot multivibrators in cascade. A 50,000 ohms potentiometer is in series with the input to attenuate the 45 volt pulse from the Delayed Trigger Generator. The first multivibrator is used to produce a delayed trigger pulse which triggers the second multivibrator. This second multivibrator produces the output pulse. The differentiator is a resistor-capacitor combination

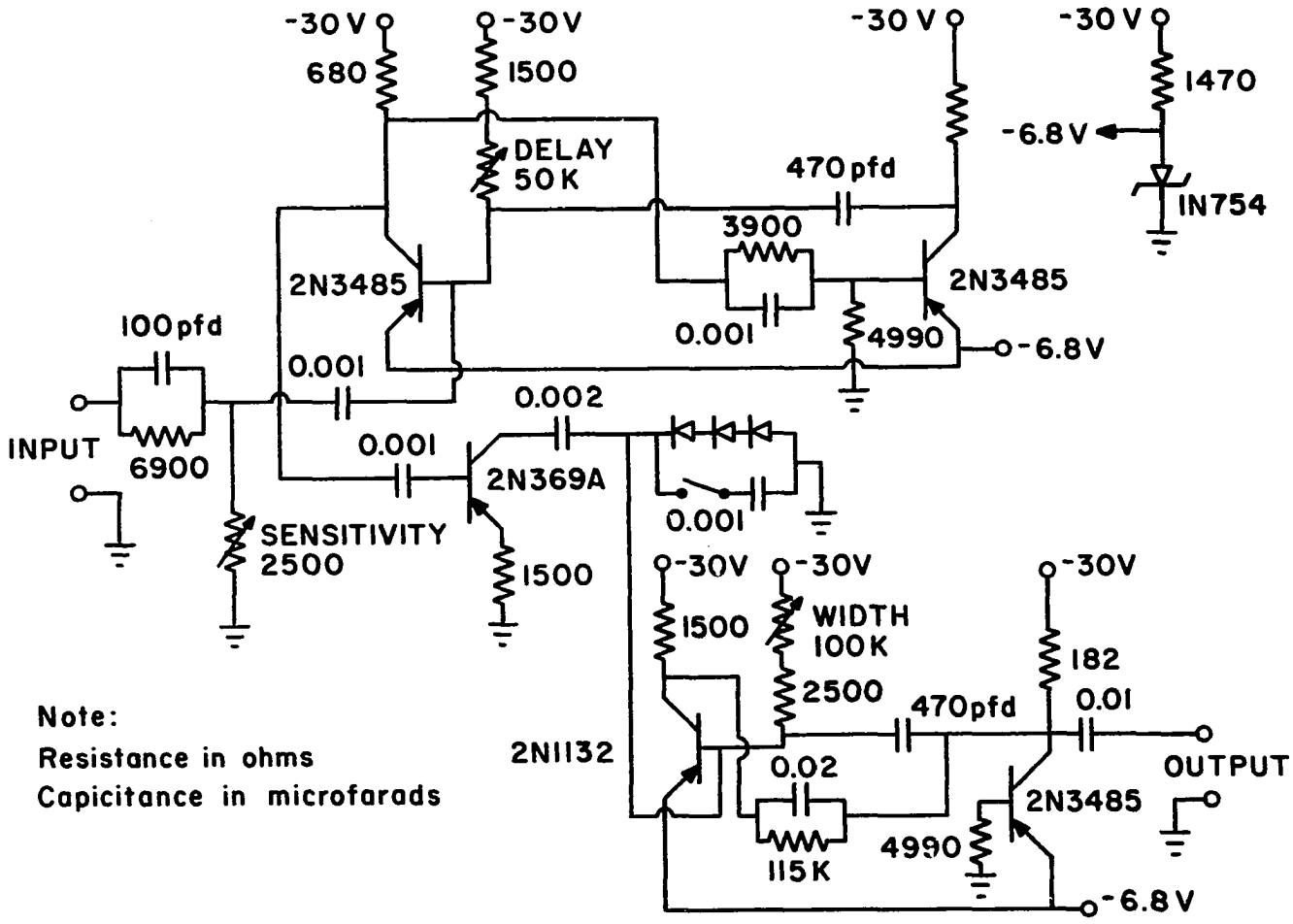

Figure 33. Gate Pulse Generator.

augmented by a diode across the resistor. The diode attenuates the pulse from the leading edge of the multivibrator's square wave output and prevents damage to the following stage from large positive signals. The possibility of misfire due to noise is also reduced by attenuating the unwanted pulse.

The second multivibrator has a range of about 100 nanoseconds to 60 microseconds, but it is very sensitive to noise at the short pulse end and should normally not be used below 1.5 microseconds.

By using silicon transistors it is possible to build multivibrators without the need for both positive and negative supplies. With gernamium transistors the saturation voltage of the "on" transistor is high enough to forward bias the base emitter junction of the "off" transistor so that this transistor is not completely off. In this case an additional supply of polarity opposite to the collector supply must be used to bias one transistor off. However, with silicon transistors the voltage required to forward bias the base-emitter junction of the "off" transistor is high enough so that the saturation voltage of the "on" transistor will not be sufficient to bring the "off" transistor into partial conduction.

It should be noted that although faster switching times are possible if multivibrators are designed to avoid saturation, this procedure will reduce output pulse amplitudes, thus requiring the use of additional amplifiers with the probable result that total switching time will not be improved.

Rate Meter Amplifier

This circuit is essentially an electronic attenuator and pulse amplifier. The output is a negative going, 45 volts pulse of approximately 10 microseconds width. This amplifier is used in conjunction with a rate meter to count the number of pulses per second generated by the Time to Pulse Height Converter. The circuit will accept input pulses from 100 millivolts to 20 volts peak to peak and produce output pulses which vary only slightly in height and width over this entire range. The maximum repetition rate is about 10,000 pulses per second, although this varies somewhat with input pulse height. The current drain in very low (about 10 milliamps with no input signal and 15 milliamps with about 6000 pulses per minute); therefore, a battery may be used as a supply.

The circuitry (Fig. 34) consists of a simple 3 stage amplifier designed to operate in a saturated mode. The first stage has a high gain and saturates with about a 100 millivolts signal input. The collector supply voltage for this stage is limited to 6.8 volts by a zener diode and, therefore, the input to the next stage is always approximately 6.8 volts regardless of the magnitude of the input to the first stage. The output pulse width is determined by the diode-capacitor pumps and not by the width of the input width.

The diode above has two functions: first, it prevents the flow of current back toward the input thus preventing a negative spike from appearing at the output; second, it isolates the capacitor from the input circuit after the capacitor has been charged. The capacitor therefore

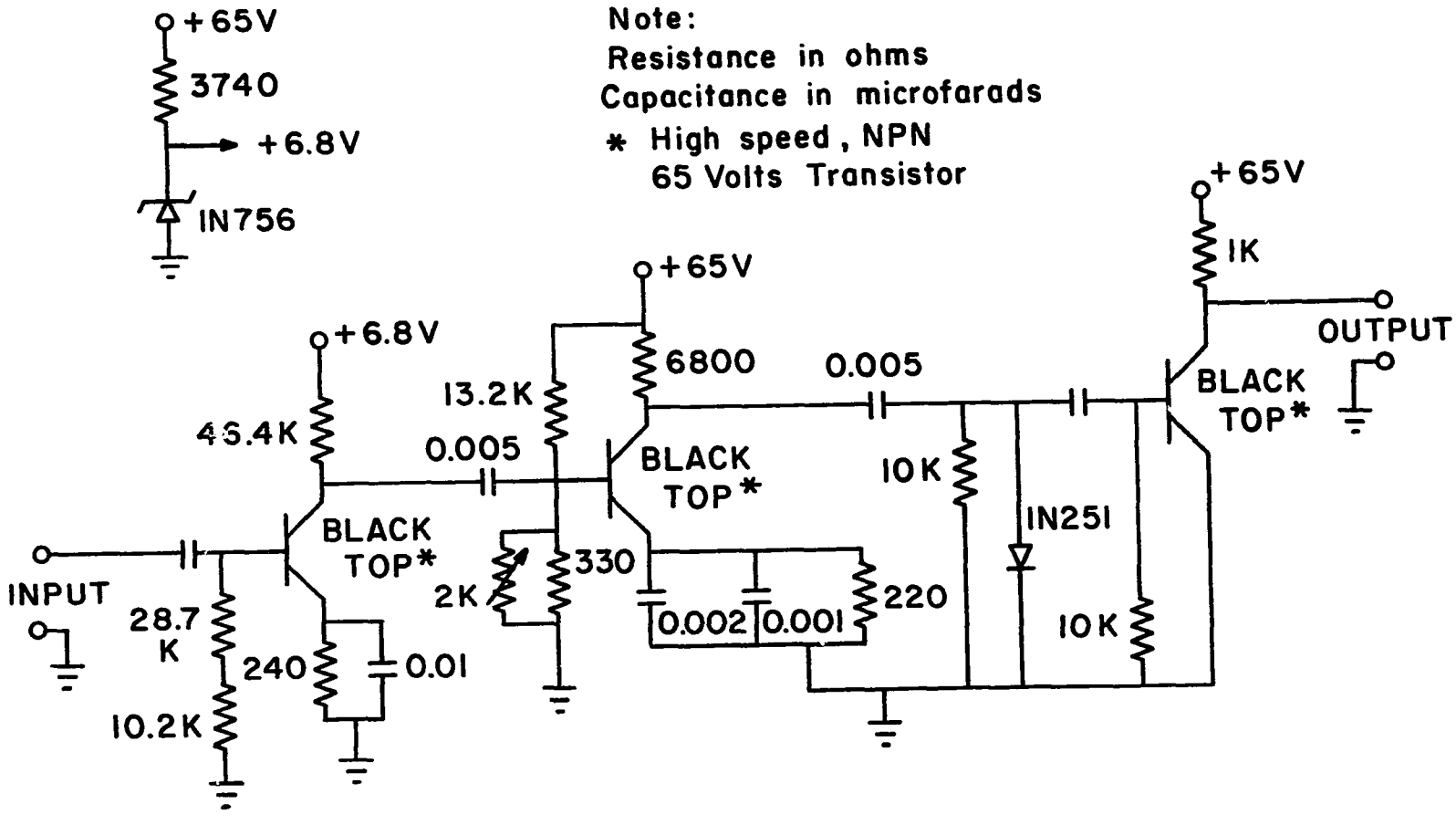

Figure 34. Rate Meter Amplifier.

remains charged to a high voltage even after the input signal has dropped to zero. When this voltage is fed to the second stage it keeps this stage saturated for a length of time determined by the resistance and capacitance of the circuit loop.

The third stage again has a high gain and saturates at a very low voltage. Its output therefore is essentially flat until the exponential from the diode-capacitor pump has decayed to a low value.

The circuit will operate with supply voltages of 25 to 70 volts; the output voltage will be approximately equal to supply voltage. Output impedance is about 10 kilohms; input impedance, about 1 kilohms. This circuit should never be coupled directly to an impedance load of less than 5 kilohms.

Delayed Trigger Generator

A time delayed trigger for the pulse forming network is necessary with Pulse Generating Device II. The Delayed Trigger Generator (Fig. 35) is used to generate this pulse. It consists of a single multivibrator followed by a pulse shaping and amplifying network. The input has a positive bias on it so that when it is shorted to ground a negative going signal is produced which activates the circuit. The output pulse is about 2 microseconds in width and 40 volts in amplitude. The decay is variable between about 1.5 microseconds and 50 microseconds. The output stage is an emitter follower with 1 kilohm emitter resistance and there is a 10 kilohms resistor in series with the output to protect the circuit from the high voltage feedback from the thyratron grid.

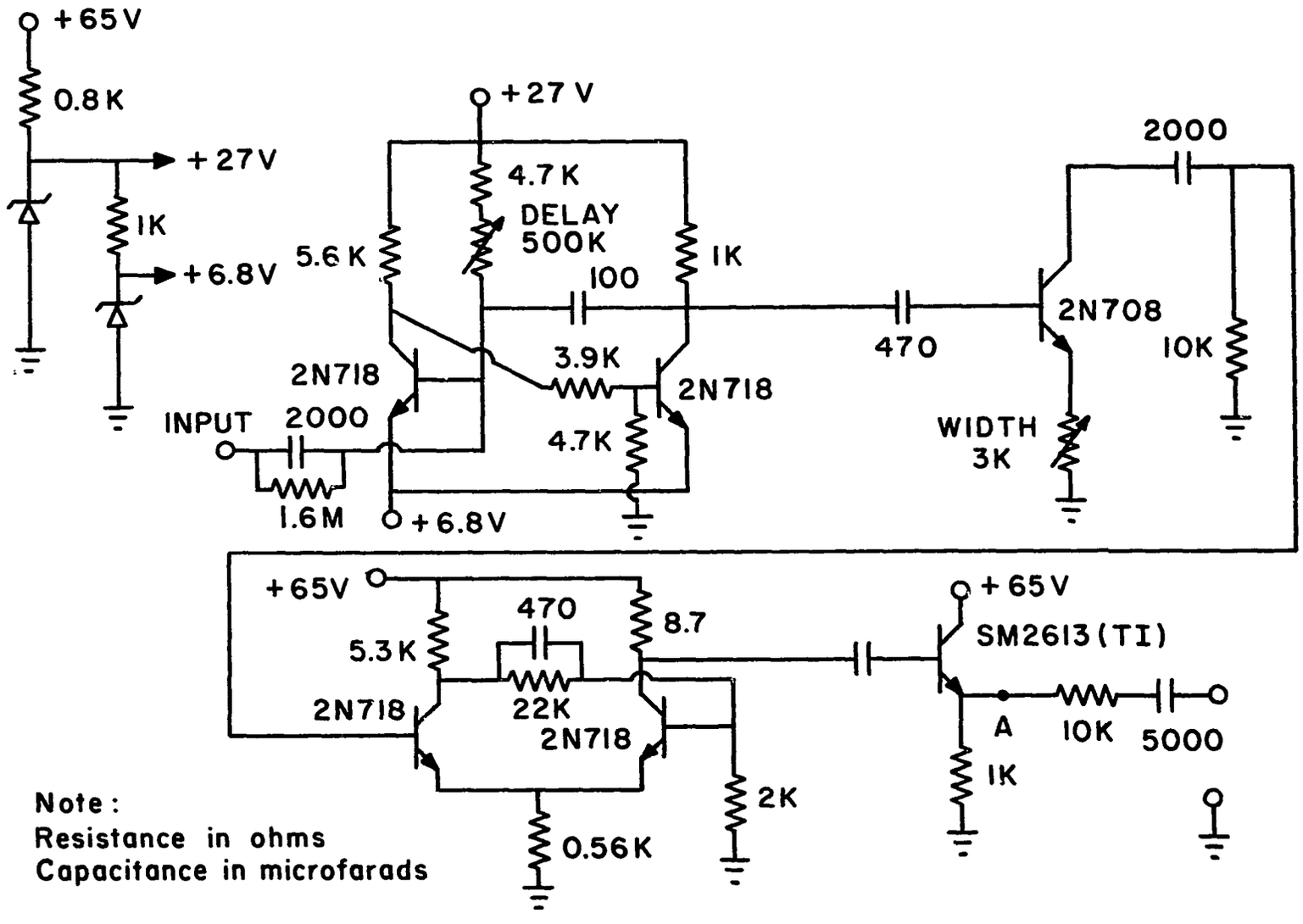

Figure 35. Delayed Trigger Generator.

A one-shot multivibrator is used to produce the delayed trigger pulse. The input is biased positively via a zener diode; a negative going signal is produced when this is shorted to ground through the mercury relay. The square wave output of the multivibrator is differentiated and fed to a Schmidt trigger generator which controls the width of the output pulse. The Schmidt trigger generator has a high output impedance and is not capable of driving more than a very light load. An emitter follower with a 1000 ohms emitter resistor provides the necessary impedance matching between the Schmidt trigger and the load.

Timer

Proper synchronization and activation of all circuits, which were used with Pulse Generating Device I, were effected with the Timer. (Pulse Generating Device II was self-activating.) A neon bulb was used as part of a relaxation oscillator to initiate all events. (See Figs. 36 and 37). The relaxation oscillator was used to trigger a 2D21. The combination of the neon bulb and 2D21 circuit is designated Oscillator and Pulse Generator in Figs. 36 and 37. The Delay Multivibrator was used to obtain a long delay time between pulses. The inverter changed the polarity of the signal from the Delay Multivibrator. The three 2D21 circuits (Pulse Shaper (Red), Pulse Shaper (Yellow), and Changeable Pulse Shaper) were used to generate fast rising pulses with large values of voltage and current. The Artificial Delay Line was used to activate any of the pulse shapers at the desired time.

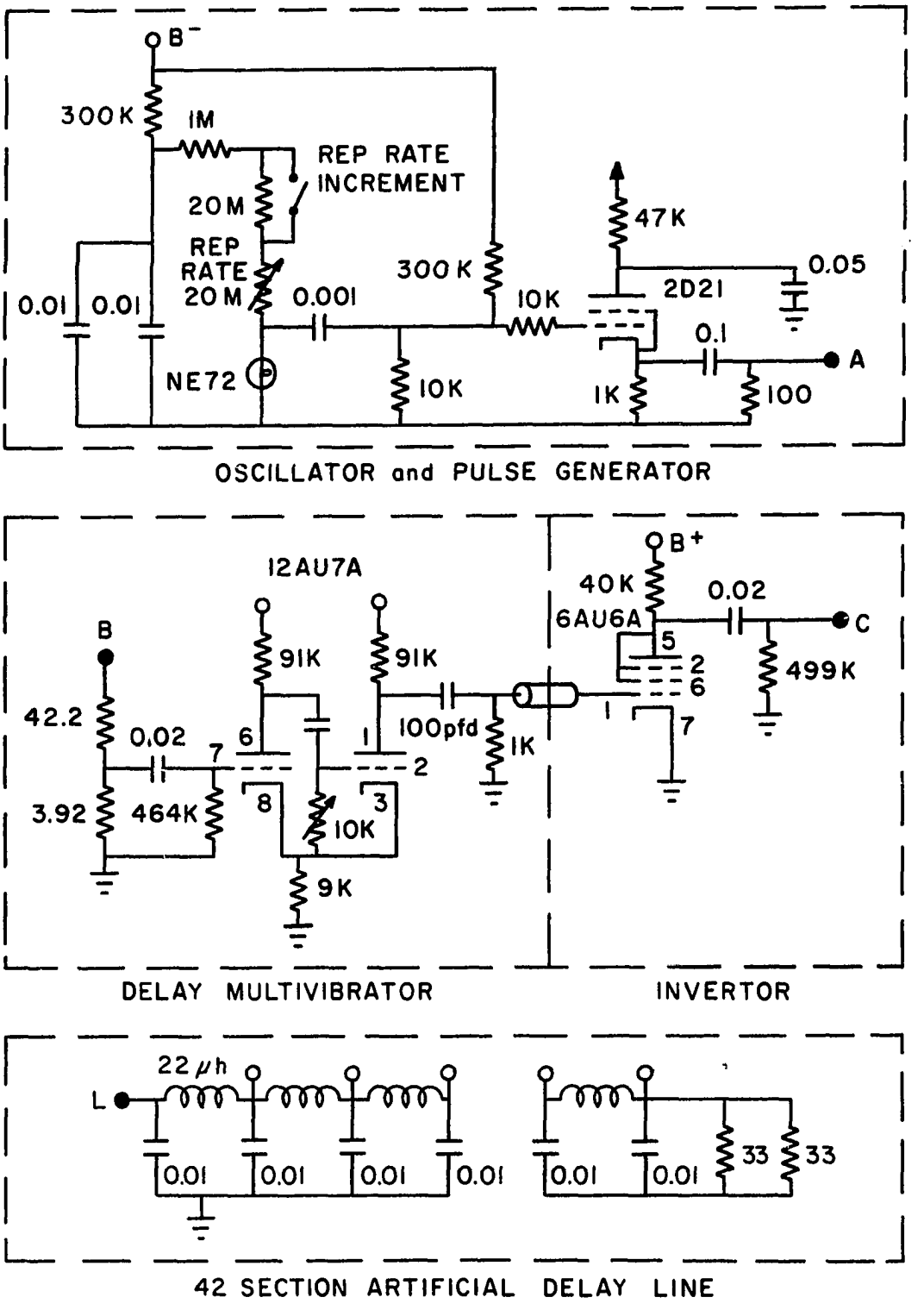

Note : Resistance in ohms , Capacitance in microfarads

Figure 36. Timer (Part I).

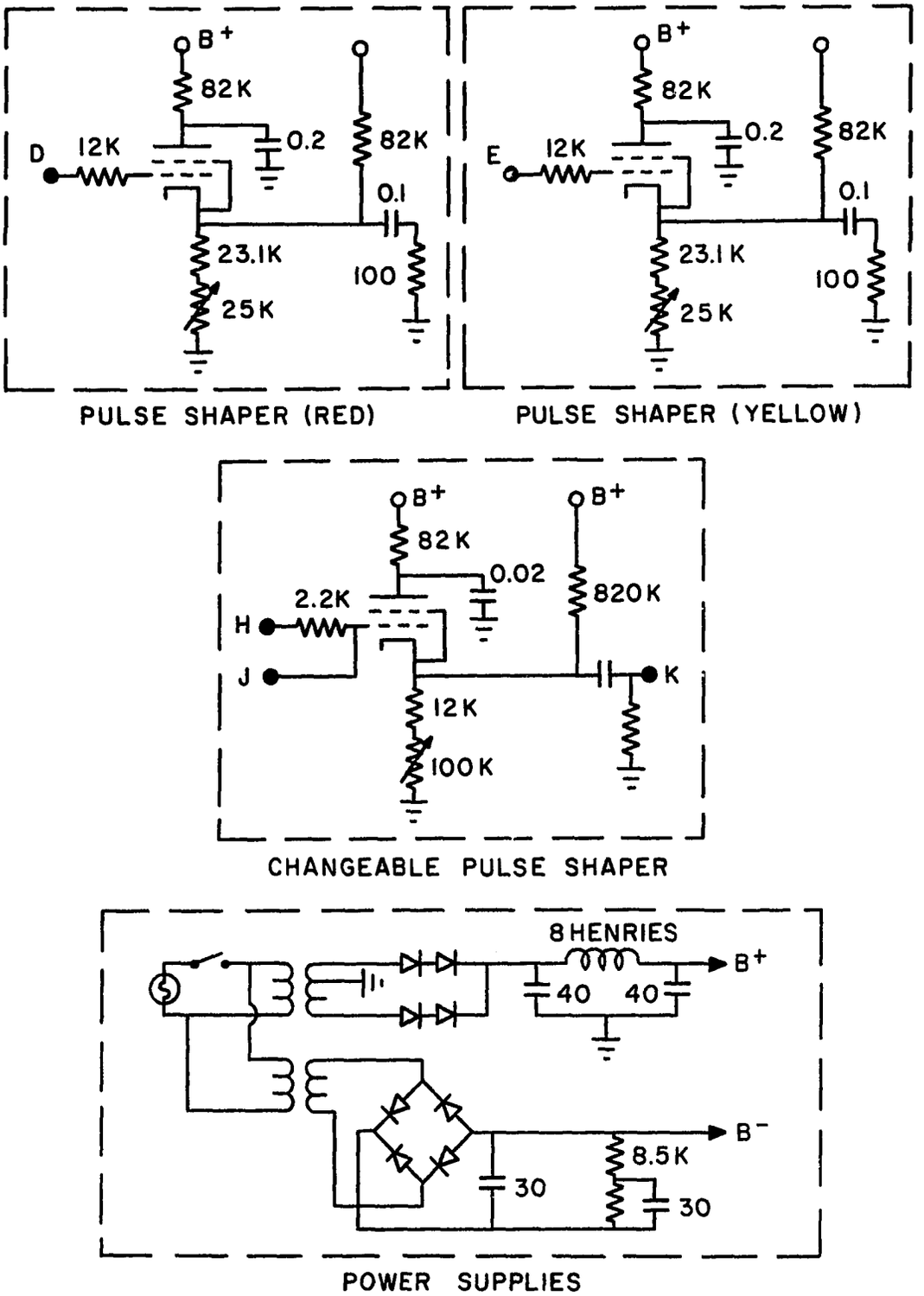

Note: Resistance in ohms , Capacitance in microfarads

Figure 37. Timer (Part II).

Each of the letters used in the circuit diagram (Figs. 36 and 37) designated a point which could be connected to any of the other designated points. The multiple point contacts of the Artifical Delay Line are not labeled.

In Fig. 38, a block diagram of the Timer is shown as it was used in conjunction with Combination System V and Preionization.

Exponential Function Synthesizer

The Exponential Function Synthesizer was used to obtain the decay constants from oscillograms of the photomultiplier output of the radiation decay. A mercury relay (Fig. 39) was used to control the charging and discharging of three R-C networks. The resulting exponential curves from each R-C circuit were mixed into one common output. Two considerations were necessary to prevent undesirable mixing of the R-C circuits. First, diodes in the charge and discharge loops were necessary to prevent the intermixing of the signals at their source. Second, the resistance used to generate the mixed output was kept small in comparison to the total output resistances from each R-C circuit to prevent feedback from the output to the source of the exponential decays. Since the output signal was small compared to the internal signals of the R-C circuits, the output leads were shielded to prevent undesirable pickup.

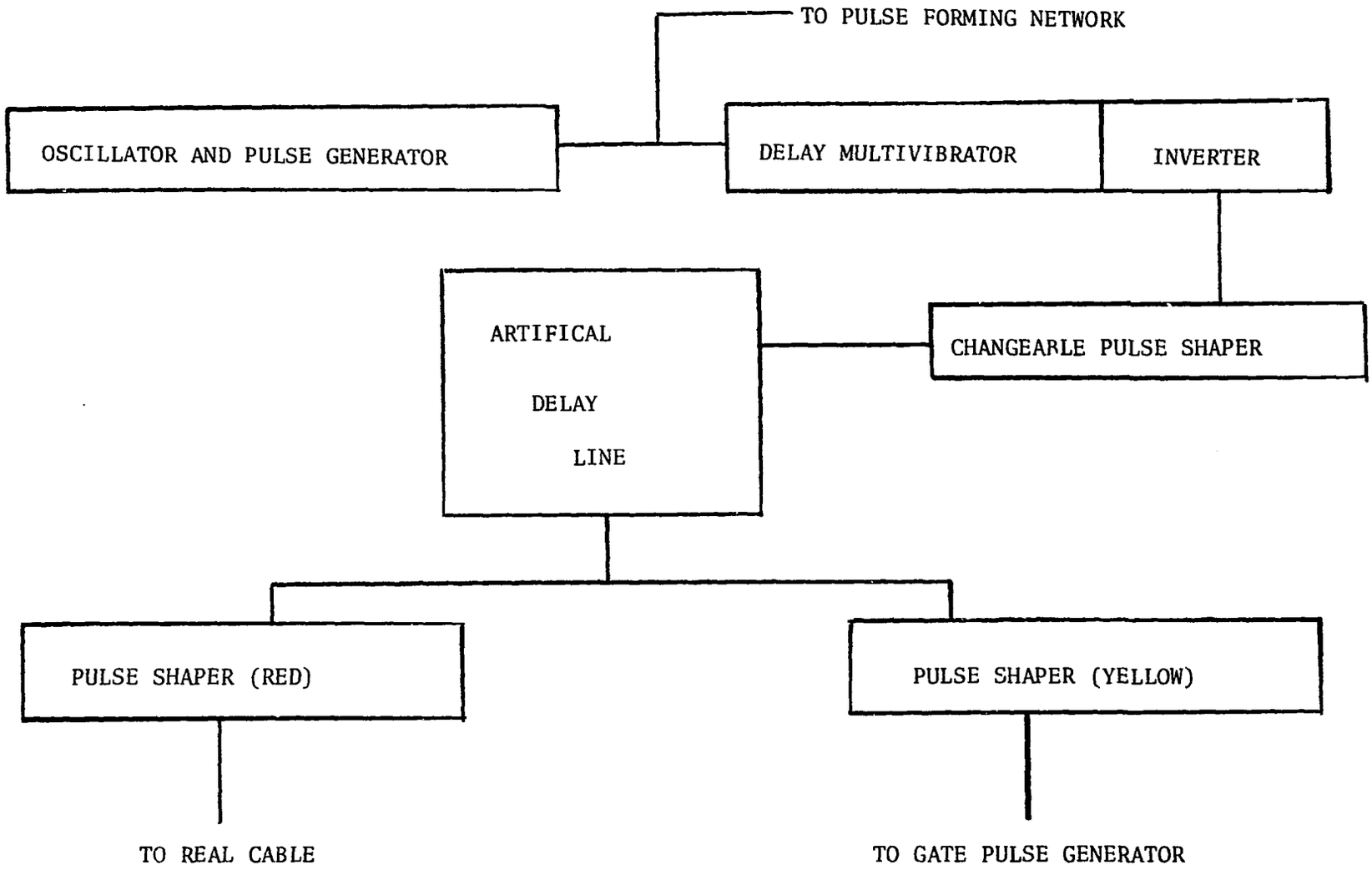

Figure 38. Block Diagram of Timer as Used with Combination System V and Preionization.

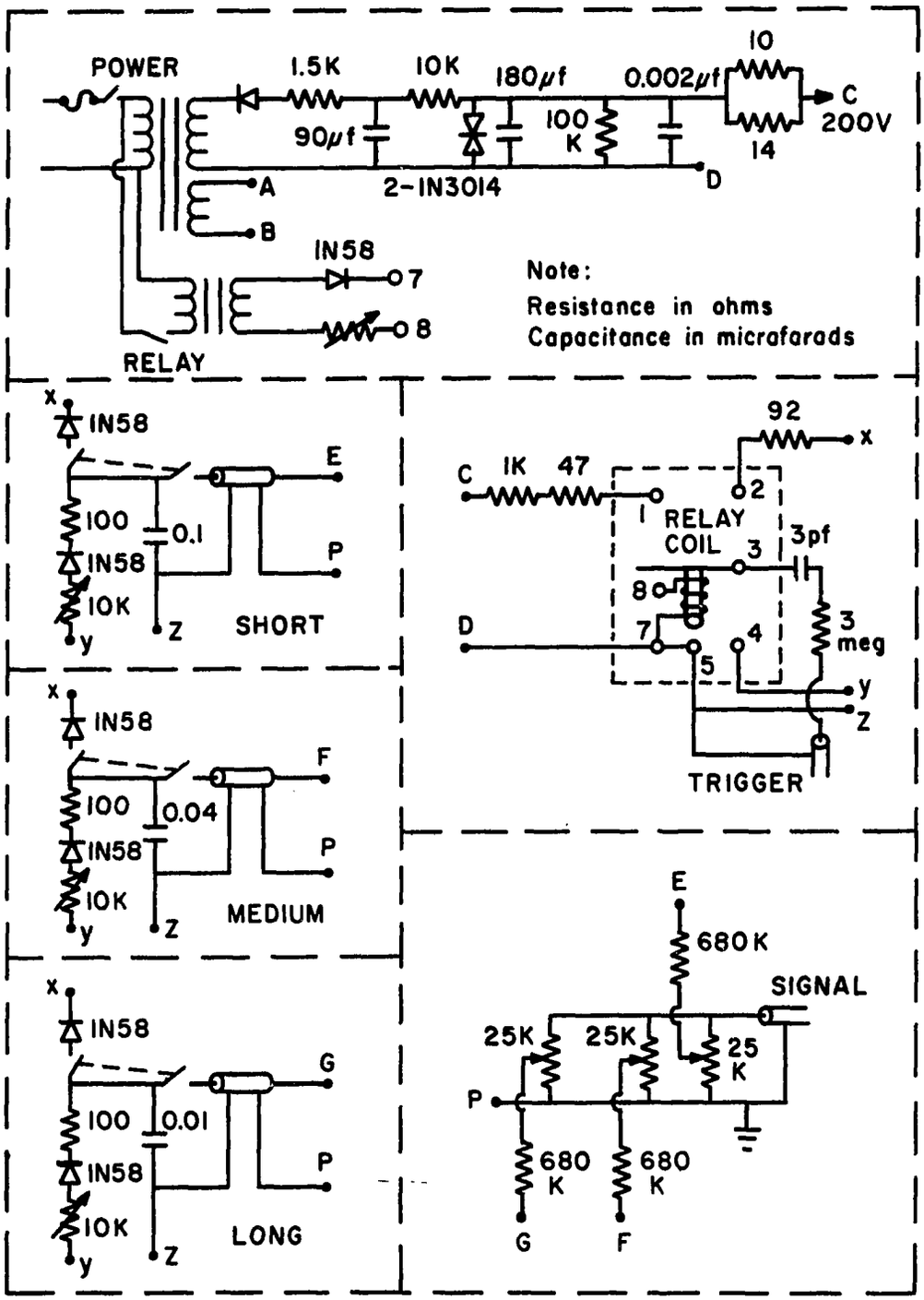

Figure 39. Exponential Function Synthesizer.

Criteria for Necessary Detection and Timing Device

The criteria to use for choosing the necessary Detection and Timing Device (DTD) can be expressed as a simple relation of the decay constant (τ) which is to be measured. When DTD I or II is to be used, the signal (S) to noise (N) ratio should be kept larger than 4 to obtain an oscillogram capable of reasonable measurement.

$$\frac{S}{N} = \left(\frac{I}{2G}\right)^{\frac{1}{2}} = 4 \tag{69}$$

I is the intensity of photoelectrons per second and G is the bandpass of the system in Hertz. To prevent distortion, the photoelectron pulse width should be kept at one fifth the decay constant (τ). If the photoelectron pulse width determines the bandpass of the system, the following expression results.

$$G = \tfrac{1}{4}\left(\frac{5}{\tau}\right) . \tag{70}$$

Combination of Eq. (69) and (70) result in the following.

$$I = \frac{40}{\tau} . \tag{71}$$

From Eq. (71) it is seen that about forty photoelectrons per lifetime are needed to maintain time resolution and signal to noise ratio for the Detection and Timing Device I: Direct View. With Detection and Timing Device II: Sampling Oscilloscope, this can be relaxed to about ten photoelectrons per lifetime if maximum smoothing is used. The use

of the Auxiliary Detection and Timing Device: Averaged Sampling, extends the useful range of the sampling oscilloscope by at least a factor of four, and thus may be used when the intensity of photoelectrons is only two or three per lifetime. When the intensity is less than this, Detection and Timing Device III: Delayed coincidence should be used.

All of the above considerations must be qualified for measurements of short lifetimes (< 20 nanoseconds) or very long lifetimes ($>$ 1 microseconds). The minimum time resolution of Detection and Timing Devices I and II is controlled by the fall time of a photoelectron pulse. The fall time of a pulse is about 50 per cent longer than the rise time, which is given by most photomultiplier manufacturers. Lifetimes which are about five times or less than the fall time of the photomultiplier should be measured with Detection and Timing Device III.

For very long lifetimes, integration (which effectively decreases the band pass) will improve the signal to noise ratio. Eq. (71) still applies if the decay constant (τ) is five times as long as the decay time of the integrator.